The human solitary nucleus and dorsal motor nucleus of vagus during fetal development

Author:
Cheng, Gang

Publication Date:
2005

DOI:
https://doi.org/10.26190/unsworks/7865

The Human Solitary Nucleus and Dorsal Motor Nucleus of Vagus During Fetal Development

Gang Cheng

Department of Anatomy, School of Medical Sciences, University of New South Wales

A thesis submitted in fulfillment of requirements for the degree of

Doctor of Philosophy at University of New South Wales

December 2005

Table of Contents

Abstract

The present study examined the embryonic and fetal development of human solitary nucleus (Sol) and dorsal motor nucleus of vagus (10N). The cyto- and chemoarchitecture of the developing Sol and 10N from 9 to 25 weeks of gestation were investigated using Nissl staining as well as immunohistochemistry for localization of calbindin, calretinin, tyrosine hydroxylase, growth associated protein 43 and substance P. Development of vagal sensorimotor circuits from 8 to 28 weeks was studied using carbocyanine dye (1, 1'-dioctadecyl-3,3,3',3' tetramethylindocarbocyanine perchlorate - DiI) tracing. Cyto- and chemoarchitectonic analysis of the developing Sol revealed that it began to gain heterogeneity and show subnucleation as early as 13 weeks, and approached cytoarchitectonic maturation from 21 to 25 weeks. The chemoarchitectonic study showed that the human Sol expressed various neurochemical substances at 13 weeks, even before cellular and neuropil differentiation. Expression of these factors may play an important role in establishment and integration of viscerosensory function. The cyto- and chemoarchitectonic study of the developing 10N showed that it begins its development as early as 9 weeks and appears as a distinctive neuronal group as early as 13 weeks. Subnucleation within 10N appeared at 15 weeks and approached a mature organization during the period from 21 to 25 weeks. The first central labeling from the thoracic vagus nerve was seen at 8 weeks. Afferent terminal segregation in the dorsomedial subnuclei of Sol was noticeable at 13 weeks, which was also the age when first retrogradely labeled 10N neurons were revealed. While there are numerous studies of the development of Sol and 10N in experimental animals, this is the first demonstration of the time course of

development of these two nuclei in human. The observation that vagal afferents terminate in a restricted zone of Sol early in development (13 weeks) suggests that there is no initial exuberance in the termination field of the nucleus. Afferents invading 10N from the medial Sol were seen only after 20 weeks and were not well developed until 24 weeks, suggesting the establishment of direct monosynaptic connections between the sensory and effector components of these two nuclei at this age.

Acknowledgement

This work would not be possible without years' of support by people around me.

First of all, I would like to say "thank you very much" to my supervisor Prof George Paxinos, who provided me with the opportunity to undertake PhD degree, and for his endeavour and enthusiasm to help me to fulfil my academic achievement.

I should also send my gratitude to my family, my parents, my wife Connie and my brother Mark. They are the closest friends to me, now and always. I know I should never let them down. Here I would especially thank my dear wife Connie, for her love, her passion and her enduring support and understanding of my scientific carrier.

People from many backgrounds have helped me in this work. The co-scientists from Wenzhou Medical College, especially Prof Jia Qu, the Principal of the college, and Prof Fan Lu, Dr Xiantian Zhou and Dr Hua Zhu have provided a great deal of support in obtaining human fetal material. Dr Luan-ling Zhang also provided many invaluable suggestions. My colleagues from Prince of Wales Medical Research Institute and Department of Anatomy in UNSW, especially Ms Hongqin Wang, Dr Yuri Koutcherov and Mr Paul Halasz, have been very generous in providing access to facilities, technical support as well as a stimulating environment for my PhD study. I hereby would say "thank you" to all the people who have kindly helped me.

Finally, a special thank you should be said to my co-supervisor, A/Prof Ken Ashwell, who has certainly acted a lot more than just as a co-supervisor. This work would never become reality without his encouragement and earnest guidance that helped me out

whenever I needed it in my studies.

Chapter 1 General Introduction

1.1. General Profile of the Solitary Nucleus and Dorsal Motor Nucleus of Vagus

The solitary nucleus (Sol) and dorsal motor nucleus of vagus (10N) are the two major structures involved in the sensorimotor function of the vagus nerve (10n). Both nuclei are located at the dorsomedial part of the medulla oblongata, and together with the area postrema, these three structures are generally termed the dorsal vagal complex (Altschuler et al., 1992). Sol is the major recipient of afferent axons of 10n, while 10N contains perikarya of efferent vagal preganglionic neurons. Both nuclei form the principal visceral sensory and motor control center in the brain that modulates cardiac, pulmonary, gastrointestinal and renal function (Barraco and Robin, 1994; Blessing, 1997; Hyde and Miselis, 1992; Jean, 1991). One example of a typical reflex involving the two nuclei is the gastrointestinal reflex; the gastrointestinal vagovagal reflex arc includes afferent, intermediate and efferent limbs. The afferent fibers innervate the visceral lumen, with receptors located in either the mucosal or muscular layers, and respond to various chemical and mechanical stimuli. Fibres carrying these visceral data are eventually convergent onto the integrating interneurons within the nucleus of the solitary tract (sol). Sol then projects to neurons in 10N. These neurons in 10N are parasympathetic preganglionic neurons which project efferent vagal nerve fibers to the intrinsic ganglia of the viscera. Thus, the esophagogastric, gastric distension-secretion, duodenogastric reflexes, as well as gastropancreatic reflex, are all examples of vagovagal reflex circuits, which maintain regional co-ordination over digestive functions (Rogers et al., 1995).

However, the autonomic controls exerted by Sol and 10N are more complicated than would be implied by these simple vagovagal reflexes, because both nuclei have

connections to a multitude of regions within the spinal cord, brainstem and forebrain (Leslie et al., 1992). The complexity of the divergence, convergence and relay functions of Sol and 10N, therefore, is underpinned by rich structural diversity of these two nuclei. The first chapter of this thesis presents a review of the structure and function of Sol and 10N across mammalian species. The current state of information concerning the development of these nuclei in mammalian species is also considered.

1.2 The Solitary Nucleus and the Visceral Sensory Process

The solitary nucleus featured prominently in work by Cajal described as early as 1899 in his *Histologie* (American translation, Cajal, 1995), and has been paid great attention ever since in studies of the autonomic nervous system. It is the major recipient and first line relay center for baroreceptor, cardiac, pulmonary chemoreceptor and other vagal and glossopharyngeal afferents (Kalia and Sullivan, 1982; Lundy and Norgren, 2004; Pritchard and Norgren, 2004; Taber, 1961; Tork et al., 1990; Torvik, 1956; Travers and Norgren, 1983; Whitehead, 1988; 1990; Zhang and Ashwell, 2001a;).

1.2.1 Subdivisions and Structural Homologies Across Species

The solitary nucleus of the mammalian brain is a heterogeneous structure located in the dorsomedial part of the medulla oblongata. The nucleus is named after a heavily myelinated fiber bundle, i.e., sol, which it surrounds. The bilateral columnar shaped nucleus extends rostrocaudally at the lateral sides of the fourth ventricle, from the level of the caudal pole of the facial motor nucleus to the obex, where the two columns merge to

form a midline structure that continues caudally to approximately the caudal level of the pyramidal decussation.

Numerous studies have attempted to identify structural and functional subdivisions of Sol, based on a number of criteria including electrophysiology, cyto- and chemoarchitecture and neuronal connections (Allen, 1923; Barry et al., 1993; Cajal, 1995; Herbert et al., 1990; Kalia and Mesulam, 1980a; Kalia and Mesulam, 1980b; Loewy and Burton, 1978; Taber, 1961; Torvik, 1956; Whitehead, 1988).

In his *Histologie* (Cajal, 1995), Cajal proposed a structural organization of Sol according to vagal and glossopharygeal afferents. He distinguished *external, internal, commissural* and *interstitial* parts of the grey matter adjacent to sol in the rat. Although this plan has been considerably changed by several authors on the basis of histological and tract tracing studies, recent studies on the nucleus have revealed that the broad features of Cajal's proposal for subdivision of Sol are still pertinent (Schwarzacher, 2002).

Also in the rat, (Torvik, 1956) divided Sol into medial and lateral portions by their location relative to sol. The *medial nucleus* is located dorsal and dorsolateral to 10N. Caudally, the cells of the medial subdivision on both sides merge in the midline to form the *commissural nucleus.* The medial subdivision contains densely packed, small, pale-staining cells with little cytoplasm. The cell bodies are generally round, pear-shaped, or triangular. The *lateral nucleus* is considerably smaller than the medial nucleus. Its lateral border is rather ill defined in caudal parts of Sol. From the level of area postrema (AP), the lateral division becomes progressively larger and more clearly outlined as it extends rostrally. The cells of the lateral division are slightly larger than those of the medial subdivision, less

densely packed, and mostly multipolar. In a more recent investigation (Kalia and Sullivan, 1982), the rat Sol was further divided into seven subnuclei by using cytoarchitectural criteria in Nissl stained material. These nuclei were the *medial, intermediate, ventral, ventrolateral, interstitial, dorsolateral* and *commissural* subnuclei (Kalia and Sullivan, 1982). Such a division pattern was in a way descriptive, but not accepted by some other investigators. Herbert and colleagues (Herbert et al., 1990) could not clearly identify any subnuclei lateral to sol and preferred to call this region the "*ventrolateral subnucleus*", instead of dividing it into ventral, ventrolateral, dorsolateral and interstitial subnuclei in the manner of Kalia and Sullivan (Kalia and Sullivan, 1982). On the other hand, the medial division was subdivided by Herbert et al. (Herbert et al., 1990) into *medial central* (also applied by Ross et al., 1985), *parvicellular*, *intermediate* (in agreement with Kalia and Sullivan, 1982), *dorsomedial*, *commissural* and *rostral* subnuclei, with an additional *subpostrema zone* (also applied by Barraco et al., 1992; Ruggiero et al., 1996; van der Kooy, 1984). The *dorsomedial* subnucleus was termed the *gelatinosus* subnucleus (Leslie et al., 1982; Ruggiero et al., 1996; Shapiro and Miselis, 1985). Van der Kooy et al. (van der Kooy, 1984) abandoned the term "commissural nucleus", and instead defined the small cell-poor area in the caudal midline as the "*midline solitary nucleus*" and included the remaining area of the commissural subnucleus into the medial subnucleus. Nevertheless, one of the most recent studies applied a 9-subnucleus division scheme based on their cytoarchitectural and neurochemical investigation of both adult and developing rats (Zhang and Ashwell, 2001b). The nomenclature of the nine subnuclei described in this study was largely adopted from the terms used by Kalia and Sullivan (Kalia and Sullivan, 1982), with the

addition of the *gelatinous* and *central* subnuclei.

Studies on other species have also arrived at divisional schemata for Sol, which are somewhat similar to those described above in the rat. In the cat, Sol was divided into *dorsomedial* and *ventrolateral* partitions by Taber (Taber, 1961). Other authors have made more detailed description of subnuclei of the cat Sol with application of autoradiographic and horseradish peroxidase experiments. Loewy and Burton (Loewy and Burton, 1978) identified 6 subnuclei in the cat Sol, whereas Kalia and Mesulam (Kalia and Mesulam, 1980a) delineated 9 subnuclei in that species, a number which was also found in the dog (Estes et al., 1989).

In studying the hamster Sol, Whitehead (Whitehead, 1988; Whitehead, 1990) suggested that the rostral and caudal parts of Sol should be regarded as two discrete regions, with each containing further different cellular groups. He made the point that the region where Sol meets the floor of the 4th ventricle represents a significant division point. In their schema, the rostral division is comparable to the so-called *prevagal* or *gustatory* part of Sol. The caudal division, which is mainly involved in vagal input according to the proposal of the author, contains a *commissural* region at its caudal extreme, where the nuclei of both sides fuse at the midline. Such a division was supported by studies on the basis of AChE, NADH-dehydrogenase, and cytochrome oxidase histochemical studies on the same species (Barry et al., 1993) and the investigations of other authors on the rat (Beckstead and Norgren, 1979).

The human Sol has also been studied cytoarchitectonically and neurochemically in developing and adult brains (Arango et al., 1988; Gai and Blessing, 1996; McRitchie and

Tork, 1993; McRitchie and Tork, 1994; Yew et al., 1990). Figure 1.1 of the present chapter shows different subnuclei of human Sol in coronal sections arranged rostrocaudally. This figure was adopted directly from Huang and Paxinos (Paxinos and Huang, 1995). The human Sol is composed of as many as 10 subnuclei: paracommissural (SolPa), commissural (SolC), gelatinosus (SolG), medial (SolM), ventral (SolV), ventrolateral (SolVL), dorsal (SolD), dorsolateral (SolDL), intermediate (SolIM), and interstitial (SolI) subnuclei. Among those subnuclei, SolI, SolD, SolDL, SolC, SolG and SolM were identified by AChE reactivity (McRitchie and Tork, 1993). The subnuclei SolG, SolM, and SolIM were apparent in substance P (SP) immunoreactive material (McRitchie and Tork, 1994). The same authors were unable to identify immunoreactivity for SP in the adult commissural subnucleus, which Yew and colleagues (Yew et al., 1990) identified in fetal brainstems treated for SP immunoreactivity. In another case, Gai and Blessing (Gai and Blessing, 1996) found a conspicuous central subnucleus on the basis of NADPH-diaphorase histochemical staining, although this could not be demarcated by other authors (Braak, 1972; McRitchie and Tork, 1993; Olszewski and Baxter, 1982). These discordant findings indicate that the divisional pattern of human Sol is inconsistent across various researchers and further studies need to be carried out to reach a definitive organizational plan.

1.2.2 Viscerotopic Organization of Afferent Terminations of Cranial Nerves in the Solitary Nucleus

The mapping of afferent fiber termination patterns within Sol has been the subject of detailed studies using degenerative, autoradiographic and anterograde and retrograde

labeling techniques (Altschuler et al., 1989; Astrom, 1953; Contreras et al., 1982; Hamilton and Norgren, 1984; Leslie et al., 1982; Norgren, 1978; Torvik, 1956; Whitehead, 1986). The major afferent cranial nerves projecting to Sol are facial nerve (7n), glossopharyngeal (9n) and vagus nerve (10n). There is also a minor portion of fibers from the trigeminal nerve (5n) terminating in Sol (Altschuler et al., 1989; Barry et al., 1993; Beckstead and Norgren, 1979; Sugimoto et al., 1997). The afferent termination of these nerves in Sol forms a viscerotopic rostro-caudal order although there is some overlap between termination territories of successive nerves. Figure 1.2 shows the orientation of the termination fields of cranial nerves 7n, 9n and 10n.

A. Gustatory afferents

The solitary nucleus provides the first synaptic interruption in the central gustatory system. A major input to Sol is provided by the geniculate ganglion cells of the facial nerve. The peripheral processes of these cells constitute the chorda tympani and the greater superficial petrosal nerves that innervate taste buds on the anterior two-thirds of the tongue and palate, respectively (Pritchard and Norgren, 2004). The centrally directed axons of geniculate ganglion cells terminate heavily in the rostral half of ipsilateral Sol (Hamilton and Norgren, 1984; Whitehead, 1986). Plasticity is present in this system during development. Dietary NaCl deprivation in postnatal developing rats has been shown to significantly reduce the area of termination of chorda tympani afferents (King and Hill, 1993). The rostral part of Sol also showed changes in neuronal dendritic and glial morphology under the same experimental regime (King and Hill, 1993). Several other

studies have also revealed that some afferents from the chorda tympani terminate in the caudal part of Sol, and are mainly of non-gustatory (perhaps somatosensory) function (Contreras et al., 1982).

Terminations of 9n in Sol is located caudal to 7n. Some of the axons extend to the commissural area (where both sides of Sol fuse to each other). The largest branch of 9n, the lingual-tonsilar branch, conveys gustatory information from the foliate and circumvallate papillae on the caudal tongue, and also serves as the somatosensory nerve for the posterior tongue, fauces, and palatine tonsils (Contreras et al., 1982). Electrophysiological stimulation of the 9n showed that the gustatory information conveyed by 9n is independent from that of 7n (Bradley and Grabauskas, 1998).

B. Cardiovascular Afferents

The chemoreceptors of the carotid body and the baroreceptors of the carotid sinus are essential in regulating blood pressure, heart rate and respiratory function. The afferent fibers from the receptor sites are conveyed in the carotid sinus nerve, which is a branch of the 9n (Housley et al., 1987). Anterograde labeling of the carotid sinus nerve showed that it terminated in the lateral division of ipsilateral Sol in the monkey (Beckstead and Norgren, 1979; Satoda et al., 1995). Contralateral labeling of the carotid sinus nerve in Sol has been reported in the cat, dog and rat (Berger, 1979; Chernicky et al., 1987; Davies and Kalia, 1981; Housley et al., 1987). A WGA-HRP study in the cat revealed that the carotid sinus nerve projects mainly to ipsilateral Sol at rostral levels, but with a strong contralateral component caudal to the obex. Afferents from the carotid sinus project to

several Sol territories that do not receive afferents from the carotid body chemoreceptors. These are the dorsolateral, the lateral extension of the commissural, the caudal intermediate, the ventrolateral and the gelatinosus subnuclei. In addition, the carotid sinus central representation includes territories occupied also by carotid body terminals: dorsal, interstitial, rostral intermediate, medial and the medial part of commissural subnuclei (Torrealba and Claps, 1988).

Not only is the carotid sinus nerve a branch of the 9n, but part of this nerve also branches into 10n. Therefore, 10n also seems to be involved in the cardiovascular receptive functions of Sol (Satoda et al., 1995; Torrealba and Claps, 1988).

C. Gastrointestinal Afferents

The vagus nerve terminates in Sol with afferents occupying most of the posterior half of the nucleus, mainly packed within the medial subdivisions. Although the distribution overlaps, the vagus nerve termination field in Sol is primarily located caudal to those of 7n and 9n, and includes almost all subnuclei of the caudal part of Sol (Contreras et al., 1982; Kalia and Mesulam, 1980b).

One of the major functions of the vagal afferent fibers to Sol is that of providing gastrointestinal sensory input to the brain. By applying intramuscular injections of HRP conjugates into different areas of the alimentary tract, visceral afferent terminations in Sol have been shown to form a viscerotopic organization in distinct subnuclei in the rat and it is apparent that a rostrocaudal segregation of terminal fields corresponds to rostrocaudal positioning of the viscera along the alimentary tract (Altschuler et al., 1989; Rinaman and

Miselis, 1987; Shapiro and Miselis, 1985). Afferents from the soft palate are represented rostrally in Sol and densely present in the interstitial subnucleus, with less densely packed labeling in the intermediate and medial subnuclei. The interstitial and intermediate subnuclei represent sites where the terminal fields of the soft palate, pharynx, and larynx overlap. Even within these two subnuclei, soft palate afferents are represented most rostrally, laryngeal afferents most caudally and pharyngeal afferents intermediate to those of the soft palate and larynx. Afferents from the esophagus, stomach and cecum terminate caudal and medial to palatal and pharyngeal afferents. Esophageal afferents terminate entirely within the central subnucleus. The terminal fields of the cervical, thoracic and subdiaphragmatic esophagus show considerable overlap in their rostrocaudal distribution within the subnucleus. The densest concentration of gastric afferents within Sol is found within the gelatinosus subnucleus, which is located dorsomedial to the central subnucleus. Gastric afferents also reach sites within the medial and commissural subnuclei, resulting in a more caudal distribution than esophageal afferents. Cecal afferents project most prominently to the commissural subnucleus, with a less dense termination field in the periventricular and ventromedial parts of the medial subnucleus. Vagal afferents from the pancreas and small intestine do not terminate in Sol. It was also noted that the palatal afferents also terminate rostrally at the lateral area of Sol, which is considered to be devoted to those fibres of gustatory relevance (Altschuler et al., 1992).

D. Respiratory Afferents

The primary afferents from the upper respiratory tract and lungs also project to Sol

via the vagus nerve. Electrophysiological studies have found that the pulmonary C fiber vagal afferents terminate mainly in the commissural subnucleus (Bonham and Joad, 1991), whereas afferent fibers from the pulmonary stretch receptors project primarily to the ventrolateral subnucleus (Berger et al., 1984). Neurons in the ventrolateral subnucleus of Sol, the so called dorsal respiratory group (Cohen, 1979), play an important role in Hering-Breuer reflex inhibition of inspiration, which consists of a shortening of inspiration and lengthening of expiration in response to afferent input from slowly adapting pulmonary stretch receptors.

1.2.3 Central Projection of the Solitary Nucleus

The solitary nucleus receives primary visceral sensory input and relays this to selected CNS structures; presumably after some significant processing of afferent input by its interneurons. Most of the central connections are reciprocal and constitute the anatomical substrate for both short and long-loop control mechanisms serving to modulate visceral reflexes and homeostatic response patterns at the level of Sol.

The regions to which Sol gives central projections are the spinal cord (Torvik, 1956), the spinal trigeminal nucleus (Menetrey and Basbaum, 1987), the dorsal motor nucleus of vagus (10N), ambiguus nucleus (Gai et al., 1995; Shapiro and Miselis, 1985), ventrolateral medulla (Ross et al., 1985), parabrachial nucleus, Kolliker-Fuse nucleus (Herbert et al., 1990; Karimnamazi et al., 2002; Whitehead, 1990), locus coeruleus, periaqueductal grey, raphe nucleus, hypothalamus, perifornical region, subfornical organ, posterior pituitary, central nucleus of the amygdala, bed nucleus of the stria terminalis, olfactory tubercle,

paraventricular nucleus of the thalamus (Beckstead et al., 1980), and accumbens nucleus (Li et al., 1990; Wang et al., 1992).

It is noteworthy that subnuclei of Sol in recipient of specific functional inputs from the cranial nerves are affiliated with the brain nuclei elaborating the same functions. For example, the ascending fibers from the rostral Sol mainly project to the gustation related area of the medial parabrachial nucleus, while the intermediate and posterior medial areas of Sol, which receive visceral inputs, project mainly to the lateral portion of the parabrachial nucleus (Herbert et al., 1990). The respiratory related area of the Kölliker-Fuse nucleus receives projections from the ventrolateral and intermediate subnuclei as well as the commissural subnucleus of Sol, all of which have been reported to receive cardiorespiratory inputs from the heart and lungs (Herbert et al., 1990). Afferents to the ventrolateral medulla mostly originate from the intermediate section of Sol. The rostral ventrolateral medulla receives inputs from the commissural, dorsal, intermediate, interstitial, ventral, and ventrolateral subnuclei of Sol, while the caudal ventrolateral medulla receives projections from neurons located in more lateral and caudal parts of Sol (Ross et al., 1985). The intermediate subnucleus of Sol receives overlapping afferents from the palate, pharynx and larynx, projects to motoneurons of the ambiguus nucleus which innervate muscle of the pharynx, larynx and esophagus and is involved in the swallow reflex and respiratory actions (Bieger, 2001). Ascending projections to the hypothalamus and other subcortical areas have once again revealed functional features of the Sol projection: the posterior visceral sensory part of Sol has ascending projections as far as the septum-diagonal band complex and gives heavy input to the bed nucleus of the

stria terminalis, and to the dorsomedial and paraventricular hypothalamic nuclei. Other projections reach some other hypothalamic nuclei, the medial and central amygdaloid nuclei and the paraventricular nucleus of the thalamus. On the other hand, the anterior part of Sol has only limited projections to the forebrain, which do not go further than the anterior dorsal hypothalamic nucleus (Ricardo and Koh, 1978; Ter Horst et al., 1989).

Connections between the ventral caudal raphe and Sol may be involved in chemoreception and central regulation of cardiorespiratory reflexes during prenatal and adult life. These pathways have been demonstrated in human fetuses aged from 18 to 22 weeks by Zec and Kinney (2003).

1.3 The Dorsal Motor Nucleus of Vagus

The dorsal motor nucleus of vagus (10N) is the largest parasympathetic nucleus of the brainstem. It is elongated in the anterioposterior extension and is located between Sol and the fourth ventricle (4V). In mammals, the caudal pole of 10N is found at the level of the pyramidal decussation dorsolateral to the central canal. Ventrally, 10N is bounded by a parvicelluar structure called the intercalated nucleus. The motor nuclei of the vagus and hypoglossal nerves (10N and 12N respectively) are separated by this intercalated nucleus. At the level of the area postrema, 10N almost reaches the periventricular gray matter, close to the 4V. Further rostrally, 10N migrates laterally together with Sol; finally, its rostral tip is replaced by the salivatory nucleus (Koutcherov et al., 2004).

1.3.1 Cyto- and Chemoarchitecture of the Dorsal Motor Nucleus of Vagus

Unlike Sol, which is structurally complex and contains numerous heterogeneous subnuclei, the cytoarchitecture of 10N is comparatively simple. In the literature, it is rare to find studies demarcating subdivisions of 10N, although topographic connectivity of 10N with different organs remains a widely discussed topic (Huang et al., 1993b). Early studies in cat have failed to identify subdivisions of 10N in Nissl preparations (Smolen and Truex, 1977), while comparative studies showed that rostral and caudal parts of 10N supplied visceral organs in different segments of the trunk (Kitchell et al., 1977). Attempts to establish a topographic map of visceral representation within 10N have also been made on the pigeon (Cohen et al., 1970; Katz and Karten, 1983; Katz and Karten, 1985), frog (Stuesse et al., 1984), rat (Dennison et al., 1981), rabbit (Getz and Sirnes, 1949) and monkey (Mitchell and Warwick, 1955). A morphometric analysis in the human fetus has identified three subnuclei (caudal, dorsal and ventral)(Nara et al., 1991).

In the humans, 10N contains a highly-AChE-reactive and cellularly dense principal part as well as less reactive and more sparsely populated fringe nuclei (with almost no AChE staining) lying dorsal and ventral to the principal part (Tork et al., 1990). Schematic graphics of subnuclei of 10N are shown in Fig. 1.1, along with Sol, drawn from *Atlas of Human Brainstem* (Paxinos and Huang, 1995).

A comprehensive subdivision of human 10N was performed by Huang et al. (Huang et al., 1993a; Huang et al., 1993b). By using Nissl staining combined with AChE histochemistry, SP and tyrosine hydroxylase (TH) immunohistochemistry, the human 10N was demarcated into eight subnuclei grouped regionally into rostral, intermediate and

caudal divisions on the basis of neuronal morphology, cell density, and differential neurochemical features. The rostral division contains the dorsorostral (10DR) and ventrorostral (10VR) subnuclei; the intermediate division contains the rostrointermediate (10RI), dorsointermediate (10DI), centrointermediate (10CeI), ventrointermediate (10VI) and caudointermediate (10CaI) subnuclei; the caudal division is not subdivided (10Ca). Along with the principal part of the nucleus, the medial fringe subnucleus is located ventromedially.

The subnucleus 10VI subnucleus is prominent in AChE preparations and also contains TH immunoreactive (TH-ir) neurons. 10DI is identified by its moderate AChE reactivity and SP immunoreactive (SP-ir) and TH-ir neurons. 10CaI and 10Ca contain mainly SP-ir neurons, while the medial fringe is identified by TH immunoreactivity (Huang et al., 1993a; Huang et al., 1993b).

Studies in other species based on labeling of peripheral organs did not give rise to such a complex subdivisional pattern. According to Fox and Powley (Fox and Powley, 1992), the rat 10N is composed of 5 subnuclei: bilaterally paired medial columnar subnuclei, bilaterally paired lateral columnar subnuclei and an unpaired column of sparsely distributed cells.

In the monkey and cat, ultrastructural cytoarchitecture of 10N has been studied. Two types of neurons have been identified under the electron microscope: medium sized neurons (20-30 μm diameter) with abundant cytoplasm and an oval nucleus, and small neurons (10-15 μm diameter) with a paucity of organelles and an invaginated nucleus. The synaptic density was comparatively higher on medium-sized neurons than on small-sized

neurons (McLean and Hopkins, 1985). These two types of neurons were also found in the hamster 10N by HRP tracing and ultrastructural investigation (Ling et al., 1987).

Along with the cytoarchitectural investigations, there were quite a few previous investigations on the chemoarchitecure of 10N. It is now known that 10N contains at least three major categories of neurotransmitters: monoamines, opioid peptides and non-opioid neuropeptides (Loewy and Spyer, 1990). Noradrenergic inputs from A5 cells of the rostral ventrolateral medulla were identified as the only source of noradrenergic innervation to 10N (Loewy et al., 1979). Dopaminergic neurons were also found in 10N in the rat. These neurons are TH positive and dopamine β hydroxylase- and phenylethanol amine-N-methyl transferase. Higher density of these TH-ir dopaminergic neurons was found in the caudal half of 10N compared to the rostral half of the nucleus (Hayakawa et al., 2004). 10N also contains neurons of opioid peptide immunoreactivity. Quite a few 10N neurons was found to be methionine-enkephalin-Arg6-Gly7-Leu8-immunoreactive in cats and dogs (Belda et al., 2003; Pego-Reigosa et al., 2000). The opioid peptide immunoreactive neurons were found to inhibit excitatory synaptic transmission to the gastrointestinal pathway (Browning et al., 2002). Non-opioid neuropeptides identified in the neuropil within 10N include cholectystokinin (De Leon et al., 1992), corticotrophin-releasing factors (Swanson et al., 1983), neuropeptide Y (de Quidt and Emson, 1986), neurotensin (De Leon et al., 1991), oxytocin (Sawchenko and Swanson, 1982), vasopressin (Sawchenko and Swanson, 1982), somatostatin (Higgins and Schwaber, 1983), and thyrotropin-releasing hormone (Kubek et al., 1983). Some of the neuropeptides-containing fibers originate from a clearly defined brain region; for example,

oxytocin and vasopressin projections to 10N are from the paraventricular nucleus of the hypothalamus (Sawchenko and Swanson, 1982). However, the origin of other neuropeptide-containing fibers of 10N is not quite clear (Loewy and Spyer, 1990).

1.3.2 Connectivity of the Dorsal Motor Nucleus of Vagus

The dorsal motor nucleus of vagus is the source of preganglionic efferent fibers of 10n that course ventral and lateral from the nucleus to exit the brain stem dorsal and lateral to the inferior olive. Preganglionic parasympathetic fibers from 10n have lengthy courses, but eventually terminate in ganglia that contain postganglionic neurons in the myenteric (Auerbach's) and submucosal (Meissner's) plexuses of the stomach, small intestines and parts of the large intestines reaching as far as the colon (Connors et al., 1983). There is no direct connection between the smooth muscle of the gastrointestinal tract and the vagal fibers originating from 10N.

The motor outflow is organized in a viscerotopographical manner. Those cells that innervate abdominal organs lie in the medial two-thirds of the nucleus, while the cells that innervate the heart and lungs lie in the lateral third of the nucleus, mainly at the caudal levels (Loewy and Spyer, 1990).

Along with 10n, 9n has also been found to project from 10N. After applying HRP to the proximal cut end of the dissected glossopharyngeal nerve in the cat, label was found in the ipsilateral side of the rostral 10N (Ciriello et al., 1981).

HRP injections reveal projections no matter what neural transmitters these projections contain. After iontophoretically infusing horseradish peroxidase (HRP) into

10N of the rat, projections to 10N were observed from several areas including the parviocellular and gigantocellular reticular nucleus, Sol, raphe obscurus nucleus, principal sensory trigeminal nucleus, and paraventricular nucleus of the hypothalamus (Rogers et al., 1980). The central nucleus of the amygdaloid complex, which was reported to have widespread influence on various structures in the subcortical area, has also been reported to send a projection to 10N as do the neuromelanin-containing cells of catecholaminergic cell group A2, which is located adjacent to 10N. Other structures which send projections to 10N are the paratrigeminal nucleus (Saxon and Hopkins, 1998), substantia innominata and bed nucleus of the stria terminalis (Price and Amaral, 1981; Schwaber et al., 1980).

1.3.3 Physiological Features of the Dorsal Motor Nucleus of Vagus

The main function of 10N is in the control of gastrointestinal and pancreatic secretions. Although its role in the control of other visceral functions such as lung (Kalia and Mesulam, 1980b) and heart (Cheng et al., 1999) has been reported, the precise physiological role of 10N is, nevertheless, still uncertain.

Gastric acid secretion can be induced by chemical or electrical stimulation of 10N. In experiments performed on cats by Kerr and Preshaw (Kerr and Preshaw, 1969), insulin-induced gastric acid secretion was dependent on the integrity of 10N and destruction of this nucleus was shown to prevent increases in gastric secretion following intravenous injection of insulin. Other hormone-induced gastric acid secretion, e.g. thyrotropin-releasing hormone or oxytocin, is also regulated by the projection from 10N to the stomach (Rogers and Hermann, 1985). 10N may also be involved in the control of

gastrointestinal smooth muscle. Electrical stimulation of the rostral part of 10N in the cat increases gastric motility (Pagani et al., 1985), while microinjections of L-glutamate in 10N of the rat causes decreased gastric smooth muscle tone (Spencer and Talman, 1986). Involvement of 10N in control of the pancreas can be exemplified by observations that electrical stimulation of 10N in the rat causes an increase in insulin and glucagon secretion. The lateral part of the nucleus appears to be responsible rather than the medial segment (Laughton and Powley, 1987).

The precise extent of the role played by 10N in control of cardiac function remains unclear. Traditionally, it was assumed that the ambiguus nucleus (Amb) is the major vagal motor neuron pool controlling the heart, whereas neurons in 10N play only a minor role in cardiac control. Recent studies with DiI antrograde labeling techniques have revealed that there are significant numbers of preganglionic neurons in 10N, which project to cardiac principal neurons in cardiac ganglia of the rat atria, suggesting a significant role of 10N in cardiac control (Cheng et al., 1999). Therefore, this anatomic evidence suggests that both 10N and Amb could be important for cardiac function. Physiological evidence has also revealed that 10N serves as an alternative vagal centre to Amb in cardiac function control: 1) electrical stimulation of vagal efferent B fibers (presumably from Amb) and C fibers (presumably from 10N) selectively evokes bradycardia, A-V bock, and reduction of cardiac contractility (Ford and McWilliam, 1986; Jones et al., 1995; Jones et al., 1998; Woolley et al., 1987); 2) stimulation of the 10N elecits bradycardia and reduces myocardial contractility (Calaresu and Pearce, 1965; Geis and Wurster, 1980; Rogers and Hermann, 1985); and 3) both 10N and Amb neurons are barosensitive (Xiong et al., 1998). Studies

by Cheng and colleagues (2003) revealed that although both 10N and Amb innervate cardiac ganglia, the axons of neurons of these two nuclei project to separate subpopulations of principal neurons in these ganglia. Furthermore, axons arising from neurons in Amb and 10N in the contralateral side of the brain stem enter the cardiac ganglionic plexus through separate bundles and preferentially innervate principal neurons near their entry regions (Cheng et al., 2003). In addition, Wang et al., (2005) revealed that mixed global application of glutamatergic NMDA and non-NMDA antagonists AP5 and CNQX significantly decreased the GABAergic synaptic events of the cardiac vagal neurons in 10N, but had no effect on the GABAergic synaptic events of the Amb counterparts. Altogether, these investigations have suggested that 10N is involved actively in parasympathetic regulation of the heart, and such a regulation is independent from and equally important to the control of Amb, which was previously regarded as the only chief cardiac control centre in the brainstem.

1.4 Development of the Solitary Nucleus and Dorsal Motor Nucleus of Vagus

The motor component of the dorsal vagal complex is derived from the ventromedial cell column of the rhombencephalon at stage 13 (Muller and O'Rahilly, 2004). Neurons of 10N migrate during stages 13 to 17, give rise to peripheral fibers at stages 14 to15, and reach their final rest site by stages 16 to 17 (Muller and O'Rahilly, 2004). Sol develops from the sensory nuclei primordium of the human rhombencephalon and appears at approximately stage 19 (Muller and O'Rahilly, 2004).

1.4.1 Development of the Solitary Nucleus

Early development of Sol has been studied in various species including humans. In the rat, it was reported that neurons destined for Sol were born at E11-E14 (E = embryonic day), with peak neurogenesis at E12 (Altman and Bayer, 1980). A recent study revealed that cytoarchitecturally the subnuclei of Sol in the rat were not identifiable until after E17 (Zhang and Ashwell, 2001b). Between E17 and E19 the nucleus undergoes profound changes as seen in Nissl stained material, and at E19 most subnuclei of Sol are discernable.

In the human, Sol becomes visible at embryonic stage 19, which is about 7 weeks after fertilization (Muller and O'Rahilly, 2004). Wang and colleagues (Wang et al., 1993) found subnuclear organization of the human Sol is apparent by at least the 16thweek of gestation, but specimens earlier than 16 weeks were not examined by the same authors. SP immunoreactivity can be seen for the first time at the 16th week of gestation, at which stage it is present in fibers distributed mainly over dorsal and dorsolateral parts of the nucleus, although the ventrolateral subnucleus also showed moderate density of SP immunoreactivity (Wang et al., 1993). The density of SP-ir fibers increased steadily in Sol over the fetal period until the last age examined by those authors (40th week of gestation). Binding of opiates to Sol and trigeminal sensory nuclei is similar to the adult by midgestation, indicating possible early maturation of the opioid system (Kinney et al., 1990).

1.4.2 Development of the Dorsal Motor Nucleus of Vagus

In the rat, 10N, like the hypoglossal nucleus (12N), belongs to the earliest arising structures of the lower medulla, with 80% of their cell populations acquired on day E12 (Altman and Bayer, 1980). 10N has a feature of rapid generation, so that completion of generation and settling in the final site occurs within just one day. This is different from the nucleus ambiguus, which completes cell migration and differentiation over a lengthier period of development. A more recent study using optical mapping techniques showed that by E13 to E14 nerve terminals in the dorsomedial area of the rat medulla showed two types of spike-like optical signals (Sato et al., 1998). One of these was a narrow signal (type I), and was associated with Sol. The other was a broader signal (type II), and appears to correspond anatomically to 10N. In the E15-16 preparations, type I signals were followed by a slow signal related to glutamate-mediated excitatory postsynaptic potentials, suggesting that synaptic function is organized in Sol by 15 day old embryonic stage (Sato et al., 1998).

The development of the human 10N has gained less attention than Sol. Only a handful of studies in the literature have reported on development of this structure. The dorsal motor nucleus of the vagus nerve can be seen to be divisible into three main subdivisions (caudal, dorsal and ventral) by 16 weeks of gestation (Nara et al., 1991), but detailed analysis of dendritic development of neurons in the vagal sensorimotor complex is not available. Nevertheless, a study of dendritic spine development in the dorsal medullary reticular formation indicates that dendritic spine density increases steadily from 20 weeks of gestation to term, before declining during early postnatal life (Becker and

Zhang, 1996). Wang et al. (Wang et al., 1993) showed by using SP immunohistochemistry, that 10N had only a low density of SP immunoreactivity at 16 weeks from last menstrual period. The density of SP-ir fibers increased as the growth of brainstem draws to a close, and by 23 weeks, 10N showed moderate to high density of SP immunoreactivity (Wang et al., 1993).

Specific disorders of human 10N appear to be rare, but some investigators have shown that there is a serotonin related abnormality specificly in 10N in Rett Syndrome. In this abnormality, which is an X-chromosome linked disorder of mental retardation resulting from mutations in the gene encoding methyl-CpG-binding protein2 (MeCP2), there is autonomic dysfunction prevalent in affected girls. Paterson et al. (2005) have found that altered 5-HT innervation and/or uptake in the 10N may contribute to abnormal 5-HT modulation of this nucleus in patients with Rett" syndrome. In a recent review of the significance of serotonergic neuron networks for sudden infant death syndrome (SIDS), Kinney et al. (2001) concluded that there was no significant differences in serotonergic receptor autoradiography in Sol and 10N between SIDS and control cases.

1.5 Hypothesis and Aims of the Present Study

The general hypothesis of the present study is that the interconnectivity of Sol and 10N is established around the time that functionally important activities such as breathing and gastrointestinal motility are first recorded by ultrasound.

The general aim of the present study was to examine the embryonic and fetal development of Sol and 10N in the human. The underlying purpose of the analysis

was to use cytoarchitectonic, chemoarchitectonic and connectivity analysis to try to determine the earliest age at which functional capacity of Sol and 10N is likely to be achieved.

Within this general aim, several specific aims can be identified and will form the subject matter of the subsequent chapters.

Specific Aim (1): to examine the cyto- and chemoarchitecture of the developing human Sol

In the present study, the development of Sol was followed during late embryonic and fetal life in order to determine when subnuclear organization and the characteristic chemoarchitectural features of Sol develop. This was intended to provide clues as to when the chemically identified neuronal circuitry responsible for particular functions of subnuclei of Sol might develop. Furthermore, examination of the distribution of various putative growth factors, neurotransmitters or their signature synthetic enzymes (e.g. GAP-43, SP, TH) may tell us something about the development of functions in which these compounds and the associated structures are involved. The cytological and chemical organization of the developing human Sol (aged from the 9th to 25th week) was examined with the aid of Nissl staining and immunohistochemistry using antibodies against calbindin (Cb), calretinin (Cr), tyrosine hydroxylase (TH), substance P and GAP-43. Immunoreactivity for these markers will allow the identification of subnuclear organization within the developing Sol as a foundation for studies of afferent connectivity.

Specific Aim (2): to examine the cyto- and chemoarchitecture of the developing 10N

The dorsal motor nucleus of the vagus nerve is the largest parasympathetic nucleus of the brainstem and contains preganglionic motoneurons. It contains populations of chemically identified neurons, e.g., TH and SP. The TH-ir neurons are dopaminergic and engage in parasympathetic projections to the alimentary tract (Hayakawa et al., 2004). SP is not only a neurotransmitter for general sensory afferent fibers (Cuello et al., 1993; Del Fiacco et al., 1983; Mai et al., 1986), but is also involved in extensive autonomic functions, such as cardiac control (Talman and Reis, 1981), stomach and esophageal function, and respiratory function (Gibbins et al., 1987; Lindh et al., 1983).

In the present work, studying the cyto- and chemoarchitectural development of 10N during late embryonic and fetal human brain, (with the focus on TH and SP, but also analyzing developmental changes in calcium-binding protein immunoreactivity), it will be possible to determine the point of development at which 10N becomes chemically differentiated. This will provide clues to when this nucleus becomes functionally capable.

Specific aim (3): to determine the time-course of maturation of the distribution of vagal afferents within the subnuclei of Sol and development of efferent neurons from 10N.

While the connections of the vagus nerve have been studied extensively in adult experimental species both morphologically and functionally (Barraco and Robin, 1994; Broussard and Altschuler, 2000a; Loewy, 1990; Ritter et al., 1992), the development of

central vagal sensory and motor connections has received much less attention. The laboratory of Kinney has undertaken an extensive series of studies using carbocyanine dye tracing techniques to explore the connections between the Sol and functionally significant brainstem centres (Zec et al., 1997; Zec and Kinney, 2001; Zec and Kinney, 2003). In the previous studies, Kinney and colleagues were interested predominantly in the connections between Sol and other parts of CNS during development, whereas the present study is focused on development of afferents to the solitary complex and efferents from 10N. In the present study, carbocyanine dye (DiI) was applied to the vagus nerve roots of embryonic and fetal human brains of various ages and the age at which afferents and neurons in Sol and 10N, respectively, were labeled was determined. This will determine the time by which the connections of vagal sensory and motor centers with the vagus nerve are established. Formation of vagal connections is clearly of major significance for the development of visceromotor and respiratory function because the vagus provides the afferent limb of respiratory reflexes and the afferent and efferent pathways in control of cardiovascular and digestive function. In humans, it remains unclear at what developmental stages the neural circuits which control the functions of these visceral organs achieve maturity. Therefore, I set out in the present study to determine the time-course of maturation of the vagal afferent and efferent centres in the brain.

Figure 1.1 Schematic graphic of rostrocaudally ordered (A-H) coronal sections showing structures of the adult human dorsomedial medulla. Note the subdivisions of Sol and 10N. Abbreviations for the names of each subnuclei as well as the structures surrounding them have been shown in the appendix of this thesis. (Figure adopted from Paxinos and Huang, 1995)

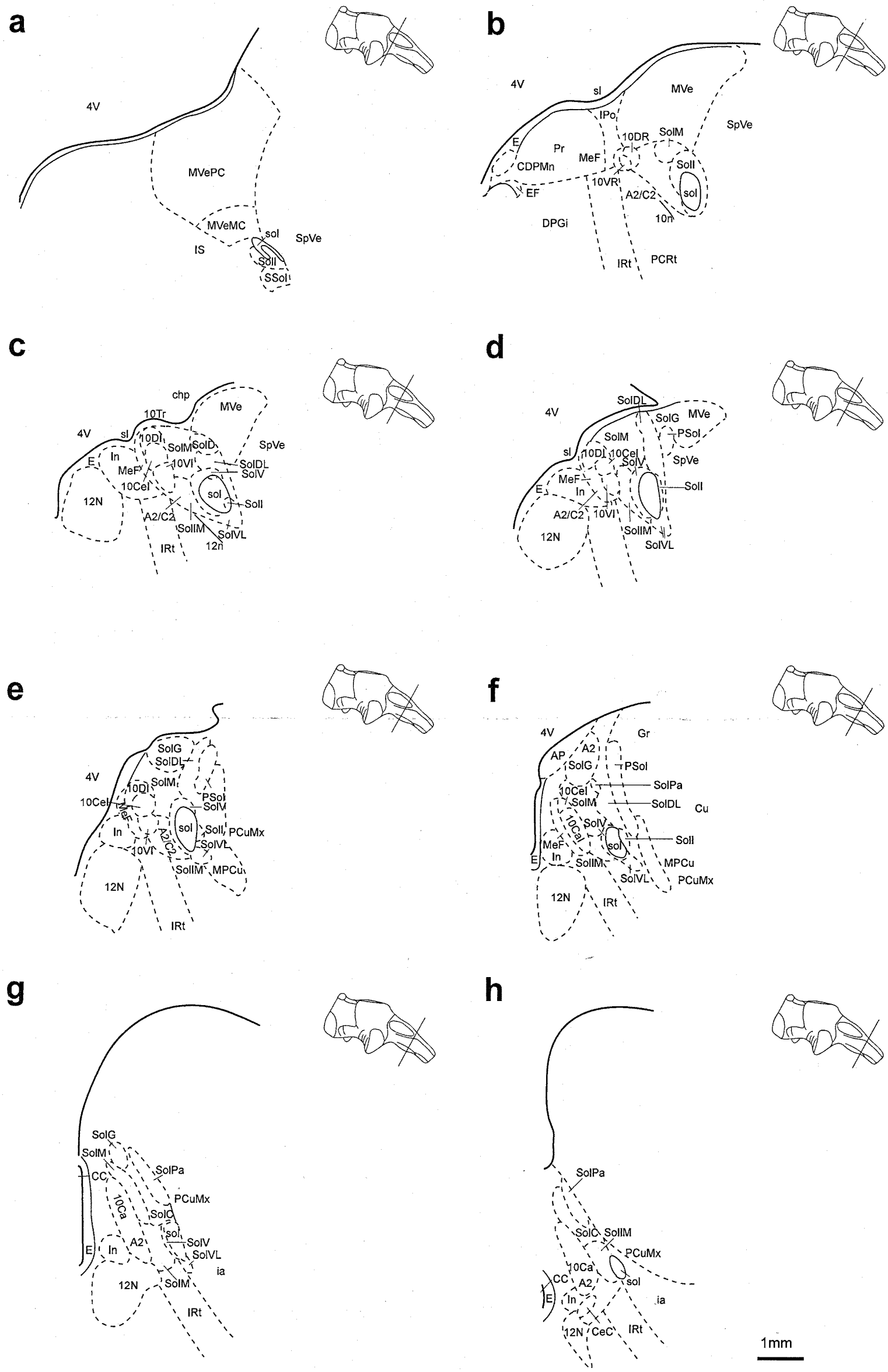
a
4V
MVePC
MVeMC
IS
sol
SpVe
SolI
SSol
b
4V
sl
MVe
IPo
SpVe
E
Pr
CDPMn
MeF
10DR
SolM
SolI
10VR
EF
A2/C2
sol
10n
DPGi
IRt
PCRt
c
chp
MVe
10Tr
4V
sl
10Dl
SolM
SolD
SpVe
In
E
MeF
10Vl
SolDL
SolV
10Cel
sol
SolI
12N
A2/C2
SolIM
SolVL
IRt
12n
d
SolDL
4V
SolG
MVe
PSol
SolM
sl
10Dl
10Cel
SolV
SpVe
MeF
SolI
E
In
A2/C2
10Vl
SolIM
12N
SolVL
e
SolG
SolDL
4V
SolM
10Dl
PSol
10Cel
MeF
SolV
In
A2/C2
sol
SolI
PCuMx
10Vl
SolVL
12N
SolIM
MPCu
IRt
f
4V
Gr
AP
A2
SolG
PSol
SolPa
10Cel
SolM
SolDL
Cu
10Ca
SolV
SolI
MeF
sol
E
In
SolIM
MPCu
SolVL
PCuMx
12N
IRt
g
SolG
SolM
SolPa
CC
PCuMx
10Ca
SolC
sol
E
In
A2
SolV
SolVL
ia
12N
SolM
IRt
h
SolPa
SolC
SolIM
PCuMx
10Ca
CC
sol
A2
E
In
ia
12N
CeC
IRt
1mm

Figure 1.1

Figure 1.2 Terminal distributions of cranial nerves 7n (a), 9n (b), and 10n (c) within Sol of an adult rhesus monkey (*Macaca mulatta*). Each panel shows an outline of Sol as it appears in the horizontal plane. The vertical dashed line represents the midline, the obex is marked by a filled circle. The medial and lateral subdivisions of the nucleus are separated from one another by a dashed line through the nucleus. Each Panel is oriented with rostral to the top of the page and lateral to the right. The yellow color area represents areas of lower density of autoradiographic label within Sol after injections of the respective ganglia for cranial nerves 7n, 9n, and 10n, while the brown color area represents areas with high density of label. The terminal areas of all three nerves in the monkey Sol show considerable overlap, especially within the rostral third of the nucleus. Of these three nerves, only the vagus projects to the contralateral side of the brain (Diagram adopted from Pritchard and Norgren, 2004).

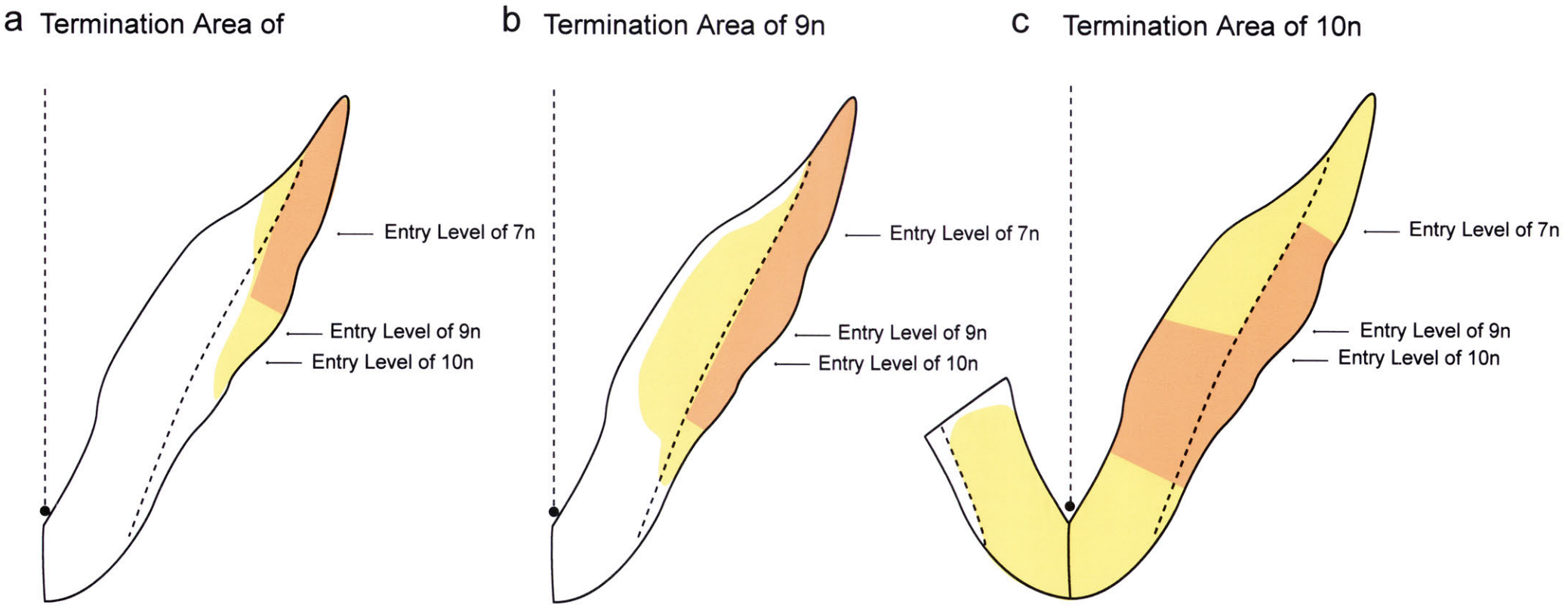
a Termination Area of
Entry Level of 7n
Entry Level of 9n
Entry Level of 10n
b Termination Area of 9n
Entry Level of 7n
Entry Level of 9n
Entry Level of 10n
c Termination Area of 10n
Entry Level of 7n
Entry Level of 9n
Entry Level of 10n

Figure 1.2

Chapter 2 Material and Methods

2.1 Brain Specimen Collection and Preparation

All the embryonic and fetal human brain tissue used in the current experiments was obtained from the Wenzhou Medical College in the People's Republic of China, under Chinese law and conforming to the regulations of the NHMRC of Australia. The collection of brain tissue in the current research work was made with approval provided by the Human Ethics Committee of the University of New South Wales and conformed to the Helsinki Declaration on Human Experimentation (WMA, 1964). All specimens were obtained from voluntary terminations of pregnancy induced by mifepristone (Danco) and prostaglandins and a written informed consent had been signed by all donors. All embryos and fetuses were obtained from mothers who had not previously given birth. This ensured that none of the women donating fetal or embryonic material were having a termination because they had been coerced to confine themselves to one child.

Sixteen specimens ranging from 9 to 28 weeks were used for Nissl staining and immunohistochemical experiments. Specimens were examined at the following ages (numbers in parentheses indicate number of specimens at each age): 9W (1); 13W (2); 14W (1); 15W (2); 17W (2); 18W (1); 20W (1); 21W (2); 23W (1); 25W (1); 26W (1). Another 8 specimens were used for DiI studies. Specimens were obtained from the following ages: 8W (1); 9W (1); 13W(2); 20W (2); 24W(1); 27W(1). With five of these brains, ages were determined by measuring the head length and crown-rump length. The correspondence between age and head length and/or crown-rump length was determined from data published by (Forutan et al., 2001). Ages of the other brains were determined by elapsed time from the first day of the last menstrual period (LMP) under the

assumption that fertilization occurs 14 days after the LMP.

All specimens were normal human embryos and fetuses. All tissue was fixed by immersion in 4% paraformaldehyde in 0.1M phosphate buffer (pH 7.4) for periods of 6 months to 1 year before experiments. In the interests of brevity I have focused on key ages (9, 13, 15, 21, 25 weeks) and not all levels will be shown for each age.

For Nissl staining and immunohistochemistry, the brain tissue of 13 week or younger conceptuses was embedded in methacrylate and paraffin as a whole block, while for older ages only the brainstems were extracted for cryostat sectioning. The brainstems were dissected with the aid of a dissecting microscope. The anterior edge of the block was at the level of the cerebral peduncles and the posterior limit of the block edge was a few mm caudal to the spinomedullary junction. This block included the entire medulla, most of the pons and a short rostral portion of the spinal cord. The blocks for cryostat sectioning were then immersed in 4% paraformaldehyde overnight and transferred to 30% sucrose for 24 hours before cryostat sectioning. All the sections were in the coronal plane. The thickness of the methacrylate or paraffin embedded tissues was 10 μm; and that of cryostat sectioned tissue was 40 μm.

2.2 Immunohistochemistry

2.1.1 Tissue Treatment

Eight series of tissue was collected sequentially. One series was prepared for cresyl violet staining, while the others were prepared for calbindin (Cb), calretinin (Cr), tyrosine hydroxylase (TH), growth associated protein 43 (GAP-43), and substance P (SP)

immunohistochemical labeling, respectively. The remaining series was retained as a control and as a backup in case of mishaps during immunohistochemical processing.

The monoclonal antibody against Cb does not cross react with Cr or other known calcium-binding proteins and specifically stains the calcium-binding spot of calbindin D-28k in tetrapods (Celio, 1990; De Leon et al., 1994). The polyclonal antiserum against Cr does not cross-react with Cb in a wide range of mammals from mouse to human (Schwaller et al., 1993). The monoclonal antibody against TH is effective in a wide range of species because it recognizes an epitope in the mid-portion of the TH molecule where extensive species homology exists. It does not cross-react with mammalian dopamine-β-hydroxylase, phenylethanlolamine-N-methyltransferase or tryptophan hydroxylase using Western blot methods (*INCSTAR* product information sheet). GAP-43 is a protein expressed at elevated levels by developing or regenerating neurons during axon growth. While this neuron-specific membrane protein is a component of axonal growth cones, it is absent from dendritic growth cones. In adult brain, GAP-43 is found in high concentrations in presynaptic areas where memory formation is thought to occur, such as frontal cortex, limbic system and hippocampus. The monoclonal mouse anti-GAP-43 antibody is able to recognize the relevant epitope on the GAP-43 protein regardless of phosphorylation state. This antibody exhibits a wide inter-species crossreactivity (e.g. human, cat, rat; *Chemicon* product data sheet). The rabbit SP antibody is able to detect substance P protein in a wide variety species including human, rat and mouse (*Chemicon* product data sheet). Anti-Cb, Cr, TH and SP immunohistochemistry has been applied in studying the chemoarchitecture of the developing Sol in the rat (Zhang

and Ashwell, 2001b). Anti-Cb, TH and SP immunohistochemistry has also been shown to reveal the structure of the developing and adult 10N in various species (De Leon et al., 1994; Huang et al., 1993a; Huang et al., 1993b; Wang et al., 1993). Moderate to intense anti-GAP-43 immunoreactivity has been shown in the rat Sol (Kapfhammer and Schwab, 1994). GAP-43 mRNA has previously been detected in the 10N, although there was no report of immunoreactivity (Yao et al., 1993).

2.2.2 Antigen Retrieval

Due to the greater fragility of human embryonic and fetal brain tissue compared to adult brain (even when careful fixation and handling has been adhered to), all the sections were mounted directly onto glass slides. The prolonged exposure of the tissues to 4% paraformaldehyde for periods of 6-12 months before coming to Australia meant that appropriate pretreatment was necessary for successful immunohistochemistry.

For the current study, a simple antigen retrieval method was applied to improve the antibody binding efficiency. The glass slides with sections mounted were immersed in 0.1M citrate buffer with 0.1% Triton X and then placed in a microwave oven (*Samsung*, 1000W) for 1.5 minutes. Boiling of buffer was avoided by heating for only 5-10 seconds at a time. Sections were then allowed to cool to room temperature for 15-30 minutes. This treatment tended to re-expose antigen binding sites on the cell surface and make them ready for antibody binding.

2.2.3 Primary Antibody Bindings

Once sections had cooled in 0.1M citrate buffer they were rinsed with distilled water and immersed in 50% ethanol with 0.3% H_2O_2 for one hour to destroy endogenous peroxidase activity. After rinsing with 0.1M phosphate buffer saline (PBST, containing 1% Triton X-100), sections were immersed in 5% normal horse serum (*Sigma-Aldrich*) for 30 minutes to block non-specific antigens. Sections were then covered with primary antibody (dissolved in PBSTA, i.e., 0.1M phosphate-buffered saline containing 2% bovine serum albumin, *Sigma-Aldrich*, and 1% Triton-X100, see below). For each section, around 30 µl of solution was needed to cover the surface.

The concentration of various antibodies is empirical, conforming to either the data sheets provided by the supplier or to previous work done with the same product. Both mouse monoclonal anti-Cb and rabbit polyclonal anti-Cr antibodies were obtained from *Swiss Antibodies* (Cb, diluted 1:2000; Cr diluted 1:4000); mouse anti-TH antibody was obtained from *INCSTAR* (1:2000); mouse anti-GAP-43 monoclonal antibody was purchased from *Chemicon* (1:4000); finally, rabbit anti-substance P polyclonal antibody was obtained from *Chemicon* (1:4000).

Slides covered with antibody solution were incubated in a sealed moisturized plastic box for 14-16 hours (overnight) at room temperature on a horizontal rotator running at 30 rpm.

2.2.4 Visualization of Immunohistochemical Labeling

Slides were rinsed in PBST and species-specific secondary antibodies (anti-mouse,

Sigma-Aldrich or anti-rabbit, *Chemicon*) were applied to the sections, diluted 1:200 in PBSTA (2 hours at room temperature). Sections were incubated in extravidin peroxidase (*Sigma-Aldrich*, diluted at 1:500 in PBSTA) for 1 hour. The immunohistochemically labeled cells were visualized by using freshly prepared 0.5% 3,3'-diaminobenzidine (DAB, *Sigma-Aldrich*) with 0.05% H_2O_2 in 0.1M phosphate buffer saline (PBS). Negative control sections were processed in an identical fashion to the above except that the primary antibody was excluded. Positive controls were provided by processing older ages in parallel and under identical conditions to those applied to younger ages. This allowed me to ensure that identical processing techniques were applied and made consistent reaction times possible.

Selected sections of various staining procedures were photographed with the aid of a bright field camera (*Zeiss Axiophot*). Photos were stored in PSD format (*Adobe* Photoshop CS 8.0). Sections immunoreactive to CB, CR and TH were viewed at a magnification of x400, and positions of immunoreactive somata were plotted with the aid of the Magellan 5.4 program (Halasz and Martin, 1985). Maps of the human fetal medulla were exported to *Adobe* Illustrator CS 11.0 for grouping and labeling.

Values for soma diameters given in the results text were derived from measurements of 50 somata in each subnucleus.

2.3 DiI Tract Tracing Techniques

The carbocyanine dye (DiI) allows both antrograde and retrograde tracing of connections. While it is broadly applicable to tracing in embryonic and fetal nervous tissue,

its effectiveness will diminish at mylination progresses during postnatal life. This may be because the close contact between axon membrane and myelin wrappings produced by oligodendrocytes will absorb large amouts of dye and prevent diffusion along the axonal length. DiI has been used in some mature nervous systems, but the length of diffusion is considerably less than is possible for embryonic and fetal nervous tissues. The identification of cell bodies in retrograde labeling with this dye ensures that the entire length of this cylinder has been labeled. (Honig and Hume, 1989) For the specimens of 8 and 9 weeks, DiI (*Molecular Probes*) was inserted into the upper right superior mediastinum at approximately the level of the sternal angle, at a point where the vagus nerve passes the aortic arch. For older fetuses (13 to 27 weeks), DiI was inserted into vagal rootlets emerging from a shallow groove along the lateral rim of the right olive. It was not possible to obtain labeling in the brainstem after insertion into the cervical or thoracic vagus nerve in specimens older than 10 weeks because of the much greater distances over which the DiI must diffuse in those older fetuses. Care was taken to ensure that the DiI crystals were inserted into the same relative position on the side of the brainstem in fetuses of all ages. From mid-gestation the olive provided a clear external landmark for this purpose. At the earlier ages (13 weeks), an appropriate level for insertion could be determined by reference to the shape of the 4^{th} ventricle. DiI was inserted into the vagal rootlets at a rostrocaudal level from 2 mm rostral to 1 mm caudal to the obex. The tissue was then stored in the above fixative at 37°C for 6 to 8 weeks to allow diffusion of the dye to central structures. This time period was chosen because experience with carbocyanine dye tracing in my supervisors' laboratories have indicated that DiI diffusion

under this conditions is at a reliable rate of one millimeter per week. Longer periods of diffusion (e.g. 6 months) may actually confuse the picture by providing too bright an image and may lead to diffusion across tight junctions between neurons.

Tissue was subsequently embedded in 5% noble agar and sectioned coronally at a thickness of 150 μm with the aid of a vibratome (*Oxford Instruments*). Sections were mounted in buffer, coverslipped and scanned with the aid of an *Olympus* Confocal Microscope (LSM-GB200). Images were cropped with Adobe Photoshop 7.0 and labeled in Adobe Illustrator 10.0. Care was taken to ensure that similar levels were studied in all embryos and fetuses. Major landmarks which confirmed that the Sol and 10N were being studied at the same rostrocaudal level included the inferior olivary nuclear complex at mid-gestation and later and comparable levels relative to the fourth ventricle topography (i.e. 2 mm rostral to the obex extending caudally as far as 1 mm caudal to the obex) in 13 week specimens. Sections as far forward as the rostral medulla as well as sections caudal to the olive were also examined, but the analysis and the illustrations focused upon the level of the middle of the rostrocaudal extent of the olive.

Table 2.1 Dilution, Data of Specificity and Manufacturer of the Antibodies Used

Table 2.1

Antibody	Dilution	Comments from Manufacturers' Datasheets	Manufacturer
Anti-Cb	1:2000	Specifically stains the 45Ca-binding spot of Calbindin D-28K (MW 28'000, IEP 4.8) in a two dimensional gel	*Swiss Antibodies*
Anti-Cr	1:4000	Does not cross-react with calbindin D-28k or other known calcium binding proteins	*Swiss Antibodies*
Anti-TH	1:2000	Recognizes an epitope in the midportion of the TH molecule where extensive species homology exist. This antibody does not cross react with dihydropterdine reductase, dopamine-B-hydroxylase, phenylethanolamine-N-methyltransferase, phenylalanine hydroxylase or tryptophan hydroxylase using western blot methods.	*INCSTAR*
Anti-GAP-43	1:4000	Will detect single 48kD band in western blot	*Chemicon*
Anti-SP	1:4000	Binding detects at least 5pg/mL substance P	*Chemicon*

Chapter 3 Cyto- and Chemoarchitecture of the Developing Human Solitary Nucleus

3.1 Introduction

The cyto- and chemoarchitecture of the adult human solitary nucleus (Sol) has been well studied (Hyde and Miselis, 1992; Koutcherov et al., 2004; McRitchie and Tork, 1993; McRitchie and Tork, 1994; Paxinos and Huang, 1995), but the early development of this important autonomic centre has received relatively little attention.

Distribution of substance P immunoreactive (SP-ir) fibers and terminals has been reported in Sol of newborn infants (Rikard-Bell et al., 1990) and of 16 weeks fetuses (Wang et al., 1993), but nothing else is known about the prenatal development of the subnuclear organization or chemoarchitecture of the human Sol.

Since the Sol plays a major role in receiving sensory information from thoracic and abdominal visceral organs (Lundy and Norgren, 2004; Pritchard and Norgren, 2004; Tork et al., 1990; Whitehead, 1988; Whitehead, 1990), and dramatic changes in cardiorespiratory and gastrointestinal functions occur during early human development, the fetal development of Sol deserves more attention. For example, Bodegard et al. (Bodegard et al., 1969) have reported that the Hering-Breuer inspiration-inhibiting reflex is weak in infants for 32 weeks, but increases in strength until 38 weeks. It is at present unknown whether this functional change is due to maturation of the vagus nerve (10n), central vagal connections or neuronal elements within the brainstem. Therefore, a study of the more detailed cytoarchitecture and chemical features of Sol in early fetal life is of value in determining the time-course of maturation of vagal reflex circuitry.

The current study aims to investigate the cyto- and chemoarchitecture of the Sol during early to mid-gestational fetal life (i.e., 9, 13, 15, 21 and 25 weeks of development)

by using Nissl staining, and calbindin (Cb), calretinin (Cr), tyrosine hydroxylase (TH), SP and GAP-43 immunohistochemistry. These markers have been chosen because they identify chemically distinct cell groups in the vagal sensory motor complex (Cb, Cr, TH - (De Leon et al., 1994; Huang et al., 1993a; Huang et al., 1993b; Wang et al., 1993; Zhang and Ashwell, 2001b) or reveal the maturational state of neuropil and afferents (GAP-43 - (Hassiotis et al., 2002; Jacobson et al., 1986; Karns et al., 1987; Meiri et al., 1986) and are applicable to human fetal postmortem material. The ages chosen for detailed study of cyto- and chemoarchitectonic, cover the period between neurogenesis and apparent cytoarchitectural maturity. The actual function of CB immunoreactivity in Sol is not certain, although it has been reported that Sol CB-ir neurons are responsible for transmitting sensory data from gustatory, cardiovascular, gastrointestinal and respiratory systems to higher integration centres such as the parabrachial area of the pons (Menetrey et al., 1992). According to Arai et al. (1991), CR-ir neurons in Sol could possibly be utilizing excitatory amino acid neurotransmitters such as glutamate. Therefore, abundance of CR-ir neurons in various subnuclei in developing human Sol might be of significance for the physiological maturation of the excitatory viscerosensory pathway. Most TH-ir neurons were located, has been reported to contain mainly noradrenergic neurons which appear to be strongly involved in esophageal-gastric reflexes (Gai and Blessing et al., 1996; Rogers, et al. 2003). GAP-43 (also termed GAP-48, B-50, F1 or pp46) is a phosphoprotein of the presynaptic membrane that is associated with the initial establishment, regeneration and functional modulation of synaptic contacts (Neve et al., 1988; Kinney et al, 1993).

In developing neurons which undergo remodeling of axonal connections, GAP-43 is expressed at high levels and transported to growth cones and immature synapses (Neve et al., 1988; Kinney et al, 1993). The receptor for SP (neurokinin 1 receptor, NK1) found on 10N neurons, plays an important role in reducing gastric motility and evoking gastric relaxation (Krowicki and Hornby, 1996; Krowicki and Hornby, 2000) and is the major factor in controlling major types of vomiting (Saito et al., 2003). Therefore, emergence of SP-ir neurons in 10N at mid-gestation in the present study may be suggestive of early establishment of a controlling mechanism on gastrointestinal motility during fetal life. It is intended that, on the basis of this study, a clearer picture of the development of Sol and its subnuclear organization will be drawn and the structural basis of maturation of central visceral sensory function can be established.

3.2 Results

3.2.1 Cytoarchitectonic Organization of the Developing Human Solitary Nucleus

The solitary nucleus is a longitudinal bilateral nucleus extending rostrocaudally throughout almost the entire medulla. To facilitate and standardize description of its developing cytoarchitecture, the nucleus was examined at three levels of its rostrocaudal extent. These levels were: a) open medulla at the rostral limit of the hypoglossal nucleus (12N), b) level of area postrema at the rostral limit of the gracile nucleus, and c) closed medulla caudal to the obex. These were comparable to Figures 1.1d, 1.1f and 1.1h, respectively.

Figure 3.1 illustrates the cytoarchitectonic organization of the Sol at 9 weeks

development. By the 9th week, postmitotic neurons have accumulated in the mantle layer of the developing medulla in 12N and the dorsal motor nucleus of vagus (10N). While the territory of Sol was present, a differentiated Sol was not yet visible (Fig. 3.1a). At high power (Fig. 3.1b and c), the cells in this region were seen to be very densely packed and darkly stained. The post-mitotic cells were small (4-5μm diameter), palely stained in the center and spindle-shaped.

Figure 3.2 shows photomicrographs of Nissl stained sections at 13 weeks of development. At the level of open medulla (Fig. 3.2a), the nucleus was identified as densely packed cells with small somata surrounding the solitary tract (sol). It was not possible at this age to discern subnuclei within Sol, but it was noticeable that two densely packed and one sparsely packed neuronal compartments had already appeared. The cell sparse compartment dorsomedial to sol was tentatively identified as the medial subnucleus (SolM) (Fig. 3.3a). Inserted between the SolM and sol was a compartment of densely packed cells, which was noted to have a close relationship to 10N on its medial side. This was tentatively identified as the combination of the intermediate subnucleus (SolIM) and ventral subnucleus (SolV) (Fig. 3.3b), whereas the dense compartment ventrolateral to the sol was identified as an immature ventrolateral subnucleus (SolVL) (Fig. 3.3c). Further caudally (Fig. 3.2b), sol was visible but with poorly defined boundaries to its lateral and ventral sides. This made it difficult to determine whether the densely packed cluster of cells ventral and lateral to the sol was the early interstitial subnucleus (SolI) or the caudal extension of SolVL as identified at the more rostral level (Fig. 3.2a). SolIM and SolV continued to appear as densely packed cells surrounding the better defined dorsomedial

border of sol. SolM contained higher cell density compared to more rostral levels (Fig. 3.2a). It was noticed that ventral to the area postrema, there was a region of high density of cells, which may represent the developing gelatinosus subnucleus (SolG) (Fig. 3.3d). At the caudal level (Fig. 3.2c), the two subnuclei seen in the adult Sol at this region, i.e., the commissural (SolC) and paracommissural (SolPa) were poorly differentiated, and appeared as a group of cells with moderately high density. At high power, cells at the dorsolateral portion of this region, which were considered to be cells of the future SolPa, appeared to be of spherical or oval shape, with 5-7 μm diameter (Fig. 3.3e), while cells at the ventromedial portion, which were considered to be of SolC, appeared to be oval or spindle shaped (Fig. 3.3f) and had their long axes arranged in a dorsomedial to ventrolateral orientation (indicated by arrows). Even though the various compartments, or more accurately, the immature subnuclei of Sol, have emerged at 13 weeks, the neuronal morphology of Sol was still quite immature. Neurons of the different subnuclei were of very similar shape: round, oval or spindle, and of small size (5-8 μm diameter, Fig. 3.3).

Photomicrographs of Nissl stained preparations of 15 weeks are shown in Figure 3.4. In contrast to the appearance at 13 weeks, subdivisions of Sol were seen to be more clearly defined. At the level of open medulla (Fig. 3.4 a), the Sol was still divisible into broad dorsomedial and a ventrolateral compartments. However, the dorsomedial compartment was now much better differentiated, with several subnuclei having emerged. Immediately dorsomedial to sol, SolV could be distinguished as a crescent shaped cell group containing oval or spindle shaped, small to moderate sized neurons (9-15 μm long axis diameter, Fig. 3.5a). It was noted that in this subnucleus, the long axes of the spindle

or oval shaped neurons were orientated parallel to the boundary of sol. Located further dorsally and medially, the SolM appeared as a large area of neurons with moderate density (Fig. 3.5b). Ventral to the SolM and immediately between the 10N and sol, SolIM had slightly higher neuronal density than SolM and a much lower density than the nearby SolV (Fig. 3.5c). At the dorsalmost area of the Sol, there was a very condensed neuronal group, which was not seen in the previous age. Neurons of this subnucleus were round, small (5-7 μm) and darkly stained (Fig. 3.5d). This was tentatively identified as the dorsal subnucleus (SolD). Dorsal to the SolD, the parasolitary nucleus (PSol) appeared as a cellular group of very high density. At the level of the area postrema (Fig. 3.4b), a more demarcated subnuclear pattern was found compared with the previous age. Ventrolateral to sol, SolVL became much smaller than it was at the more rostral levels, indicating the progressive reduction in size of the subnucleus as it courses caudally. High power showed that neurons of SolVL were medium to large size (14-20 μm diameter) and spindle shaped with the long axis parallel to the boundary of sol (Fig. 3.5e). SolV continued to be visible as a crescent shaped cellular condensation surrounding the medial border of sol. SolD, which was substantial at the open medulla level, had disappeared by this level. SolIM, SolM and SolDL (high power image of SolDL in Fig. 3.5f) appeared as neuronal groups of lower density than surrounding regions. SolG featured very high cellular density and was located most dorsally, immediately ventral to the area postrema. Neurons of this subnucleus were found to be medium sized (9-11 μm diameter) and darkly stained, with a few small putative glial cells (5 μm diameter, Fig. 3.5g). Located in the ventrolateral side of sol, SolI was now clearly identified as a compacted group of small to medium sized (7-11

μm diameter) cells (Fig. 3.5h). At the caudal level (Fig. 3.4c), SolC was still not very well differentiated from the nearby SolPa, since both SolPa and SolC appeared to contain cellular groups of moderate density. Neurons within SolC were of oval to spindle shape (Fig. 3.5i), while the neurons of SolPa were mainly of spherical shape (Fig. 3.5j). By 15 weeks of development, although subnuclei began to appear, cytoarchitecture of Sol as a whole was still at a very early stage and neuronal density remained high and subnuclei compact (Fig. 3.5).

At 21 weeks of development, the subnuclear pattern of Sol was approaching the adult appearance (Fig. 3.6). Fig. 3.6a shows low power photomicrographs and schematic diagrams of the Sol at the open medulla level. At this level, the SolVL, SolIM, SolM, SolV, SolDL and SolD (high power images of each subnucleus in Fig. 3.7a-f), which had all been seen at earlier ages, were clearly visible as differentiated subnuclei with differing cellular densities. SolI, which had been found at a more caudal level at the previous age, was also identified at this level. Most of the cells of SolI were small and spherical (5-9 μm diameter), while some neurons were comparatively larger and elongated (11-13 μm diameter, Fig. 3.7g). At the level of area postrema level (Fig. 3.6b), SolG became prominent in the dorsal part of Sol, immediately ventral to the the area postrema (Fig. 3.7h). SolI was now visible as a very distinct cluster of neurons in the ventrolateral quadrant of sol. At the caudal level (Fig. 3.6c), SolC, which had been difficult to differentiate from SolPa at earlier ages, appeared to be well demarcated at this age. It was composed of a cellular group with moderately low density. Neurons within this subnucleus were of medium size (10-12 μm diameter) and spindle shaped with their long

axis orientated dorsomedial to ventrolateral (Fig. 3.7i). On the other hand, SolPa contained relatively densely packed cells (Fig. 3.7j). In summary, at 21 weeks of development, the various subnuclei of Sol were all visible. Neurons were not as densely packed as was seen at the previous ages, with more putative glial cells (as indicated by arrows in various photomicrographs in Fig. 3.7) appearing between the neurons.

At 25 weeks of development, as is shown in Fig. 3.8, the subnuclear pattern as revealed by low power photomicrographs had changed little compared to 21 weeks and was similar to the adult structure (Paxinos and Huang, 1995). In higher power photomicrographs, SolVL was seen to contain a few large neurons (15-20 μm diameter; Fig. 3.9a), whereas neurons in the other subnuclei were smaller than those in SolVL (Fig. 3.9b-j). In particular neurons in SolDL and SolI were very small (somata diameter <10 μm, Fig. 3.9e, g).

3.2.2 Chemoarchitecture of the Developing Sol

Table 3.1 shows a summary of immunoreactivity in Sol and 10N throughout development.

A. Calbindin Immunoreactivity

Figure 3.10 illustrates the distribution of cells immunoreactive for Cb (Cb-ir) in the developing Sol at 13, 15, 21 and 25 weeks, while Figure 3.11 shows high power photomicrographs of Cb-ir cells in Sol at these ages. At 13 weeks, the rostral level of Sol contained few Cb-ir neurons. The most striking feature of Cb immunoreactivity in the Sol was the presence, even at this young age, of a cluster of Cb-ir neurons in the developing

SolG at the level of the area postrema (Fig. 3.10b). There were also scattered neurons in SolM throughout the rostro-caudal extent of the nucleus and labelled neurons were present in the SolC at the most caudal levels. As can be seen in high power figures, Cb-ir neurons in the SolG had spherical somata about 5-6 μm diameter with no dendritic processes (Fig. 3.11a). The scattered neurons in the SolM and SolC were also spherical. Neurons of SolM were small (3-4 μm diameter) and of low Cb immunoreactivity (Fig. 3.11b), while neurons in SolC were slightly larger (6-9 μm diameter, Fig. 3.11c). Except for a few weakly labelled dendritic process found on the cells of SolC, only weak neuropil immunoreactivity was present at this age.

At 15 weeks (Fig. 3.10d-f), the rostral level of Sol continued to show very little Cb immunoreactivity, with only a few round neurons seen in the SolM. Neurons of the SolM were larger than those at 13 weeks, but remain palely stained and without labelled dendrites (Fig. 3.11d). Close to SolM, some Cb-ir neurons were seen located in SolD with a similar appearance as those in SolM (Fig. 3.11e). At the level of area postrema (Fig. 3.10e), a cluster of Cb-ir neurons was visible in SolV (Fig. 3.11f). The morphological features of the labelled neurons in SolV were similar to those seen in SolM, but more densely packed. Scattered Cb-ir neurons were also visible in the area of SolIM (Fig. 3.11g). The field of immunoreactive neurons in SolG was now more dispersed and extensive, leading up to the border with the area postrema. Neurons of SolG were larger (6-9 μm diameter, Fig. 3.11h) compared to those of 13 weeks. Some neurons continued to be spherical with no dendritic processes, whereas others had became polarized and displayed growing processes with labelled dendrites about 15-20 μm long (Fig. 3.11h). By 15 weeks,

there was Cb immunoreactivity in the neuropil of SolG (Fig. 3.11h). The caudal parts of Sol had very few Cb-ir neurons at this age (Fig. 3.10f).

By 21 weeks (Fig. 3.10g-i), more Cb-ir neurons appeared in SolM and SolD at the open medulla level (Fig. 3.10g). Cb-ir neurons in SolM were seen displaying primary dendrites of about 40-50 μm length (Fig. 3.11i). At the level of the area postrema, SolG continued to be the structure with the highest density of Cb-ir neurons (Fig. 3.10h). At this age, Cb-ir neurons were no longer round or oval shaped, but had taken on a spindle or trigonal shape (Fig. 3.11j). Neurons were slightly larger than those at 15 weeks (10-13 μm diameter) and the dendrites extended to about 30-40μm in length. More Cb-ir neurons were apparent at the caudal parts of Sol at this age, especially in the SolC area (Fig. 3.10i). Primary dendrites about 25-40 μm long were seen in Cb-ir neuron of SolC (Fig. 3.11k).

Figures 3.10j-l show the distribution of Cb-ir neurons in the Sol at 25 weeks. At this age, at the level of the open medulla (Fig. 3.10j), SolM contained more Cb-ir neurons than at 21 weeks and these neurons were of multipolar and bipolar shape (Fig. 3.11l). Only very few neurons were found in sol at the rostral level (Fig. 3.10j), in contrast to sol at more caudal levels (Fig. 3.10k), where many Cb-ir neurons were concentrated in the ventrolateral quadrant where SolI was located. Although cells within SolI had palely stained small somata (5-7 μm diameter), these, nevertheless, were the first Cb-ir neurons seen in SolI (Fig. 3.11m). At the level of area postrema (Fig. 3.10k), SolG continued to be a region with strong Cb immunoreactivity, where neurons were large (15-20 μm diameter long axis) and of monopolar, bipolar or multipolar morphologies (Fig. 3.11n). At the

more caudal level (Fig. 3.10l), Cb-ir neurons were found both in SolPa and SolC.

B. Calretinin Immunoreactivity

Line diagrams showing the distribution of Cr immunoreactive (Cr-ir) somata in Sol are shown in Figure 3.12, while photomicrographs of Cr-ir neurons are shown in Figure 3.13. At 13 weeks, immunoreactivity for Cr was present in scattered neurons throughout SolM, SolV, SolDL, SolVL and SolIM at the level of open medulla (Fig. 3.12a). Somata in those subnuclei were spherical in morphology and of small size (7-9 μm average diameter, Fig. 3.13a-e). It was noteworthy that SolM was composed of two distinct regions with a difference in Cr immunoreactivity: the ventromedial part of the SolM contained a cluster of Cr-ir neurons, while the dorsolateral portion of this nucleus was almost devoid of Cr-ir neurons. Cells of some subnuclei, e.g., SolIM, SolVLand SolV (Fig. 3.13c-e respectively), had visible dendritic processes (15-20 μm long), while those within other subnuclei, e.g., SolM and SolDL, had very few Cr-ir processes (Fig. 3.13 a, b). At the level of area postrema (Fig. 3.12b), Cr-ir neurons were concentrated in the area ventrolateral to sol, i.e., SolVL and part of SolIM, leaving the area dorsomedial to sol almost blank. There were also a few somata found in sol, but these neurons were unclustered and it was difficult to determine whether they belong to SolI. At the caudal level (Fig. 3.12c), only a few scattered neurons were found in the SolC. Cr-ir somata of SolC were spherical and of small size (about 5-7 μm diameter), but also contained labelling of a few dendritic processes (10-15 μm long, Fig. 3.13f).

At 15 weeks (Fig. 3.12d-f), distribution of Cr-ir somata was similar to that of the

previous age. At the level of open medulla (Fig. 3.12d), SolM continued to have two distinct regions on the basis of Cr immunoreactivity. The dorsolateral part, which did not contain Cr-ir somata, was strongly Cr-ir in neuropil (not shown); while the ventromedial part of SolM, together with more caudally localized SolV, contained a field of strongly Cr-ir somata with only moderate intensity of neuropil. Neurons in SolM were no longer spherical, but appeared to be oval or spindle shaped, and had dendritic process up to 40 μm long (Fig. 3.13g and h). Also at this level, SolD began to show a cluster of small Cr-ir neurons (Fig. 3.13i). At the level of area postrema (Fig. 3.12e), although the region ventrolateral to sol (SolVL) continued to have higher density of Cr-ir neurons (Fig. 3.13j), the dorsomedial region (mainly SolM and SolV) which was devoid of Cr-ir somata at previous ages (Fig. 3.12b) began to acquire a few Cr-ir cells. At this age, distribution of Cr-ir somata at the caudal level appeared to be similar to the previous ages (Fig. 3.12f), but cells of SolC and SolPa were larger (15-18 μm diameter) and oval shaped (Fig. 3.13k, l).

The distribution of Cr-ir neurons in Sol at 21 weeks is shown in Figures 3.12g-i. This was found to be broadly similar to the previous ages. At high power, SolD was seen to have small (8-10 μm diameter) round neurons (Fig. 3.13m), while neurons of SolIM were trigonal with multiple dendritic processes (Fig. 3.13 n). SolVL continued to have densely packed Cr-ir neurons. The somata of these cells were large (18-20 μm diameter of long axis) and spindle shaped. The long axes of the somata were parallel to the border of sol (Fig. 3.13o). Neurons of other subnuclei, i.e, SolM, SolV, SolC and SolPa, appeared to be similar to previous ages (not shown).

By 25 weeks (Fig. 3.12j-l), many more Cr-ir neurons were present in Sol compared to

previous ages. At the rostral level, more neurons appeared to be Cr-ir in SolV, SolIM and the ventral part of SolM, while the dorsal part of SolM continued to be devoid of any Cr-ir somata, but had strong neuropil immunoreactivity (not shown). It was difficult to differentiate SolV from the nearby SolM and SolIM if merely judging by their cellular distribution, but can be delineated on the basis of the neuronal morphology. Neurons in SolV were small (5-7 μm diameter) and spherical with no dendritic process (Fig. 3.13p), this can be contrasted by neurons of SolM and SolIM, which appeared to contain large (13-18 μm diameter) spindle shaped and trigonal cells with dendritic processes up to 60μm long (Fig. 3.13 q, r). The lateral subnuclei (SolVL and SolDL) contained densely packed Cr-ir cells with large cell bodies (15-20 μm diameter) with multiple dendritic processes. In addition, the boundary of SolG could be clearly distinguished because it appeared to be a cell-free area surrounded by structures having clusters of Cr-ir neurons (Fig. 3.12k). At caudal levels (Fig. 3.12k and l), more Cr-ir neurons had appeared in the SolC and SolPa. The morphology of Cr-ir neurons in SolC and SolPa appeared to be similar. A higher power photomicrograph of Cr-ir neurons in SolC is shown in Figure 3.13u.

C. Tyrosine Hydroxylase Immunoreactivity

The distribution of TH immunoreactive (TH-ir) perikarya in Sol is illustrated in Figure 3.14, while photomicrographs of TH-ir neurons of Sol subnuclei are shown in Figure 3.15. At 13 weeks, sparsely distributed TH-ir neurons were found in SolV, SolM and SolIM at the level the of open medulla (Fig. 3.14a). At the level of the area postrema

(Fig. 3.14b), TH-ir neurons were concentrated mainly in the medial portion of Sol, i.e., SolG, SolM and SolIM. At the caudal level (Fig. 3.14c), a few TH-ir neurons were found to be spread over SolC. At this age, TH-ir neurons in Sol appeared to have small to medium sized somata (10-13 μm diameter) of bipolar or multipolar morphology with dendritic processes of about 15-20 μm long (Fig. 3.15 a-d).

At 15 weeks, distribution of TH-ir neurons in the Sol was largely similar to that of the previous age (Fig. 3.14d-f), but with the exception that the area lateral to sol, i.e., SolVL and SolDL, which did not contain TH-ir neurons at 13 weeks (Fig. 3.14a), now contained clusters of TH-ir neurons. At this age, TH-ir neurons in SolVL SolIM, SolV, SolM and SolDL had large somata (15-20 μm diameter) and dendritic process up to 70 μm in length (Fig. 3.15 e-i), while neurons of SolG and SolC had relatively smaller (10-15 μm) oval or trigonal neurons (Fig. 3.15j, k). A high density of TH-ir dendrites was also seen in SolG (Fig. 3.15j).

The distribution and morphology of TH-ir neurons at 21 and 25 weeks was similar to that seen in the earlier ages (Fig. 3.14g-l; Fig. 3.15l-s), but it is noteworthy that at 25 weeks, SolG contained a very dense cluster of small to medium sized TH-ir neurons (10-13 μm diameter) along with high neuropil density, which made it a very striking feature in the caudal medulla at the level of area postrema (Fig. 3.15p). Compared to previous weeks, neurons of SolDL and SolVL were relatively larger (20-25 μm diameter, Fig. 3.15q, r), and dendritic fields of TH-ir neurons now extended for up to 200 μm from the somata (not shown).

D. GAP-43 and Substance P Immunoreactivity

Figure 3.16 shows photomicrographs of GAP-43 immunoreactivity at 13 weeks (Fig. 3.16a-c) and 21 weeks (Fig. 3.16d-f). At 13 weeks, sol was seen as a distinctive fiber bundle with strong GAP-43 immunoreactivity, and the regions surrounding it also showed medium to high immunoreactivity. Among them, SolM, SolV and SolVL showed medium immunoreactivity, while SolDL, which was a cell-sparse area in Nissl preparations, showed a high density of GAP-43 immunoreactivity (Fig. 3.16a). At the level of the area postrema (Fig. 3.16b), the dorsomedial regions of Sol, i.e., SolM, SolV, SolG showed medium density of GAP-43 immunoreactivity, which made those subnuclei difficult to differentiate. On the other hand, SolVL and SolIM continued to contain lower immunoreactivity as seen at the previous level. At the caudal level (Fig. 3.16c), SolPa and SolC, which were not discernable in Nissl stained preparation, could be demarcated from each other by the fact that SolPa had slightly higher GAP-43 immunoreactivity than SolC. By 21 weeks, there had clearly been a substantial decline of GAP-43 immunoreactivity in general (Fig. 3.16d-f), but sol was still quite strongly immunoreactive. There was no differential staining of subnuclei of Sol with GAP-43 at the level of the open medulla (Fig. 3.16d). At the level of the area postrema, SolG and SolV had moderately high GAP-43 immunoreactivity (Fig. 3.16e). At the caudal level, SolPa had stronger GAP-43 immunoreactivity than SolC, similar to that seen at 13 weeks (Fig. 3.16f).

Immunoreactivity for SP was very difficult to obtain in the human material due to problems with antigen retrieval and antibody sensitivity. For this reason, only a 21 week specimen has been illustrated (Fig. 3.17). At the rostral level (Fig. 3.16a), medium intensity

of SP immunoreactivity was mainly found in SolM and SolIM, and strong SP immunoreactivity was found in fibers but not neurons in SolI and SolD (Fig. 3.17d, e). It was noted that SolI at this level was not identifiable in Nissl preparation, but could be identified by SP immunohistochemstry. At the level of the area postrema (Fig. 3.16b), immunoreactivity was quite weak, but SolV, SolM and SolDL showed moderate immunoreactivity. At the caudal level (Fig. 3.16c), SolPa had comparatively higher immunoreactivity than SolC (Fig. 3.16f).

3.3 Discussion

3.3.1 Name of the Game: Nomenclature of Sol Subnuclei

There is some disagreement concerning the subdivisional pattern of Sol across mammalian species, and even within one species (Schwarzacher, 2002) and this is seen in humans as much as any other species. Nageotte (Nageotte, 1906) used the term "*gustatory nucleus*" instead of Sol and divided it into the superior and inferior portions. In the inferior portion he identified the *nucleus gelatinosus* and the *commissural nucleus of Cajal.* Subsequently, Olszewski and Baxter (Olszewski and Baxter, 1954) outlined the entire Sol but only identified the commissural and gelatinosus subnuclei. A more detailed investigation of Sol has been presented by Braak (Braak, 1972), in which he applied the term *glossopharyngeal-vagus-complex* (ala cinerea) and considered Sol to be a relatively small component of this complex, basically as two subnuclei immediately dorsomedial and ventrolateral to the solitary tract, with the rest of what we have considered to be Sol designated as parts of the ala cinerea.

Recent studies of the cytoarchitecture of human Sol have provided a more detailed schema of subdivision in this nucleus. Hyde and Miselis (Hyde and Miselis, 1992) identified 10 subnuclei in the caudal Sol. They defined SolC as being the only subnucleus below the obex and other subnuclei being above the obex. Within the pre-obex subnuclei, they identified SolV as the *ventromedial* subnucleus and inserted the *subpostrema* subnucleus between the area postrema and SolG. Moreover, in their study, *SolD* was considered to be a more extensive area including what was designated SolD and SolDL in my study. SolG, which they called the *substantia gelatinosus*, was regarded as a cell sparse area and SolI was further divided into the *lateral* and *interstitial* subnuclei at caudal levels.

Relying on AChE histochemical and substance P immunohistochemical techniques, McRitchie and Tork (McRitchie and Tork, 1993; McRitchie and Tork, 1994) have also identified 10 subnuclei in adult human Sol. In that way, they separated a SolPa from the caudally located SolC, and defined SolD as a subnucleus with short rostro-caudal extent and intense AChE reactivity. Such a divisional schema was adopted by Paxinos and Huang (Paxinos and Huang, 1995).

The present study has used the nomenclature of Paxinos and Huang (Paxinos and Huang, 1995) and set out to study systematically the development of human Sol. During fetal life, Sol can be considered as a dynamic structure with evolving complexity, rather than a fixed structure with stable topography. Therefore, although the names of each subnucleus used in the present study are adopted from those applied in the adult, some fluidity of boundaries is to be expected.

3.3.2 Development of Cytoarchitecture of the Subnuclei of the Human Solitary Nucleus

Subnuclear development of Sol has been investigated in other species. Altman and Bayer, (1980) showed that neurons destined for Sol in the rat are generated between E11 and E14, with peak neurogenesis on E12. Zhang and Ashwell (Zhang and Ashwell, 2001b) reported that a rapid and profound change of differentiation of Sol in the rat occurred between E17 and E19, with most subnuclear features being present at E19.

Humans have a longer gestational period than rodents and the developmental process is expected to be prolonged and perhaps more complicated than that of rats. Neuronal multiplication giving rise to Sol probably occurs at stage 19 or slightly earlier (6-7 weeks) (Muller and O'Rahilly, 2004), after which time no new nerve cells appear to be generated, though neuronal arborization and the formation and re-organisation of synapses most likely continues until late gestation.

Nine weeks of development was the earliest age investigated in the present study. No subnuclei were discernable at this age. The cytoarchitectonic appearance of Sol at that age is similar to that seen in the rat between E15 and E17 (Zhang and Ashwell, 2001b). Profound changes in cytoarchitecture occurred between 9 and 13 weeks, at the end of which Sol was noticeably heterogeneous. In our study, SolM, SolV, SolIM, SolVL were among the earliest subnuclei to be clearly differentiated, although SolV and SolIM did not have a clear boundary between each other and appeared as one compact cell cluster dorsomedial to sol. Other subnuclei, e.g., SolG and SolDL could not be identified at this age. At the caudal level at 13 weeks, although there were densely packed cells dorsomedial to sol, the two subnuclei located in this area in the adult, i.e. SolPa and SolC (McRitchie

and Tork, 1993; Paxinos and Huang, 1995), were not discernable. From the cytoarchitecture of human Sol at 13 weeks, this age could be tentatively correlated to rodent Sol at between E17 and E19 (Zhang and Ashwell, 2001b).

The period between 13 and 15 weeks represented another significant shift in human Sol development. By 15 weeks, more subnuclei were discernable, although the general cytoarchitecture of Sol continued to be densely packed. SolD for the first time could be identified dorsal to SolV and the boundary between SolV and SolIM became clear. SolG continued to be difficult to discern, but a dense cell group between the area postrema and SolM hints at its site of development.

Development of cytoarchitecture of Sol slowed after 15 weeks, thus there was little difference in the subnuclear pattern at 21 weeks compared with that at 15 weeks, although more neuropil has formed between 15 and 21 weeks, thereby reducing the neuronal density. The only significant difference between 15 and 21 weeks was probably at the caudal level, where the two subnuclei, SolC and SolPa, could be easily differentiated for the first time.

Cytoarchitecture of fetal Sol at 25 weeks is very similar to that of the adult human (McRitchie and Tork, 1993; Paxinos and Huang, 1995), with all subnuclei that were described in the adult having been identified. A noticeable difference of cytoarchitecture between 21 and 25 weeks was SolG. At 25 weeks, SolG was as clearly present as seen in the adult, where it is described as being conspicuously cell poor and palely stained (McRitchie and Tork, 1993). It is possible that the neurons of SolG have either not been generated at 21 weeks or that the compact cell mass ventral to the area postrema is

actually an underdeveloped SolG. Since Altman and Bayer (Altman and Bayer, 1980) have not found any evidence for SolG neurons being generated from the ventricular germinal zone significantly later than any other subnuclei of the rat Sol, it is unlikely that human SolG neurons have delayed birthdates either.

In conclusion, development of the cytoarchitecture of human fetal Sol can be correlated with that of rats (Zhang and Ashwell, 2001b), but has a more prolonged progress. It is noteworthy that human Sol completed its subnuclear differentiation by the beginning of the second trimester. The significance of this for the functional maturation of central vagal regulation is to be discussed below.

3.3.4 Development of Chemoarchitecture of the Human Solitary Nucleus

Both Cb and Cr belong to the large family of EF-hand calcium-binding proteins, which comprises more than 200 members in the human brain (Schwaller et al., 2002). Functionally, the two proteins are involved in regulating calcium pools critical for synaptic plasticity (Schwaller et al., 2002). Distribution of Cb-ir neurons in Sol has been revealed in several species (De Leon et al., 1994; Menetrey et al., 1992; Zhang and Ashwell, 2001b). In the present study, perikarya of Cb-ir neurons appeared in human Sol quite early (at 13 weeks). Neurons immunoreactive to Cb firstly appeared in the medial gastrointestinal area, i.e., SolM, SolC and presumptive SolG, and as the fetus grew, other subnuclei, i.e., SolD, SolV, SolIM, SolVL, SolDL and SolPa were also found to contain Cb-ir neurons. The distribution of Cb-ir neurons in human fetal Sol was similar to that which has been reported in the rat (Zhang and Ashwell, 2001b). The actual function of Cb

immunoreactivity in Sol is not certain, although it has been reported that Sol Cb-ir neurons are responsible for transmitting sensory data from gustatory, cardiovascular, gastrointestinal and respiratory systems to higher integration centres such as the parabrachial area of the pons (Menetrey et al., 1992). A recent study revealed that Cb-ir neurons in the paratrigeminal nucleus of the rat receive nociceptive information from orofacial and visceral organs and have projections to Sol (Ma et al., 2005). Early development of Cb-ir neurons in Sol and increasing numbers of these neurons may suggest that Sol is involved in the wide range of viscerosensory relay functions as early as the second trimester.

Information about the role of Cr immunoreactivity in the adult Sol is relatively scarce, which is surprising in view of the large numbers of Cr-ir neurons found in the adult Sol. A previous report in the developing rat showed that Sol contains Cr-ir neurons as early as E15 and that these are abundant at E17, especially in SolI (Zhang and Ashwell, 2001b). In the adult rat, Arai et al. (Arai et al., 1991) reported abundant Cr-ir neurons and strong neuropil immunoreactivity in medial parts of Sol, whereas only a few Cr-ir neurons were identified in the lateral portion of the nucleus. However, in the present study, such a pattern could not be discerned, since there were also many Cr-ir neurons lateral to sol. On the other hand, SolM at the open medulla level was not homogeneous with respect to Cr immunoreactivity, with the ventromedial part containing quite a few Cr-ir neurons and the dorsolateral part containing more intensive neuropil, but no neurons. This was not reported by other investigators and the significance of this finding remains unclear. It could be that either there is another subnucleus, such as the central subnucleus (Gai and

Blessing, 1996) mixing with SolM, or SolM itself might be heterogeneous with various functions. It should be noted that the significance of Cr immunoreactivity in Sol is also unknown. According to Arai et al. (Arai et al., 1991), Cr-ir neurons in Sol could possibly be utilizing excitatory amino acid neurotransmitters such as glutamate. Therefore, abundance of Cr-ir neurons in various subnuclei in developing human Sol might be of significance for the physiological maturation of the excitatory viscerosensory pathway.

Neurons expressing catecholamines in developing Sol were identified in the present study by TH immunohistochemistry. As early as 13 weeks, there were TH-ir neurons in the medial subdivisions of Sol, i.e., SolM, SolV, SolIM and SolC. SolG, although immature in appearance in Nissl preparation, also contained small perikarya of TH-ir neurons. Immunoreactivity for TH became progressively more intense, with increasing number and cellular size of TH-ir neurons as Sol developed. The broad distribution of TH-ir neurons in the fetal Sol is comparable to both adult human (Gai and Blessing, 1996; Lynn et al., 1996) and rat (Hokfelt et al., 1984; Rogers et al., 2003; Zhang and Ashwell, 2001b) from 13 weeks, though the population continued to rise until 25 weeks. The area medial to sol, where most TH-ir neurons were located, has been reported to contain mainly noradrenergic neurons which appear to be strongly involved in esophageal-gastric reflexes (Gai and Blessing, 1996; Rogers et al., 2003). Therefore, early formation of TH-ir neurons in fetal human Sol, along with the known establishment (12 weeks) of vagal connections to the stomach (Abel et al., 1998), implies the early setting up of gastrointestinal function within Sol. Gastrointestinal regulation is likely to become more sophisticated as Sol develops during the second trimester.

GAP-43 (also termed GAP-48, B-50, F1 or pp46) is a phosphoprotein of the presynaptic membrane that is associated with the initial establishment, regeneration and functional modulation of synaptic relationships (Kinney et al., 1993; Neve et al., 1988). In developing neurons which undergo remodeling of axonal connections, GAP-43 is expressed at high levels and transported to growth cones and immature synapses (Kinney et al., 1993; Neve et al., 1988). In the present study, strong immunoreactivity of GAP-43 was found in sol at both young (13 weeks) and mature (21 weeks) ages. This might suggest robust neural plasticity of this fiber tract throughout fetal life. There is so far no analysis of subnuclear distribution of GAP-43 in the developing Sol in any mammalian species, although Sol as a whole has been reported to have high GAP-43 expression during fetal and infantile life in the human (Kinney et al., 1993), pouch young wallaby (Hassiotis et al., 2002) and adult opossum (Zou and Martin, 1995). The present study showed that high GAP-43 immunoreactivity was present in Sol at 13 weeks, especially in SolDL and SolC, while at 21 weeks, there was a significant decline of GAP-43 expression of Sol. This significant decline in GAP-43 immunoreactivity indicates that axonal elongation is largely completed by 21 weeks and thereby provides critical information about the formation of sol. It is known that in early development GAP-43 is concentrated along the entire length of axons as they elongate, then in the distal elements of axons during terminal branching and synaptogenesis, with levels subsequently declining markedly with the maturation of stable synaptic relationships (Kinney et al., 1993). The declining expression of GAP-43 from 13 to 21 weeks in our study may suggest maturation of stable synapses in Sol during the second trimester.

Distribution of SP immunoreactivity in Sol has been reported in the adult (McRitchie and Tork, 1994) and developing (Nomura et al., 1982; Rikard-Bell et al., 1990; Wang et al., 1993; Yew et al., 1990) human as well as in the rat (Zhang and Ashwell, 2001b). This undecapeptide tachykinin is known to be a neurotransmitter in sensory and autonomic pathways (Chang et al., 1971; Hokfelt et al., 1975a; Hokfelt et al., 1975b; Schoenen and Faull, 2004). In the fetal human, SP immunoreactivity at 11 weeks of gestation is abundant in subnuclei SolM, SolIM, SolV, SolVL and SolDL (Yew et al., 1990). SP immunoreactivity was found in the so called *subnucleus dorsalis* of Sol (regions correlated to SolD and SolDL of the present study) at 16 weeks of gestation, and was shown to be of low to moderate density in Sol at 23 weeks of gestation (Wang et al., 1993). In the infant human, strong SP immunoreactivity was found in SolPa, while SolM, SolV, SolD, SolVL and SolC had moderate immunoreactivity (Rikard-Bell et al., 1990). In the adult human, SP-ir neurons have been observed most frequently in SolG, with moderate numbers in SolM, SolIM and very few in SolV, SolD SolDL and SolC (McRitchie and Tork, 1994). In the present study, only one specimen of 21 weeks was available for chemoarchitectural study of SP distribution. No SP-ir neurons could be seen in the Sol at 21 weeks, although strong immunoreactive neuropil could be seen in SolD, SolI and SolPa. Moderate immunoreactivity was present in SolM, SolDL and SolIM; SolG SolV and SolC had the lowest levels SP immunoreactivity. Such a distribution is similar to what was found in early fetal (Yew et al., 1990) and infant (Rikard-Bell et al., 1990) humans but quite different from the adult (McRitchie and Tork, 1994). Therefore, it seems that the subnuclear expression of SP is a developing process and its correlation with the development of

cardiovascular and gastrointestinal regulation of Sol remains an open question (Abdala et al., 2003; Liu et al., 2004).

3.3.5 Functional Correlations of Subnuclear Development of the Solitary Nucleus

It is now certain that various subdivisions of Sol are responsible for processing different viscerosensory information (Altschuler et al., 1989; Armstrong et al., 1981; Broussard and Altschuler, 2000a; Kalia et al., 1984; Katz and Karten, 1983; Yamazoe et al., 1984). In the rat, SolVL and SolV receive projections from the lower respiratory system, while SolI and SolIM receive projections from the common pathway of gastrointestinal and respiratory tracts, i.e., oropharynx and upper laryngopharynx (Altschuler et al., 1989; Broussard and Altschuler, 2000a; Kalia et al., 1984). SolG, SolM, SolC and the central subnucleus (which is not identified in humans) receive projections from the esophagus and stomach (Altschuler et al., 1989; Gai and Blessing, 1996), whereas SolD and SolDL are functionally linked to the baroreceptors and chemoreceptors (Armstrong et al., 1981; Kalia et al., 1984; Yamazoe et al., 1984). In the cat (Kalia and Mesulam, 1980b), a more complicated distribution of visceral afferents in various subnuclei has been revealed. SolM, SolD, SolC receive projections from larynx, trachea, main bronchus, lung, heart, and stomach; SolDL and SolVL receive projections from all visceral organs above except the stomach; SolIM receives projections also from the visceral organs above, but not the larynx. The other three subnuclei receive projections from relatively few organs: SolG contains afferent terminals only after labeling trachea, heart and stomach, SolI receives

projections from larynx, trachea, bronchus and lung, while SolV receives projections from larynx, trachea, bronchus and heart (Kalia and Mesulam, 1980b). Therefore, distribution of visceral afferents in Sol subnuclei is largely similar across species.

Embryological studies in the human have shown that the cardiovascular system is one of the earliest functioning systems during prenatal development, with the heart contracting as early as 18 days (Wang et al., 1993). The respiratory and digestive systems of the fetus also develop at early stages of prenatal development, whereas the development and formation of the oral-facial structures which originate from the first and second pharyngeal arches occurs relatively later (Wang et al., 1993). Muller et al (Muller et al., 1981) found that, by the end of embryonic stages 23 (8 weeks postovulatory), most major laryngeal muscles are present, and their innervation closely follows the adult pattern. While reflexes involving the oral area have been identified as early as 9 weeks, swallowing does not appear in response to lip stimulation until 13 weeks (Humphrey, 1968). This is the age at which sol was identified as a distinct fiber tract in the present study, and SolM, SolV, SolIM, SolVL were among the earliest subnuclei to be clearly discernable. As noted above, SolM and SolIM are involved in processing sensory information from the pharynx and esophagus (Broussard and Altschuler, 2000a; Gai and Blessing, 1996).

Breathing activity in the human fetus can be detected by 11 weeks gestation (Boddy and Dawes, 1975). SolVL, which receives projections from the larynx, trachea, main bronchus and lung (Kalia and Mesulam, 1980b), appeared as a densely packed cell group ventrolateral to sol at 13 weeks, whereas SolV, which also receives pulmonary afferents,

did not become discernable from the adjacent SolIM until 15 weeks. Cb immunoreactivity appeared at 15 weeks in SolV and SolVL, which as noted above, may be involved in projections to the parabrachial area in the pons (Menetrey et al., 1992). From these observations, it is clear that the first breathing movements occur at approximately the same time as the cytoarchitectural and chemoarchitectural maturation of the relevant parts of Sol. At present the precise role the Sol plays in control of early respiratory movements is unknown, but it is unlikely that fetal breathing movements at 13 weeks involve a fully functional Sol circuitry.

3.4 Concluding Remarks

The present study focused on the development of cyto- and chemoarchitecture of human Sol from fetal age 9 weeks to 25 weeks, by using Nissl staining and Cb, Cr, TH, GAP-43 and SP immunohistochemical techniques. Sol began to gain heterogeneity and show different subnuclei as early as 13 weeks, and approached maturation from 21 to 25 weeks. The subnuclear division pattern observed in the fetal Sol is consistent with the subnuclear pattern that has been found in the adult (McRitchie and Tork, 1993; Paxinos and Huang, 1995). Results from the chemoarchitectural study showed that human Sol expressed various neurochemical substances at early developmental ages, even before fully cellular and neuropil maturation was attained. Expression of these neurotransmitters or neuromodulators may play an important role in establishment and integration of the viscerosensory function of Sol. For the first time, the present study analyzes the development of subnuclei of Sol in human fetuses, and further connectional or functional

studies on the fetal development of Sol are expected to provide additional evidence for the early role of this important autonomic brainstem nucleus.

Table 3.1 Distribution and Age of Emergence of Immunoreactive Markers in Subnuclei of Sol and 10N. (NA not applicable; - no immunoreactive neurons or fibers identified; + scattered immunoreactive neurons or fibers as applicable; ++ moderate density of immunoreactive neurons or fibers +++ high density of immunoreactive neurons or fibers)

Table 3.1

a) Cb

Age	SolM	SolV	SolVL	SolI	SolDL	SolD	SolIM	SolG	SolC	SolPa	10DI	10CeI	10VI	10CaI	10Ca
13W	+	-	-	NA	-	NA	-	++	+	NA	+	++	NA	NA	NA
15W	+	-/+	-/+	NA	-	+	-/+	++	+	NA	+	++	++	NA	NA
21W	++	-/+	-/+	NA	-/+	+	-/+	++	+	++	+	++	+++	NA	NA
25W	+++	+	-/+	+/++	+	+	-/++	+++	++	+++	+	+++	+++	NA	NA

b) Cr

Age	SolM	SolV	SolVL	SolI	SolDL	SolD	SolIM	SolG	SolC	SolPa	10DI	10CeI	10VI	10CaI	10Ca
13W	+/-	+/-	-/+	NA	+/-	NA	+	-	+	NA	-				
15W	+	+/-	+	NA	+	+	+	-	+	+	-				
21W	+	+	+/++	NA	+	+	+	-	+	+	-/+				
25W	++	+	++	NA	++	++	++	-/+	++	++	-/+				

c) TH

Age	SolM	SolV	SolVL	SolI	SolDL	SolD	SolIM	SolG	SolC	SolPa	10DI	10CeI	10VI	10CaI	10Ca
13W	+	+	-	NA	-	NA	+	+	+	NA	-/+	+	NA	+	+
15W	+	+	+	NA	+	NA	+	+	+	+	++	+	++	+	+
21W	+	+	+	NA	+	NA	+	++	+	+	+/++	++	++	+	+
25W	+	+	+	NA	+	NA	+	++	+	+	++	++	+++	+/++	+

d) GAP43

Age	SolM	SolV	SolVL	SolI	SolDL	SolD	SolIM	SolG	SolC	SolPa	10DI	10CeI	10VI	10CaI	10Ca
13W	+	++	++	+++	++	NA	+	++	+	+	++	++	NA	++	++
21W	+	+	+	++	+/-	NA	+/-	+	+	+	+	+	+	+	+

e) SP

Age	SolM	SolV	SolVL	SolI	SolDL	SolD	SolIM	SolG	SolC	SolPa	10DI	10CeI	10VI	10CaI	10Ca
21W	+/-	-	++	++	-	++	+/-	-	-	++	++	+	+	++	++

Figure 3.1 Photomicrographs of Nissl stained section of fetal Sol at 9 weeks: a) low power image showing the location of developing Sol and 10N and their positions relative to adjacent structures (12N and sl); b) medium power image showing Sol with its surroundings c) high power image showing cellular morphology of Sol.

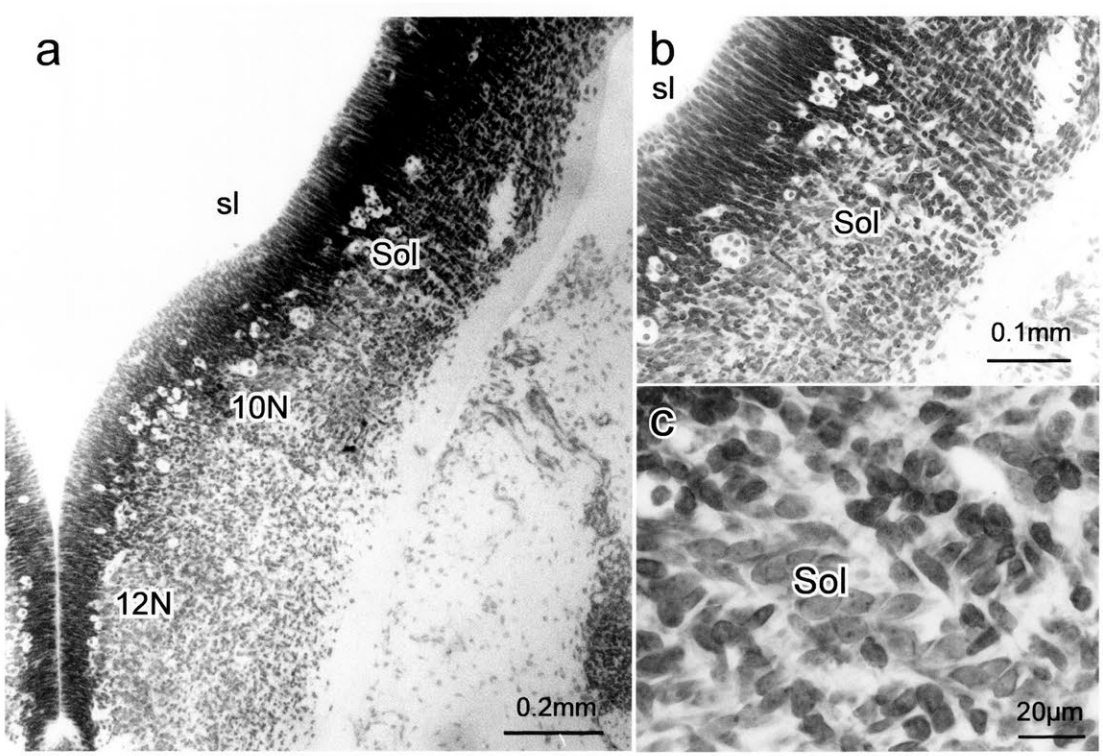

Figure 3.1

Figure 3.2 Line diagrams and their accompanying photomicrographs of Nissl stained sections of Sol and 10N and adjacent structures in the dorsomedial medulla at 13 weeks. Levels chosen at (a) the open medulla at the rostral limit of 12N; (b) the area postrema at the rostral limit of the gracile nucleus (Gr); (c) caudal to the obex close to the medulla-spinal cord junction.

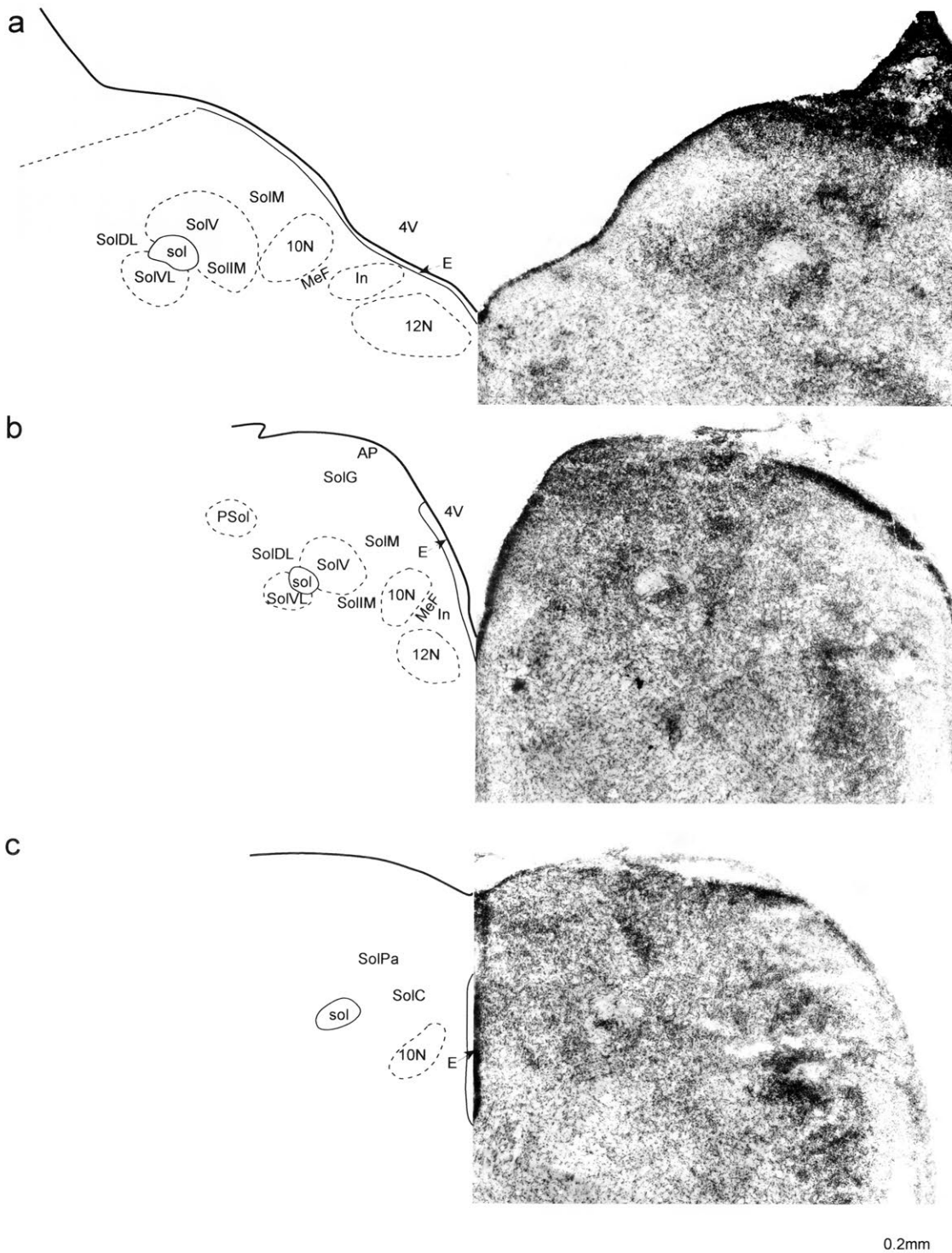
a
SolM
SolV
SolDL
sol
SolVL
SolIM
10N
4V
E
MeF
In
12N
b
AP
SolG
PSol
4V
SolM
E
SolDL
SolV
sol
SolVL
SolIM
10N
MeF
In
12N
c
SolPa
SolC
sol
10N
E
0.2mm

Figure 3.2

Figure 3.3 High power images of Nissl stained sections of Sol at 13 weeks. Cellular morphology and density of each subnucleus are illustrated in individual photomicrographs. The arrows in figure (f) indicate cells in SolC with a dorsomedial-to-ventrolateral orientation.

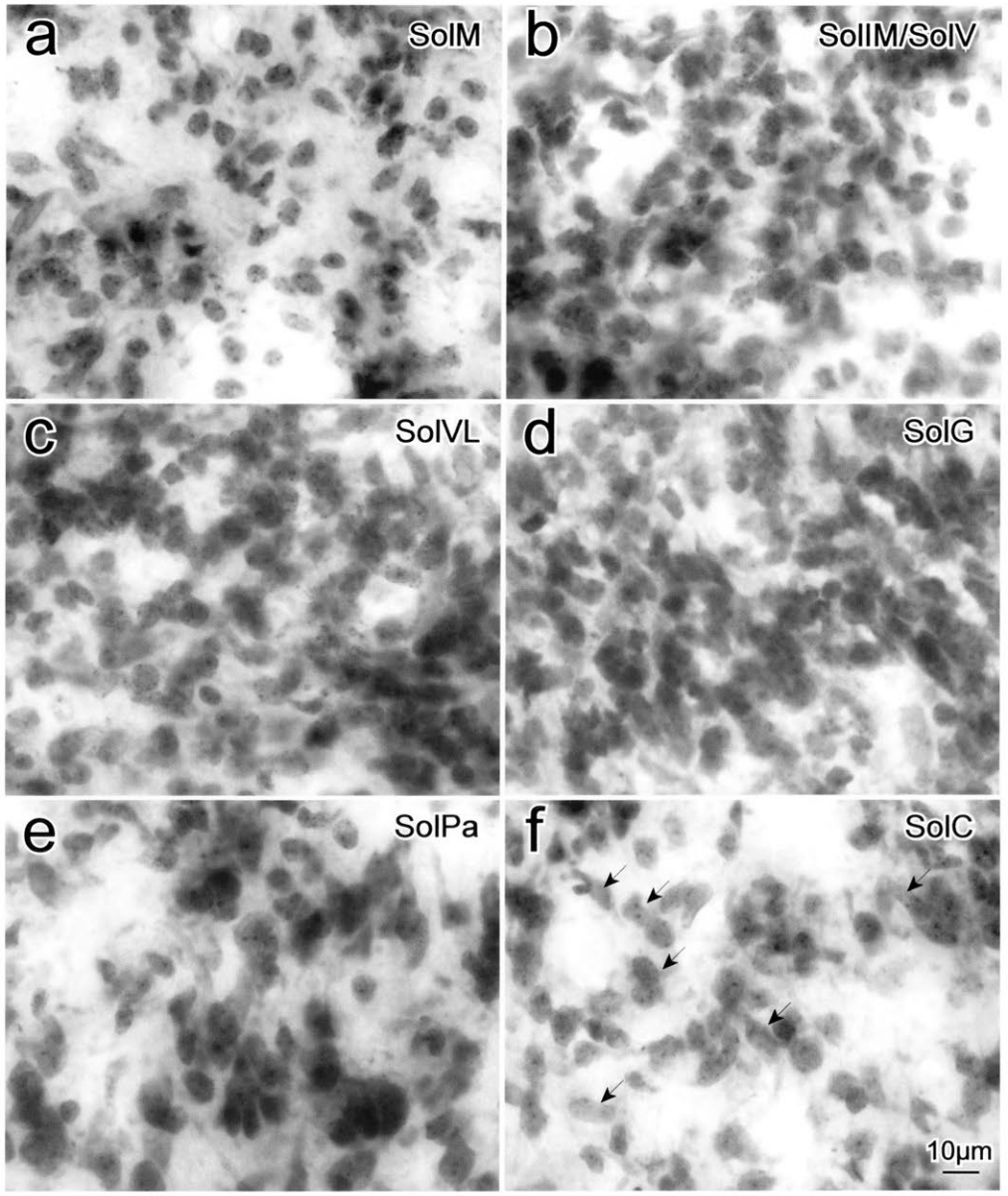

Figure 3.3

Figure 3.4 Line diagrams and their accompanying photomicrographs of Nissl stained sections of Sol and 10N and adjacent structures in the dorsomedial medulla at 15 weeks. Levels chosen in accordance with those of Figure 3.2.

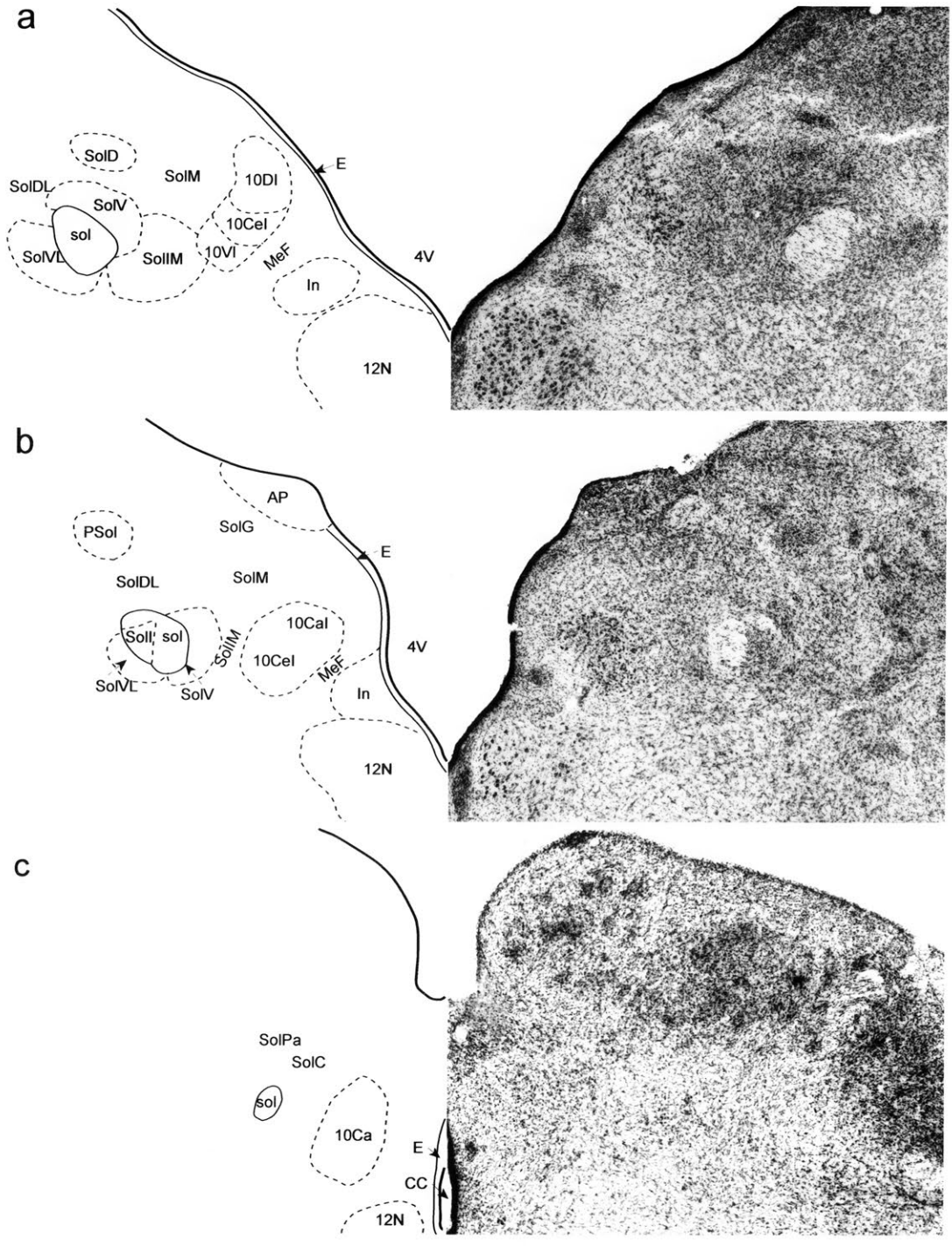
a
SolD
SolM
10DI
E
SolDL
SolV
sol
10CeI
SolVL
SolIM
10VI
MeF
4V
In
12N
b
AP
PSol
SolG
E
SolDL
SolM
10CaI
SolI
sol
SolIM
4V
10CeI
MeF
SolVL
SolV
In
12N
c
SolPa
SolC
sol
10Ca
E
CC
12N
0.2mm

Figure 3.4

Figure 3.5 High power images of Nissl stained sections of Sol showed cellular morphology and density of individual subnuclei at 15 weeks.

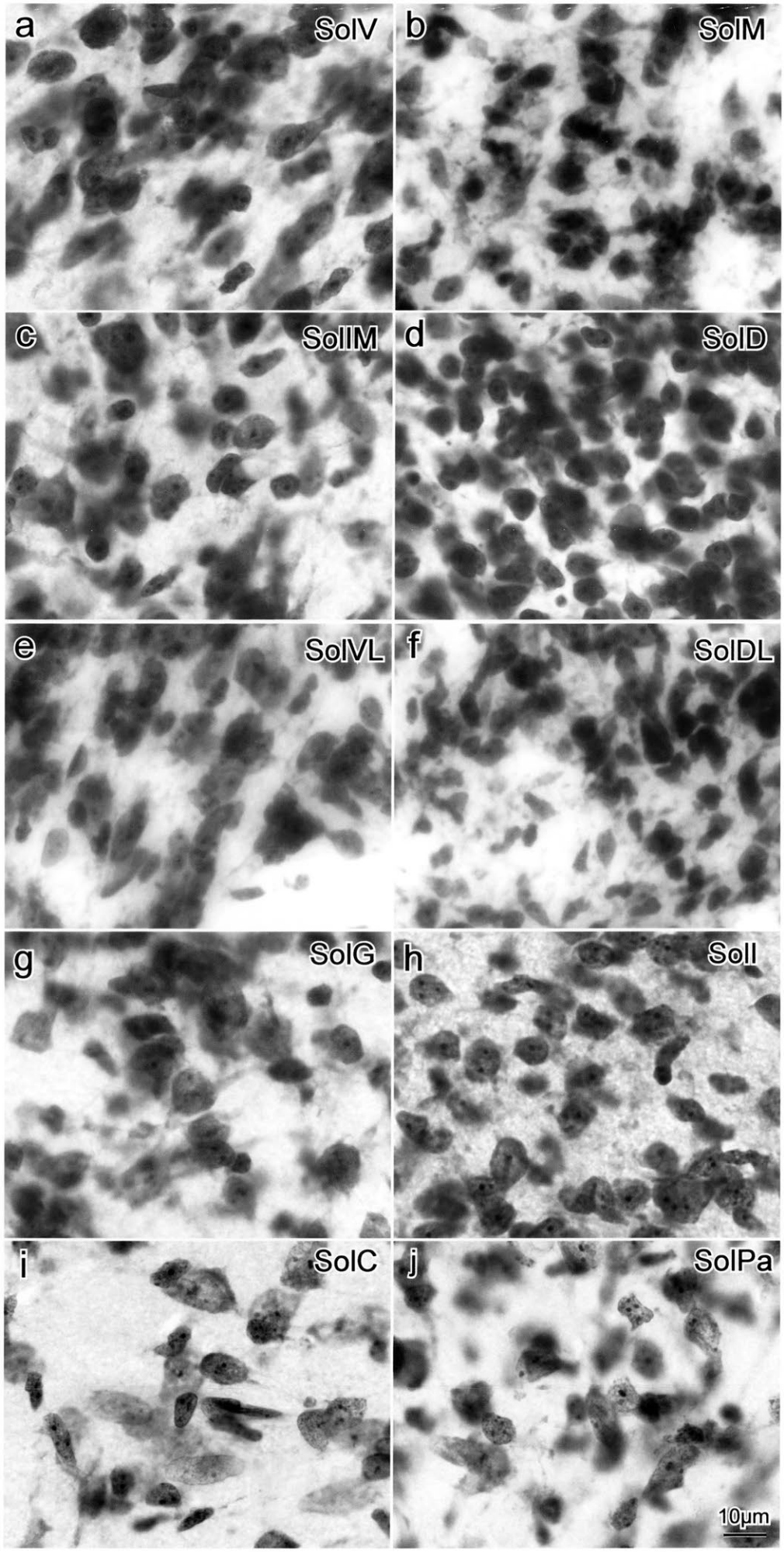
a
SolV
b
SolM
c
SolIM
d
SolD
e
SolVL
f
SolDL
g
SolG
h
SolI
i
SolC
j
SolPa
10µm

Figure 3.5

Figure 3.6 Line diagrams and their accompanying photomicrographs of Nissl stained sections of Sol and 10N and adjacent structures in the dorsomedial medulla at 21 weeks. Levels chosen in accordance with those of Figure 3.2.

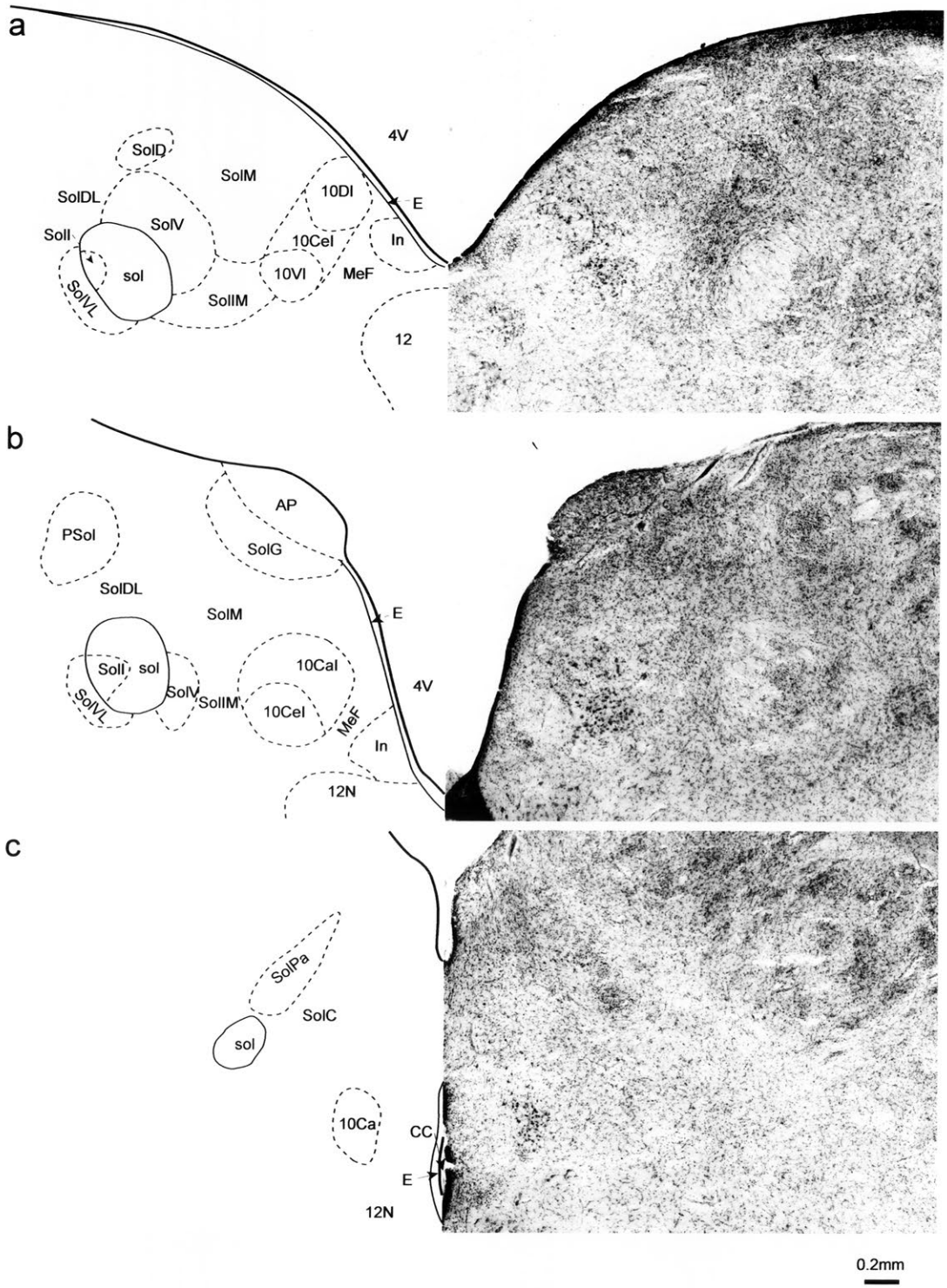
a
4V
SolD
SolM
SolDL
10Dl
E
SolV
SolI
10Cel
In
sol
10Vl
MeF
SolVL
SolIM
12
b
AP
PSol
SolG
SolDL
E
SolM
SolI
sol
10Cal
4V
SolVL
SolV
SolIM
10Cel
MeF
In
12N
c
SolPa
SolC
sol
10Ca
CC
E
12N
0.2mm

Figure 3.6

Figure 3.7 High power images of Nissl stained sections of Sol showing cellular morphology and density of individual subnuclei at 21 weeks. White arrows in figures (a), (b), (c), (d) and (g) indicate putative glial cells at this age.

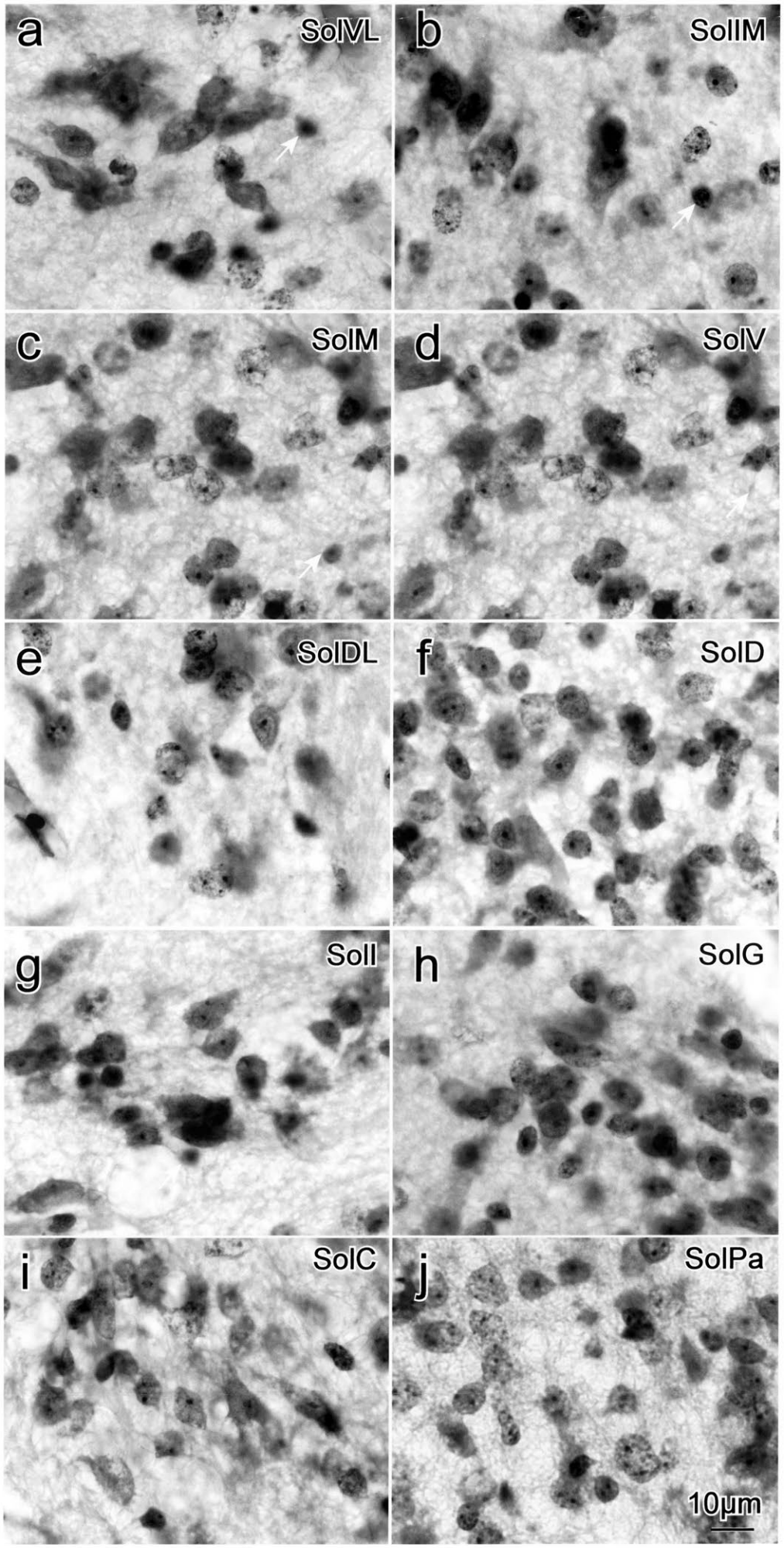
a
SolVL
b
SolIM
c
SolM
d
SolV
e
SolDL
f
SolD
g
SolI
h
SolG
i
SolC
j
SolPa
10µm

Figure 3.7

Figure 3.8 Line diagrams and their accompanying photomicrographs of Nissl stained sections of Sol and 10N and adjacent structures in the dorsomedial medulla at 25 weeks. Levels chosen in accordance with those of Figure 3.2.

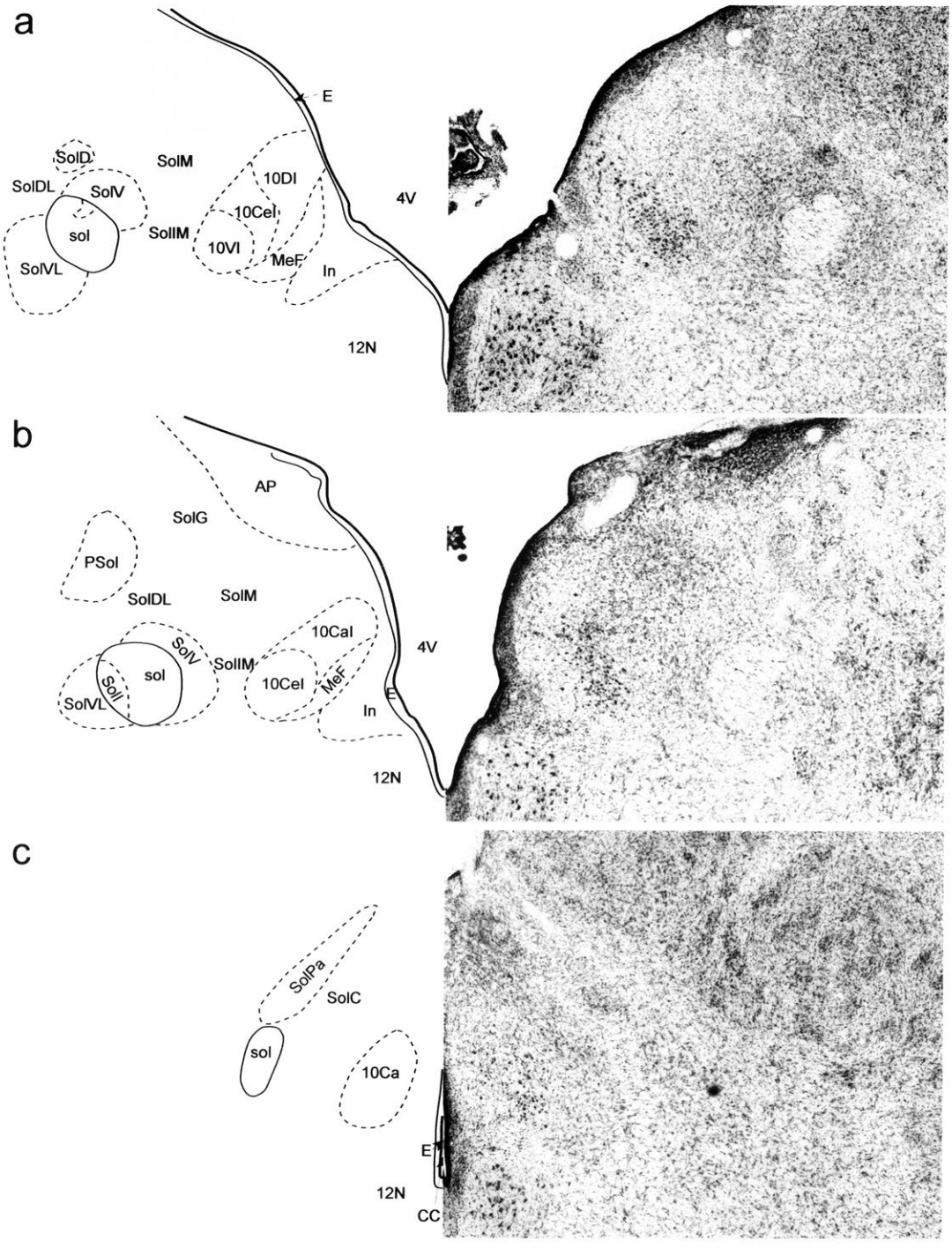
a
E
SolD
SolM
SolDL
SolV
10DI
10CeI
4V
sol
SolIM
10VI
MeF
SolVL
In
12N
b
AP
SolG
PSol
SolDL
SolM
10CaI
SolV
SolIM
4V
sol
SolI
10CeI
MeF
SolVL
E
In
12N
c
SolPa
SolC
sol
10Ca
E
12N
CC
0.2mm

Figure 3.8

Figure 3.9 High power images of Nissl stained sections of Sol showing more mature cytology of constituent cells of individual subnuclei at 25 weeks compared to previous ages. Note the presence of cytoplasm in many of the neurons.

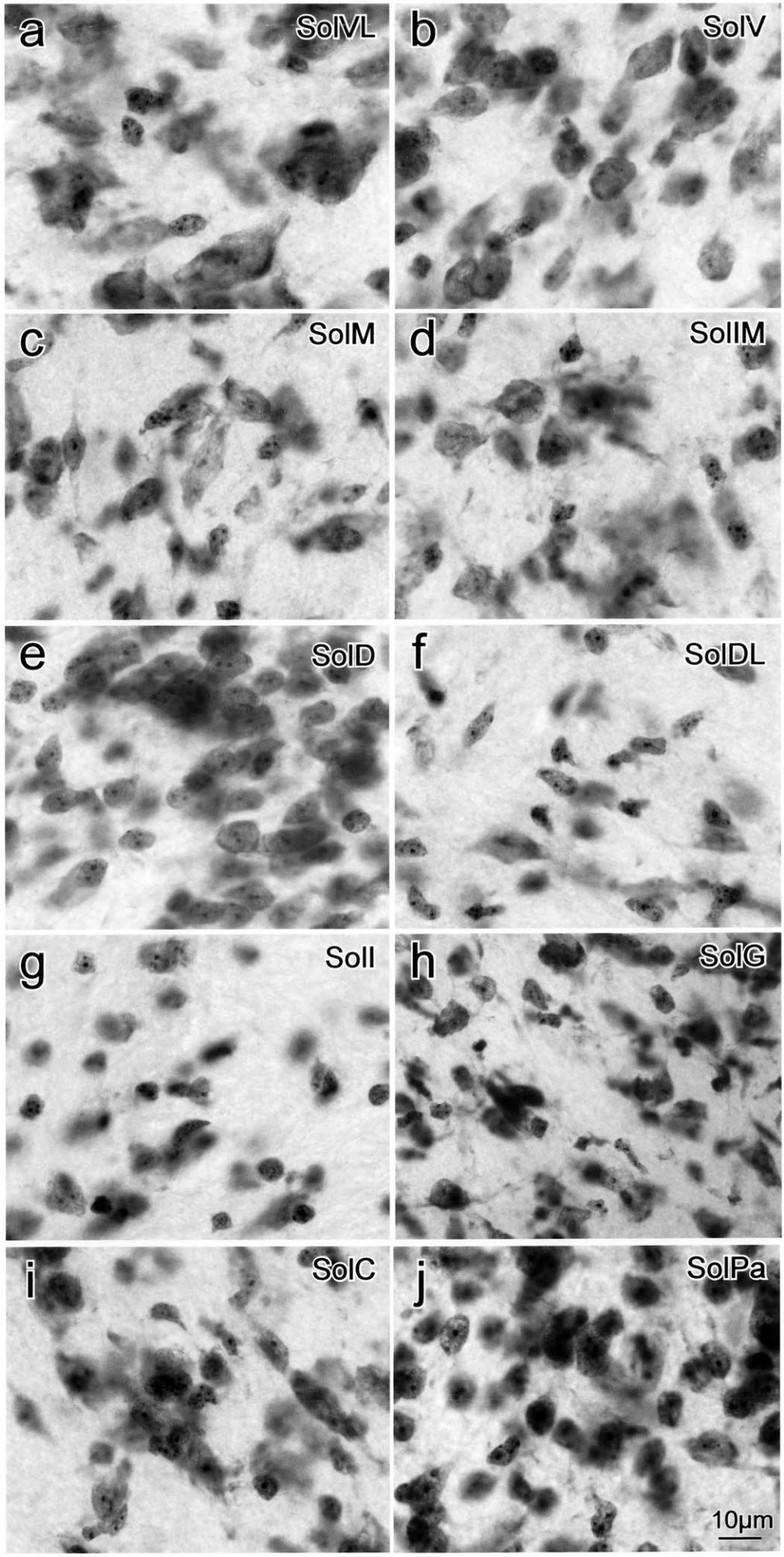
a
SolVL
b
SolV
c
SolM
d
SolIM
e
SolD
f
SolDL
g
SolI
h
SolG
i
SolC
j
SolPa
10μm

Figure 3.9

Figure 3.10 Line diagrams illustrating the distribution of CB-ir neurons in Sol and 10N at various ages: (a)-(c) 13 weeks, (d)-(f) 15 weeks, (g)-(i) 21 weeks; (j)-(l) 25 weeks. Figures (a), (d), (g) and (i) represent sections at the rostral limit of 12N for each age; figures (b), (e), (h) and (k) represent sections at the level of the area postrema and the rostral limit of Gr, whereas figures (c), (f), (i) and (l) represent sections at the level of the spinomedullary junction.


13W
a
4V
SolM
SolDL
SolV
10N
sol
SolIM
SolVL
b
AP
SolG
SolM
4V
sol
c
SolC
sol
15W
d
SolD
SolM
4V
10Dl
SolDL
SolV
10Cel
sol
SolIM
SolVL
e
AP
SolG
SolDL
SolV
SolM
4V
sol
SolIM
10N
SolVL
f
SolC
sol
CC
21W
g
4V
SolM
SolD
SolDL
10Dl
SolV
10Cel
sol
SolIM
SolVL
h
AP
SolG
4V
SolDL
SolM
SolV
sol
SolIM
10N
SolVL
i
SolPa
SolC
sol
CC
25W
j
SolD
SolM
4V
SolDL
SolV
10Dl
10Cel
sol
SolIM
SolVL
k
AP
SolG
4V
SolDL
SolV
SolM
10N
sol
SolIM
SolVL
SolI
l
SolPa
SolC
sol
0.2mm

Figure 3.10

Figure 3.11 High power images of CB-ir somata in various subnuclei of Sol at different ages: (a)-(c) 13 weeks, (d)-(h) 15 weeks, (i)-(k) 21 weeks, (l)-(n) 25 weeks.

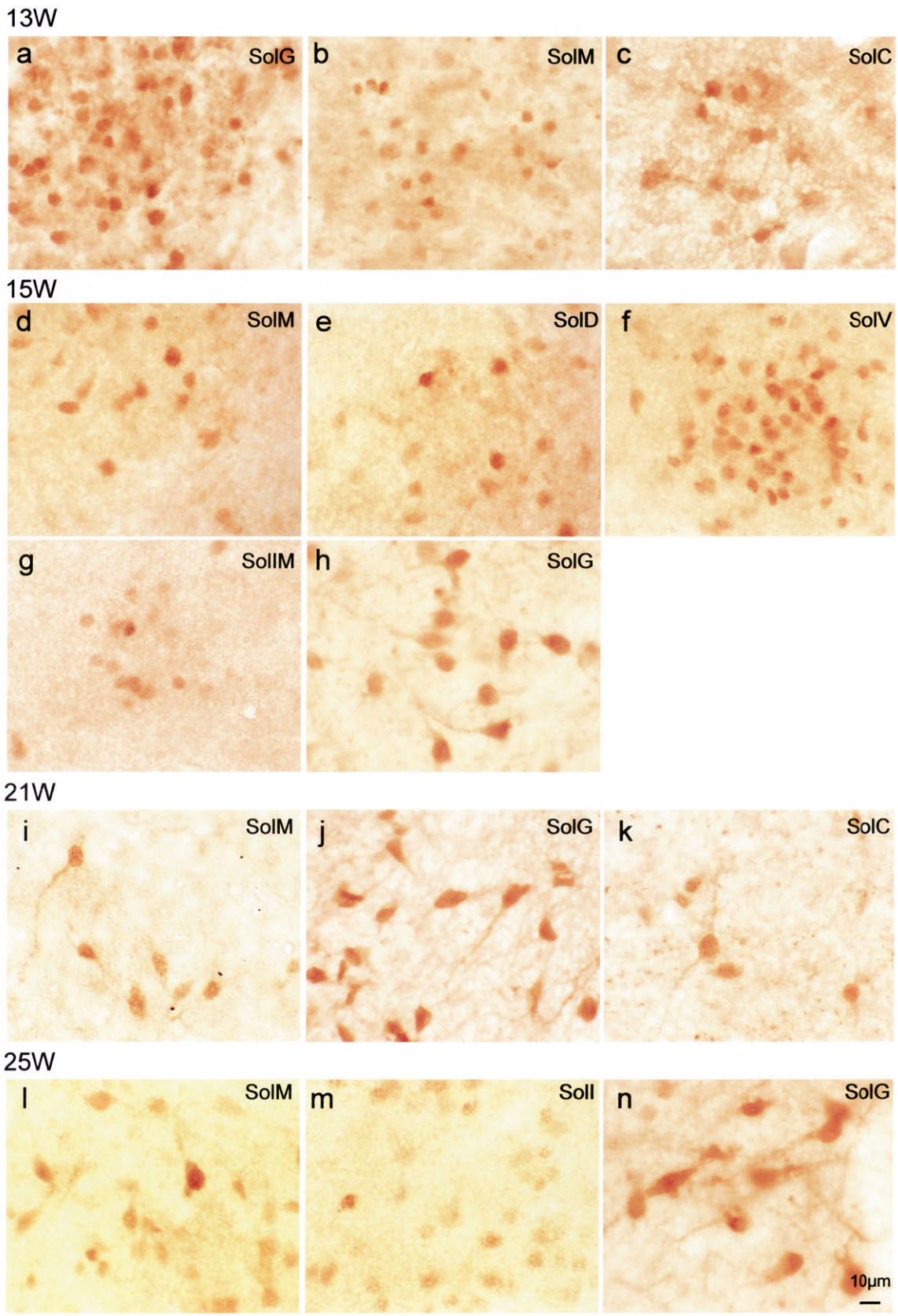
13W
a
SolG
b
SolM
c
SolC
15W
d
SolM
e
SolD
f
SolV
g
SolIM
h
SolG
21W
i
SolM
j
SolG
k
SolC
25W
l
SolM
m
SolI
n
SolG
10μm

Figure 3.11

Figure 3.12 Line diagrams showing the distribution of CR-ir neurons in Sol and 10N at various ages: (a)-(c) 13 weeks, (d)-(f) 15 weeks, (g)-(i) 21 weeks; (j)-(l) 25 weeks. The levels of sections chosen for each age are the same as those in Figure 3.10.

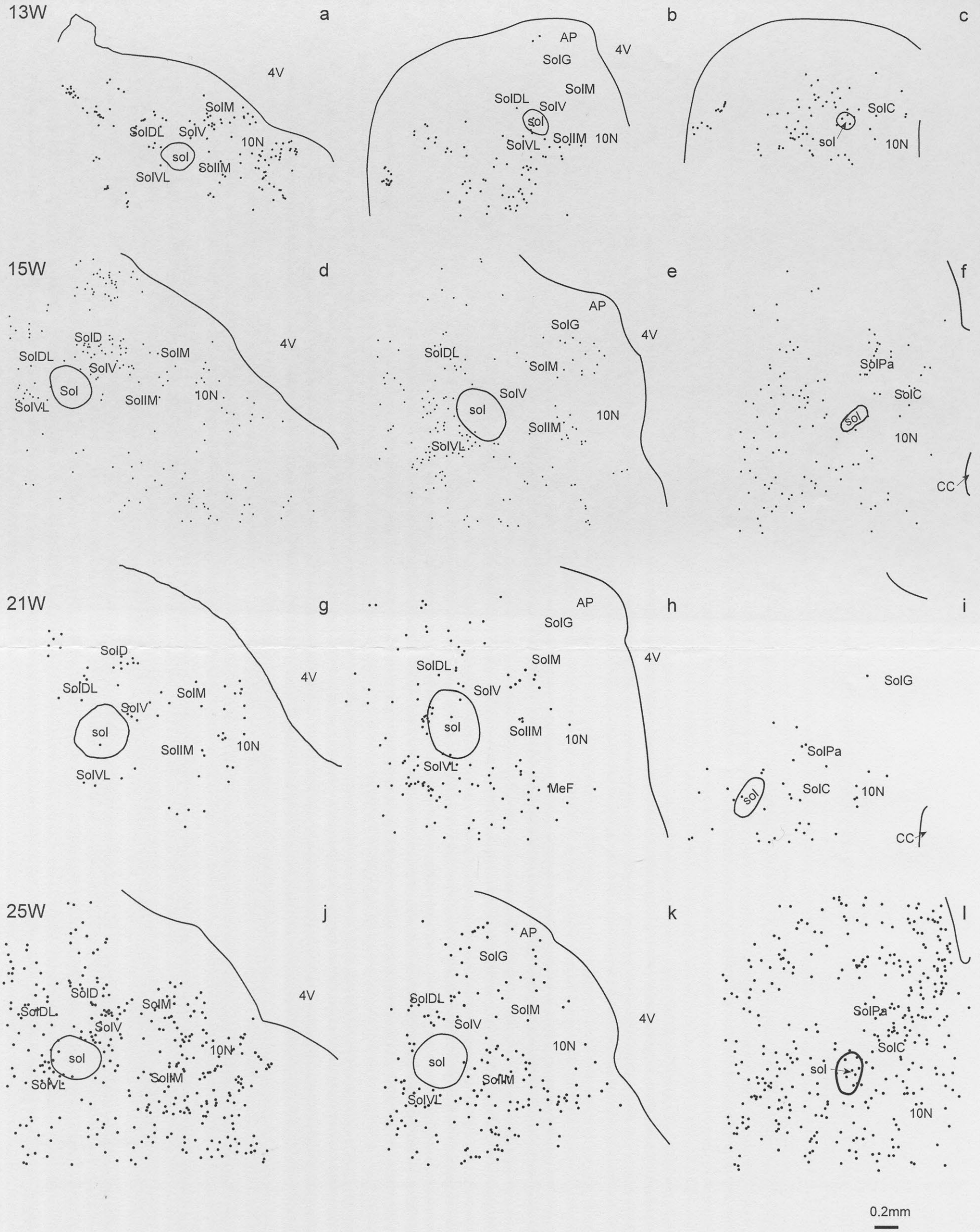
13W
a
4V
SolM
SolDL
SolV
sol
10N
SolIM
SolVL
b
AP
SolG
4V
SolM
SolDL
SolV
sol
SolVL
SolIM
10N
c
SolC
sol
10N
15W
d
SolD
4V
SolDL
SolM
SolV
Sol
SolVL
SolIM
10N
e
AP
SolG
4V
SolDL
SolM
SolV
sol
10N
SolIM
SolVL
f
SolPa
SolC
sol
10N
CC
21W
g
SolD
4V
SolDL
SolM
SolV
sol
SolIM
10N
SolVL
h
AP
SolG
SolDL
SolM
4V
SolV
sol
SolIM
10N
SolVL
MeF
i
SolG
SolPa
sol
SolC
10N
CC
25W
j
SolD
4V
SolDL
SolM
SolV
sol
10N
SolVL
SolIM
k
AP
SolG
SolDL
SolM
4V
SolV
10N
sol
SolVL
l
SolPa
SolC
sol
10N
0.2mm

Figure 3.12

Figure 3.13 High power images of CR-ir somata in various subnuclei of Sol at different ages: (a)-(f) 13 weeks, (g)-(l) 15 weeks, (m)-(o) 21 weeks, (p)-(u) 25 weeks.

13W

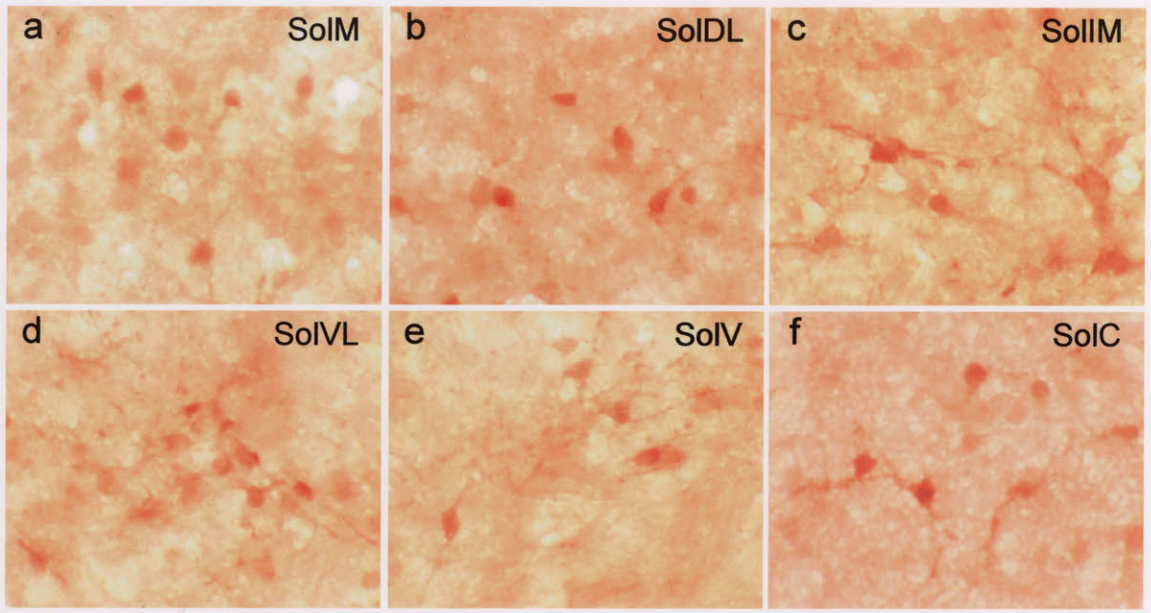

15W

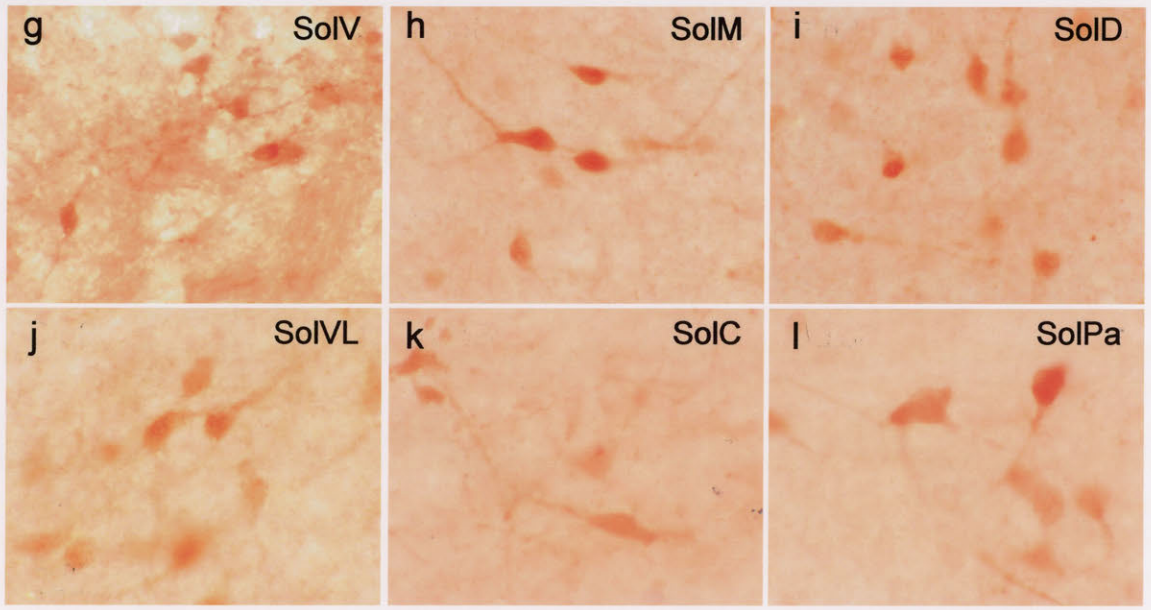

Figure 3.13

21W

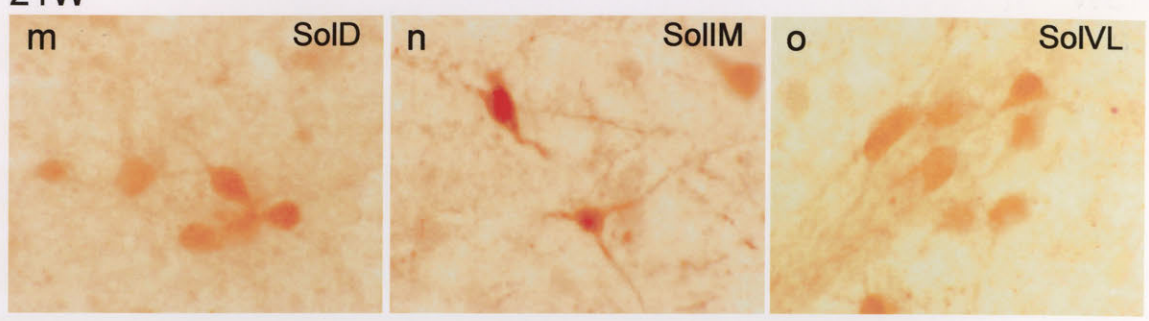

25W

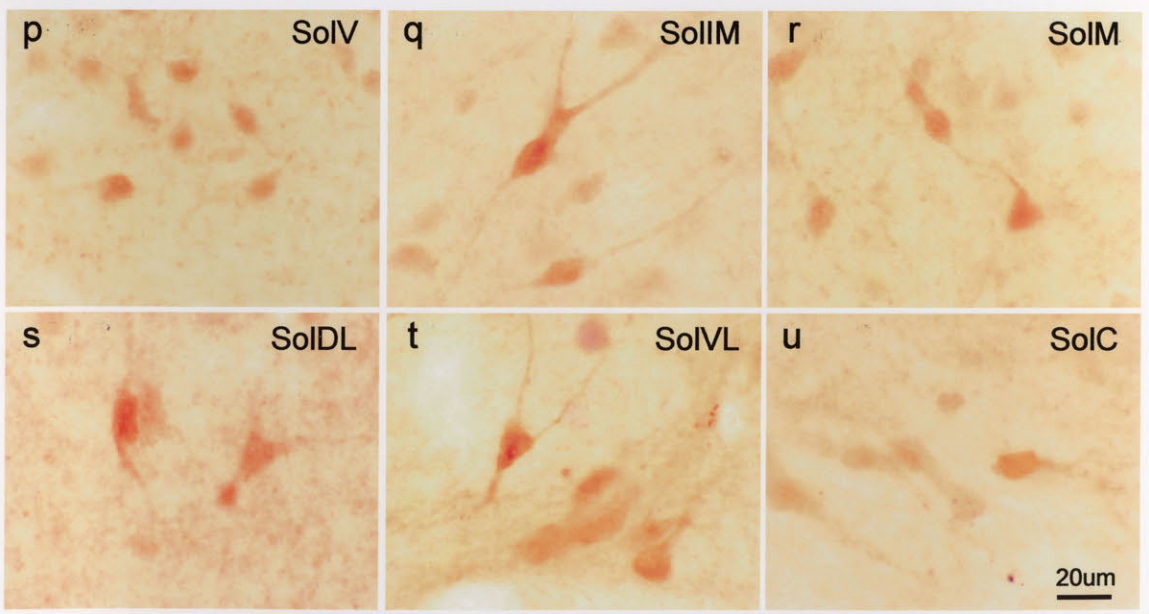

Figure 3.14 Line diagrams showing the distribution of TH-ir neurons in Sol and 10N at various ages: (a)-(c) 13 weeks, (d)-(f) 15 weeks, (g)-(i) 21 weeks; (j)-(l) 25 weeks. The levels of sections chosen for each age are the same as those in Figure 3.10.

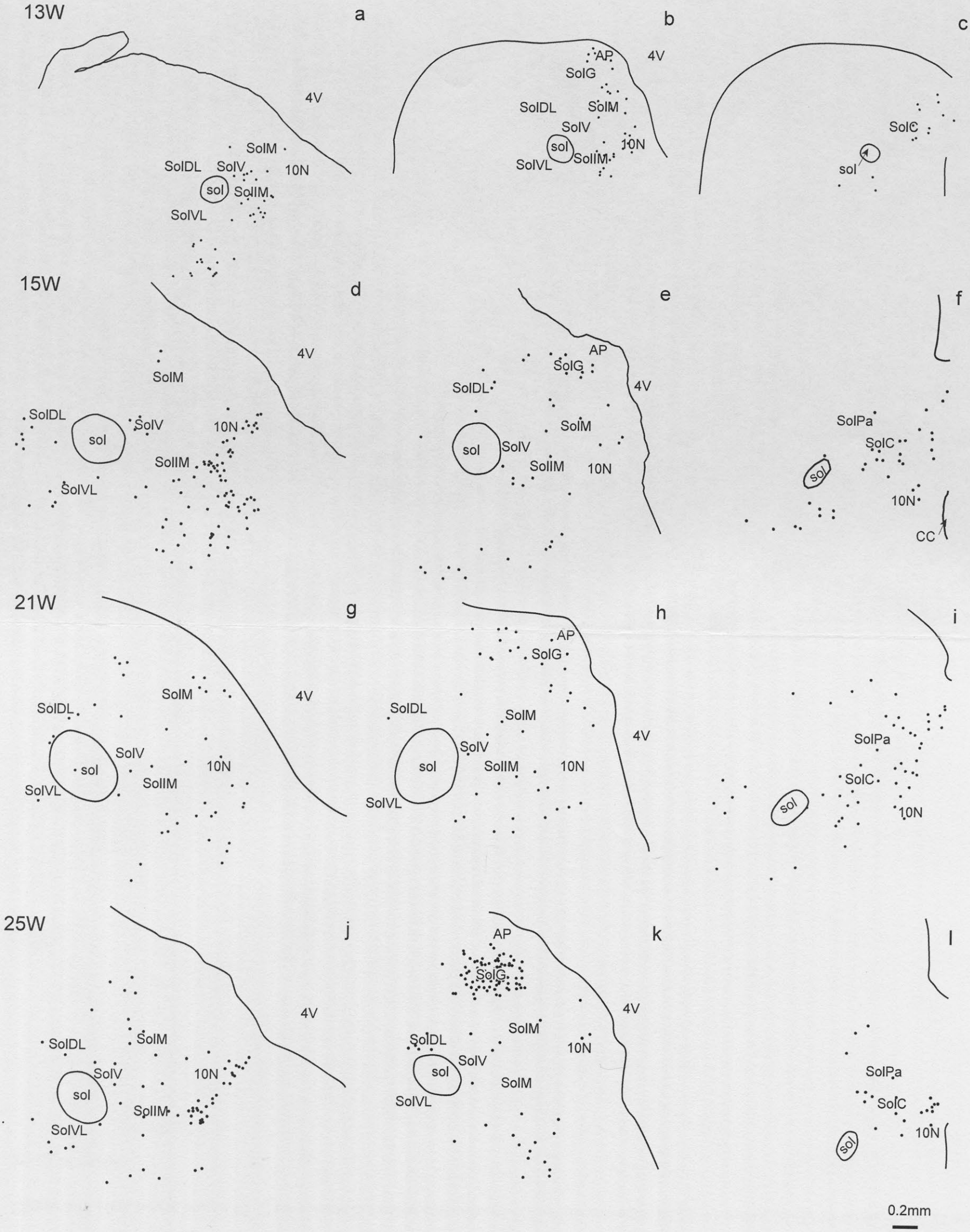
13W
a
4V
SolM
SolDL
SolV
10N
sol
SolIM
SolVL
b
AP
4V
SolG
SolDL
SolM
SolV
sol
10N
SolVL
SolIM
c
SolC
sol
15W
d
4V
SolM
SolDL
SolV
10N
sol
SolIM
SolVL
e
AP
SolG
4V
SolDL
SolM
sol
SolV
SolIM
10N
f
SolPa
SolC
sol
10N
CC
21W
g
SolM
4V
SolDL
SolV
sol
10N
SolIM
SolVL
h
AP
SolG
SolDL
SolM
4V
SolV
sol
SolIM
10N
SolVL
i
SolPa
SolC
sol
10N
25W
j
4V
SolDL
SolM
SolV
10N
sol
SpIIM
SolVL
k
AP
SolG
4V
SolM
SolDL
10N
SolV
sol
SolM
SolVL
l
SolPa
SolC
sol
10N
0.2mm

Figure 3.14

Figure 3.15 High power images of TH-ir somata in various subnuclei of Sol at different ages: (a)-(d) 13 weeks, (e)-(k) 15 weeks, (l)-(o) 21 weeks, (p)-(s) 25 weeks.

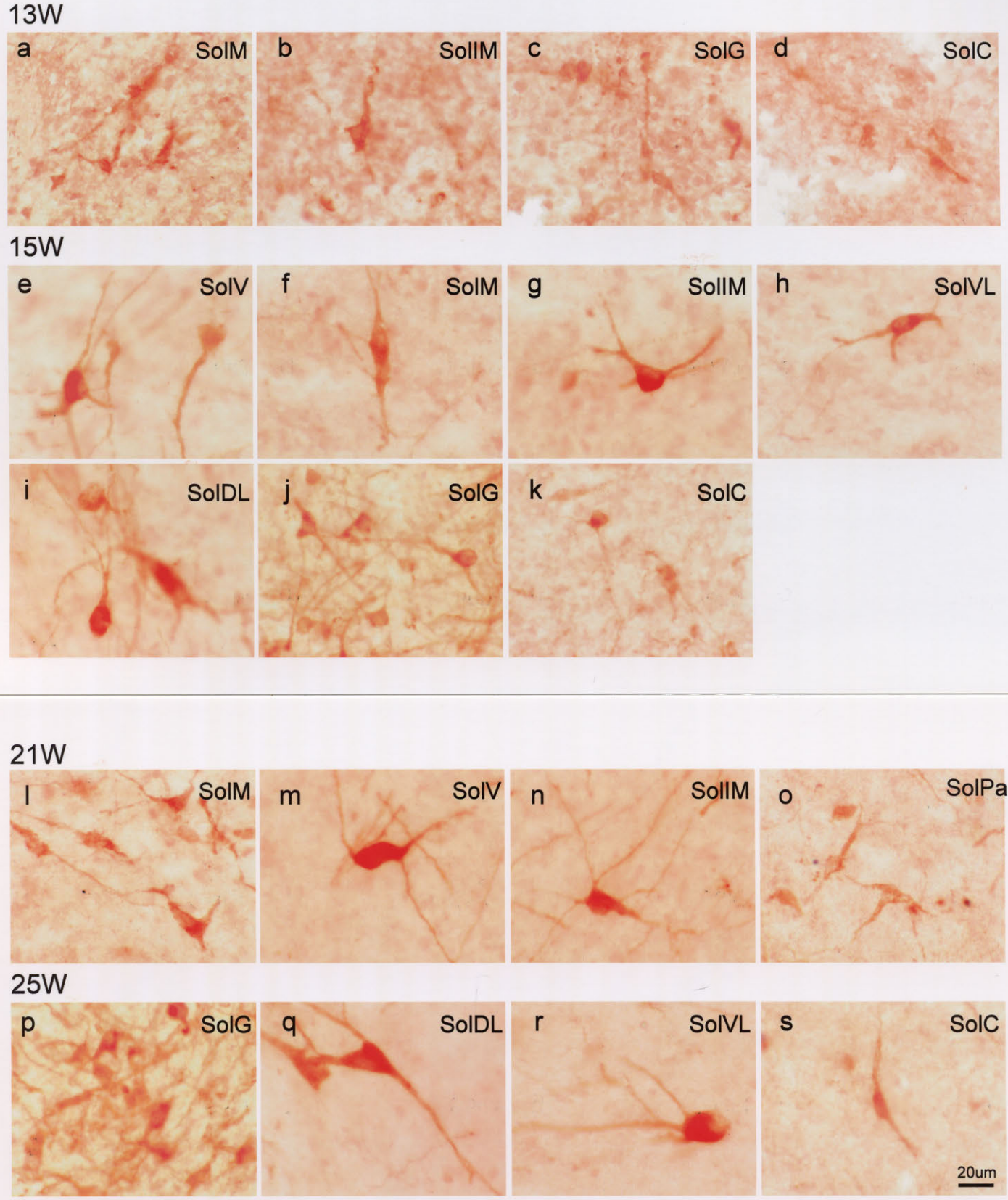
13W
a
SolM
b
SolIM
c
SolG
d
SolC
15W
e
SolV
f
SolM
g
SolIM
h
SolVL
i
SolDL
j
SolG
k
SolC
21W
l
SolM
m
SolV
n
SolIM
o
SolPa
25W
p
SolG
q
SolDL
r
SolVL
s
SolC
20um

Figure 3.15

Figure 3.16 Low power photomicrographs of GAP-43 immunoreactivity in Sol and 10N at (a)-(c) 13 weeks and (d)-(f) 21 weeks. Rostrocaudal levels of sections chosen for each age are the same as those in Figure 3.10

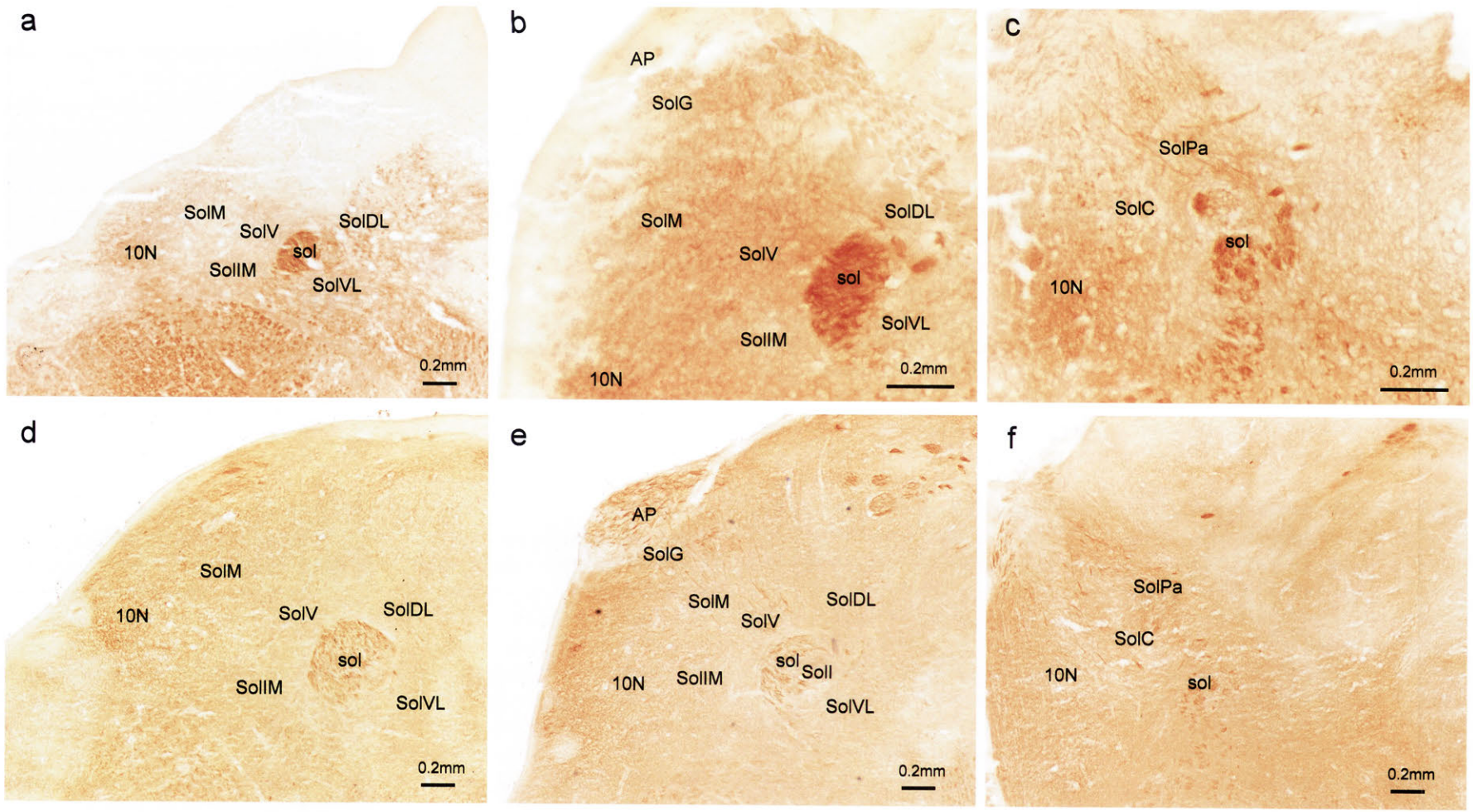
a
SolM
SolV
SolDL
10N
sol
SolIM
SolVL
0.2mm
b
AP
SolG
SolM
SolDL
SolV
sol
SolVL
SolIM
10N
0.2mm
c
SolPa
SolC
sol
10N
0.2mm
d
SolM
10N
SolV
SolDL
sol
SolIM
SolVL
0.2mm
e
AP
SolG
SolM
SolDL
SolV
sol
SolI
10N
SolIM
SolVL
0.2mm
f
SolPa
SolC
10N
sol
0.2mm

Figure 3.16

Figure 3.17 (a)-(c) Low power photomicrographs of SP immunoreactivity in Sol and 10N at 21 weeks. Rostrocaudal levels of sections are the same as those in Figure 3.10; (d)-(f) High power images of SP immunoreactivity in Sol subnuclei SolI, SolD and SolPa, respectively.

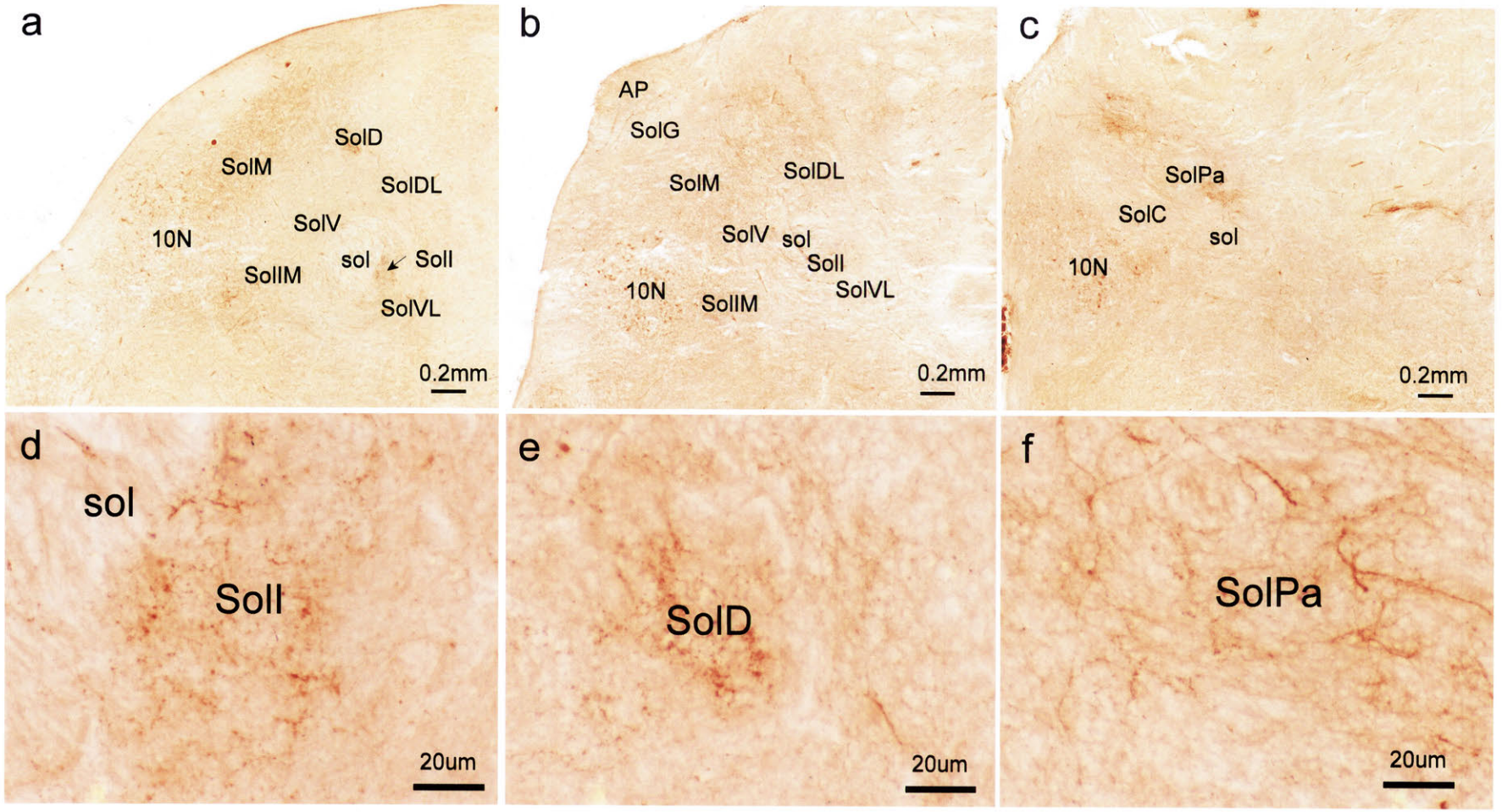
a
SolD
SolM
SolDL
SolV
10N
sol
SolI
SolIM
SolVL
0.2mm
b
AP
SolG
SolM
SolDL
SolV
sol
SolI
10N
SolIM
SolVL
0.2mm
c
SolPa
SolC
sol
10N
0.2mm
d
sol
SolI
20um
e
SolD
20um
f
SolPa
20um

Figure 3.17

Chapter 4 Cyto- and Chemoarchitecture of the Developing Human Dorsal Motor Nucleus of Vagus

4.1 Introduction

It is now well known that the parasympathetic motor control of smooth muscle and glands of thoracic and abdominal visceral organs is mediated by efferent fibers of the vagus nerve (10n) originating from the dorsal motor nucleus of the vagus nerve (10N) and/or the nucleus ambiguus (Amb) (Nara et al., 1991).

Cyto- and chemoarchitecture of adult human 10N has been thoroughly studied by Huang and colleagues (Huang et al., 1993a; Huang et al., 1993b). According to their study, the 10N is composed of dorsorostral, ventrorostral, rostrointermediate, dorsointermediate, ventrointermediate, centrointermediate, caudointermediate and caudal subnuclei and has various types of neurons with different morphological features (Huang et al., 1993a).

However, such a detailed subdivisional pattern was not observed in a developmental study of 10N by Nara et al. (Nara et al., 1991), in which only three subnuclei, i.e., dorsal, ventral and caudal, were distinguished. Their study mainly focused on the morphometry of neurons of 10N and did not examine the chemical features of those neurons during fetal life. In another study by Wang and colleagues (Wang et al., 1993), substance P (SP) immunoreactivity was shown to be strongly expressed in human fetal 10N at 16 weeks of development.

Except for these previous studies, there has been no comprehensive investigation of the development of this nucleus in the human. By contrast, neural circuits involved in the vagal reflex are known to be established early in fetal life (Humphrey, 1968; Muller et al., 1981) and physiological function of this nucleus in adult experimental animals has gained

extensive attention (Loewy and Spyer, 1990). The current study set out to initially investigate the cyto- and chemoarchitecture of 10N during early to middle fetal development (9 to 25 weeks) and was aimed at revealing more detail about the time-course of the establishment of those subnuclei seen in adult 10N and the neurochemical features of neurons in the nucleus. It was hoped that combined with a connectional study with DiI (Chapter 5, Cheng et al., 2004), an integrated view of the morphological maturation of the efferent part of the vagus nerve could be derived.

4.2 Results

4.2.1 Cytoarchitecture of the Developing Dorsal Motor Nucleus of Vagus

The rostro-caudal levels chosen for study of the cyto and chemoarchitecture of the developing 10N were the same as those in the previous chapter. Except for the 9 week specimen, at which only one level was taken, the levels chosen for 13 to 25 weeks were invariably a) open medulla at the rostral limit of the hypoglossal nucleus (12N), b) level of area postrema at the rostral limit of the gracile nucleus, and c) closed medulla caudal to the obex. Thus, low power photomicrographs and accompanying schematic diagrams of 10N at ages from the 13th to 25th week of prenatal life are shown in the Figure 3.2, 3.4, 3.6 and 3.8, respectively. In the present chapter, photomicrographs particularly showing the 10N area were extracted and magnified from the figures mentioned above and embedded in Figure 4.1-4.5, in order to yield a clearer presentation. Abbreviated names of subnuclei of 10N were defined according to Paxinos and Huang (Paxinos and Huang, 1995).

The fetal 10N at 9 weeks has been depicted in low and high power images in Figure

4.1. At this age, 10N was a densely packed cell group in the mantle layer of the caudal brainstem, adjacent to the sulcus limitans. There is a cell-sparse area lateral to it (Fig. 4.1a). Cells within the 10N were of small size (< 10μm diameter), and darkly stained and it was difficult to differentiate cells of 10N from those of surrounding structures (Fig. 4.1b).

At 13 weeks, as shown at the level of the open medulla (Fig. 4.2a), 10N was seen to contain two groups of cells which could be differentiated according to their different cellular density. The dorsomedial group contained relatively low cell density and probably corresponds to the dorsointermediate subnucleus (10DI) in the adult brain (Paxinos and Huang, 1995), while the ventral group was of relatively high cell density and probably corresponds to the centrointermediate subnucleus (10CeI) of adult brain. A third nucleus, found in the adult 10N at this level, is known as the ventrointermediate subnucleus (10VI), but this subnucleus could not be identified in Nissl preparations at this age. Cells of 10DI and 10CeI contained spherical darkly stained somata, which were about 6-11 μm in diameter (Fig. 4.2 d, e). The morphology of these cells was not noticeably different from that of small cells in adjacent structures, e.g., Sol, a feature which made it difficult to define the lateral border of 10N (Fig. 4.2a). At the level of the area postrema (Fig 4.2b), two groups of densely packed cells were seen in 10N. The ventrolateral group contained densely packed cells which appeared to be similar to those seen at the rostral level (Fig. 4.2e) and was identified as a continuation of 10CeI. The dorsomedial group was also densely packed and contained cells with appearances similar to 10CeI (Fig. 4.2f). In addition to these small to medium-sized cells, there were occasional darkly staining larger cells (>15 μm diameter, indicated by arrows). This group was therefore identified as the

caudointermediate subnucleus (10CaI). At the caudal level (Fig. 4.2c), 10N appeared to be a single group of darkly stained spherical or oval shaped cells. According to their position, this group of cells was tentatively identified as the caudal subnucleus (10Ca) (Fig.4.2g)

Figure 4.3 shows photomicrographs of 10N at the 15th week. At this age, unlike the previous ages (Fig. 4.1, 4.2), 10N appeared to be a prominent structure with densely packed darkly stained cells located at the dorsomedial region of the medulla and this nucleus could be easily differentiated from the nearby Sol. At the level of open medulla (Fig. 4.3a), the ventrolateral part of 10N displayed higher cell density than the dorsomedial part. The intermediate region was of moderately higher cell density; therefore, it was clear that at this age three subnuclei (i.e., 10DI, 10CeI and 10VI) could be identified. Cells within 10DI were mainly of small to medium size (7-11 μm diameter, Fig. 4.3d), though there were also occasional larger neurons (15-17 μm average diameters, not shown). These large neurons were only about 5% of the total cell number in 10DI. Ventrally, more large neurons appeared in 10CeI (Fig. 4.3e). These neurons were oval or trigonal in shape and may represent the parasympathetic preganglionic neurons of 10N. More ventrolaterally, 10VI had the highest density of large, darkly stained neurons of the three subnuclei. About 80% of all cells in this subnucleus were large neurons (20-25 μm diameter). At the level of the area postrema (Fig. 4.3b), 10N continued to be a prominent nucleus in contrast to surrounding structures. At this level, 10CeI continued as a subnucleus with moderately high cell density, but at this level it was located in the dorsomedial position. Dorsally, 10CaI appeared as a cell group with similar cell density as 10CeI (Fig4.3g), but contained neurons which appeared to be similar as those of 10DI

(Fig. 4.3d). At the caudal level (Fig. 4.3c), 10Ca occupied only a small area and was difficult to differentiate from surrounding structures. Under high power, large neurons with similar appearance to those of 10CeI were observed (Fig. 4.3h).

At 21 weeks, subdivisions of the 10N were more clearly visible (Fig. 4.4). At the open medulla level (Fig. 4.4a), 10DI continued to show low cell density of large cells. More large neurons (19-20 μm diameter) were visible in 10DI at this age than previously. They were of multipolar morphology (Fig. 4.4d). Among those large neurons, there were also presumptive glial cells of only about 3-4 μm diameter. Ventrally, 10CeI had relatively higher cellular density compared to 10DI; neurons of 10CeI were of either multipolar or bipolar shape (Fig. 4.4e). 10VI continued to have the highest cell density among the three subnuclei and neurons of 10VI also appeared to be bipolar and multipolar (Fig. 4.4f). At the level of the area postrema (Fig. 4.4b), 10CeI appeared to have comparatively higher cell density than the dorsally located 10CaI; however, large neurons within 10CeI were no different to that seen in 10CaI (Fig. 4.4g). At the caudal level (Fig. 4.4c), more large neurons were concentrated in the region of 10N (Fig. 4.4h), making 10Ca a more clearly demarcated subnucleus at this level.

By 25 weeks (Fig. 4.5), subdivisions which had appeared at the previous age (21 weeks) remained unchanged, but simply became better defined at all levels examined (Fig. 4.5 a-c), indicating that development of the subnuclear patterning of 10N had come to its final stage. In higher power images (Fig. 4.5d-h), the large neurons of various subnuclei, which were seen in previous ages had similar morphology to that at 21 weeks, however, the size of neurons was larger (25-30 μm diameter). Cells at this age were not as tightly

clustered as at previous ages.

4.2.2 Chemoarchitecture of the Developing Dorsal Motor Nucleus of Vagus

A. Calbindin Immunoreactivity

Cb immunoreactivity in 10N was mainly found at the open medulla with the caudal limit at the level of area postrema (Fig. 4.6). Caudal to the level of area postrema, Cb immunoreactive (Cb-ir) neurons were scarcely seen in 10N at any age (not shown).

At 13 weeks (Fig. 4.6a), Cb-ir neurons were mainly found in the ventral area, i.e., 10CeI, while 10DI was mainly devoid of Cb-ir neurons. It was not possible at this age to identify 10VI. Neurons of Cb immunoreactivity in 10CeI were of medium size (10-13 μm diameter) and of spherical shape. There were a few dendritic processes found in these neurons (Fig. 4.6b).

At 15 weeks (Fig. 4.6c), neurons with intense Cb immunoreactivity continued to be found mainly in the ventral subnuclei of 10N, i.e. 10CeI and 10VI. 10DI also contained a few Cb-ir neurons, but these were palely stained. CB-ir neurons with 10CeI and 10VI were of about 11-15 μm diameter and mainly round or oval shaped. Dendritic processes of Cb-ir neurons continued to be scarce and extended for only a few micrometers. 10VI had slightly higher cell density than 10CeI (Fig. 4.6d, e).

At 21 weeks (Fig. 4.6f), the distribution of Cb-ir neurons were similar to that seen at the previous age, with a few more neurons found in 10DI. CB-ir neurons in 10CeI and 10VI were trigonal, oval or spindle shaped. Dendritic processes of Cb neurons were more elongated, extending more than 20 μm (Fig. 4.6g and h).

At 25 weeks (Fig. 4.6i), distribution of Cb-ir neurons remained unchanged. Cb-ir neurons in 10CeI and 10VI were similar to the previous age, except that they were slightly larger (15-24 μm diameter) (Fig. 4.6j and k).

B. Tyrosine Hydroxylase Immunoreactivity

Neurons immunoreactive to TH in 10N at 13 weeks were sparsely distributed. At the open medulla level, neurons of various sizes (12-20 μm diameter) were found both in 10DI and 10CeI (Fig. 4.7a). The dendritic processes of TH immunoreactive (TH-ir) neurons were more than 30 μm long (Fig. 4.7e, d). At more caudal levels (Fig. 4.7b and c), only sparsely distributed TH-ir neurons could be identified in the 10CaI and 10Ca. Neurons of these subnuclei were of small to medium size (5-10 μm diameter) and spherical in morphology (Fig 4.7f).

At 15 weeks, a more intensive TH immunoreactivity appeared in 10N (Fig. 4.8). At the open medulla level (Fig 4.8a), 10DI continued to contain a dense cluster of TH-ir neurons of various sizes (15-22 μm, Fig 4.8d), whereas neurons aggregated at the ventrolateral area, which belonged to 10CeI at 13 weeks, were scattered in both 10CeI and 10VI. Neurons of both subnuclei have similar appearance, being oval or spindle shaped (15-20 μm diameter of long axis), with dendritc processes extending for about 40-50 μm (Fig. 4.8e, f). At more caudal levels (Fig. 4.8b, c), there were once again a few TH-ir neurons distributed in 10CaI and 10Ca. Neurons of both subnuclei appeared to be more mature than those of the previous age (10-20 μm diameter), being spherical or spindle shaped. Dendritic processes of these neurons extended as long as 25-30 μm (10Ca, Fig.

4.8g).

Distribution of TH-ir neurons in 10N at 21weeks was similar to that of the previous age (Fig. 4.9a-c), with more densely aggregated neurons found in the rostrally located 10DI, 10CeI and 10VI, and sparsely distributed neurons in the 10CaI and 10Ca. In high power images (Fig. 4.9d-f), TH-ir neurons in 10DI, 10CeI and 10VI featured as having medium to large somata (15-20 μm) and multiple dendritic processes (20-40 μm length). TH-ir neurons in and 10Ca (Fig. 4.9g) were elongated in shape, being either trigonal or spindle.

At 25 weeks (Fig. 4.10a-c), distribution of TH-ir neurons in 10N were similar to that of 21 weeks. A dense dendrtic plexus was present in 10DI, 10CeI and 10VI (Fig. 4.10d-f). Dendritic processes of some neurons extended for more than 100 μm (Fig. 4.10a). TH-ir neurons in 10CaI and 10Ca (Fig. 4.10g) were similar in morphology to those found in 21 weeks.

C. Calretinin and GAP-43 Immunoreactivity

After application of anti-Cr immunohistochemistry on the sections of medulla, 10N was found to be devoid of Cr-ir neurons, leaving it a negative area surrounded by the Cr positive Sol (Fig. 3.12). Therefore, in the present chapter, Cr immunoreactivity is not described in detail.

GAP-43 immunoreactivity was observed in specimens of 13 weeks and 21 weeks (Fig. 4.11). At 13 weeks (Fig. 4.11a-c), strong immunoreactivity was found in all subnuclei, i.e., 10DI, 10CeI, 10CaI and 10Ca, with the strongest presentation in the 10CaI (Fig. 4.11b).

The difference of strengths of GAP-43 immunoreactivity between subnuclei of 10N and the surrounding structures provided a clearer boundary of 10N than in Nissl preparations. At 21 weeks (Fig. 4.11d-f), the strength of GAP-43 immunoreactivity had declined greatly, indicating the maturation of axons by the age of 21 weeks, although 10N still had relatively intensive immunoreactivity compared with the surrounding structures.

D. Substance P Immunoreactivity

Immunohistochemistry against SP was only applied on the specimen at 21 weeks. At 21 weeks, 10N in general contained strong immunoreactivity compared to the surrounding structures, with 10CeI and 10CaI had higher intensity of SP immunoreactivity, while 10DI, 10VI and 10Ca having lower (Fig. 4.12a-c). In high power images (Fig. 4.12d-h), medium sized neurons (10-13 μm diameter) as well as dendritic fibers were identified in all subnuclei of 10N. These neurons were multipolar in morphology and had short dendritic processes about 10-20 μm in length.

4.3 Discussion

4.3.1 Development of Cyto- and Chemoarchitecture of Dorsal Motor Nucleus of Vagus

The present study delineated the cyto- and chemoarchitecture of 10N in the fetal human brain. Generally, 10N refers to the longitudinal group of magnocellular vagal preganglionic neurons that extends rostrocaudally in the dorsomedial medulla. However, the band of areas dorsal and ventral to this cell cluster, which contain smaller neurons, are also regarded as a part of 10N, namely the dorsal fringe (DrF) and medial fringe (MeF)

(McRitchie and Tork, 1993). Accordingly, the prefered name for10N in international anatomical terminology (*Paris Nomina Anatomica*) is dorsal nucleus of the vagus (Nara et al., 1991) rather than the commonly used "dorsal motor nucleus of vagus", since DrF and MeF do not directly serve motor function. However, it was not possible in the present study to differentiate DrF from the adjacent SolM and SolIM, probably due to the immaturity of the cytoarchitecture during fetal life. While MeF has been clearly identified in the present study, it was not found to present much structural diversity and will not be considered in detail here. Consequently, the present study focuses only on the principal part of 10N, which contains vagal preganglionic neurons.

In the adult human, 10N was found to be inhomogeneous and discontinuous, with higher AChE reactivity found in the ventral and caudal parts of the nucleus (McRitchie and Tork, 1993). Huang et al. (Huang et al., 1993b) further divided 10N into 9 subnuclei according to their rostrocaudal position and reactivity of neurons and neuropil to AChE and homology with the 10N of pigeon brain (Katz and Karten, 1983). Heterogeneity of 10N preganglionic neurons has also been found in other species such as rat (Laughton and Powley, 1987) and rabbit (Getz and Sirnes, 1949), although the described subdivisional patterns of 10N in these species were not as comprehensive as that for the human (Huang et al., 1993b).

Neurogenesis of 10N commences at embryonic stage 13 (approximately 5 weeks) and cell migration occurs during stages 13 -17 (6 weeks) (Muller and O'Rahilly, 2004). In the present study, at 9 weeks, 10N consisted of merely a group of immature cells, while by 13 weeks, all parts of 10N were composed of densely packed immature cells.

Subnuclear divisions of 10N were not clear in Nissl preparations until 15 weeks, at which time the ventrally and caudally located subnuclei, i.e., 10CeI, 10VI and 10Ca contained higher densities of neurons compared to the dorsally located 10DI and 10CaI. Cytoarchitectural development of 10N has been reported in the human (Nara et al., 1991) as well as in the rat (Kalia, 1992). In the human, Nara and co-workers (Nara et al., 1991) found that 10N was divisible from 16 weeks into ventral, dorsal and caudal subnuclei on the basis of Kluver-Barrera staining, with higher cellular density found in the ventral and caudal subnuclei. Such an early division into subnuclei is also supported by the present study, although the ventral and caudal parts were further divided into various subnuclei in the present study.

Immunoreactivity for Cb in 10N has only been briefly mentioned previously by several investigators in laboratory animals (Celio, 1990; De Leon et al., 1994; Menetrey et al., 1992). These reports were in some ways controversial, and none of the investigators have made a close examination of this nucleus. Low to moderate density of Cb-ir neurons was found in the cat 10N (De Leon et al., 1994), but not in the rat (Celio, 1990). This negative finding was supported by Menetrey (Menetrey et al., 1992) who investigated Cb immunoreactivity in the nearby Sol in rats. The present study found a group of Cb-ir neurons at the rostral levels of 10N, mainly located in the ventral subdivisions, i.e., 10CeI and 10VI. This distribution was consistent from age to age and these neurons showed a trend of gradual maturation as fetal life progressed. This finding shows that in fetal humans, like in adult cats (De Leon et al., 1994), there is a distinct group of Cb-ir neurons within 10N. Although De Leon and co-workers (De Leon et al., 1994) have suggested that

the Cb-ir neurons in 10N, together with those in Sol, may be involved in cardiovascular and respiratory mechanisms, the actual function of this group of neurons remains to be tested. Nevertheless, in the present study, as judged by distribution of Cb-ir neurons, those neurons of the rostral 10N probably belong to a distinct subgroup. Therefore, the territory of 10CeI at different levels in the Nissl preparations in this study probably includes diverse groups of Cb-ir and Cb negative neurons.

Catecholamines are among the earliest neurotransmitters detected in the human brain. They are assumed to be morphogens (Pendleton et al., 1998) and are known to stimulate neuronal maturation in the fetal brain (Verney et al., 2001). The ventrolaterally located A1 and dorsomedially located A2 groups of neurons in the medulla have been shown to be TH-ir by 4.5 to 6 weeks (Puelles and Verney, 1998). TH-ir neurons in 10N were identified as part of A2/C2 catecholaminergic neuronal group at 14.5 weeks and showed mature morphology by 21 weeks (Lorke et al., 2003). In the present study, the regional distribution of the TH-ir neurons in fetal 10N was studied in more detail than that by Lorke et al. (Lorke et al., 2003). TH-ir neurons were detected in subnuclei 10DI, 10VI, 10CaI and 10Ca as early as 13 weeks and increased in number by 15 weeks. By 21 weeks, TH-ir neurons in 10N were shown to be quite mature and the morphology of neurons was very similar to that of the adult 10N (Huang et al., 1993a).

Regional distribution of TH-ir neurons is distinctive in the human 10N. Huang and colleagues (Huang et al., 1993a) reported that TH-ir neurons are mainly distributed in the periphery of 10N, which is the area adjacent to MeF, while the central parts of the principal subnuclei do not contain many TH-ir neurons. Such a distribution of TH-ir

neurons could also be seen in the present study at 15 weeks at the open medulla level. At this age, TH-ir neurons extended as a dorsomedial-to-ventrolateral band along the ventromedial border of the principal part of 10N. It is not certain if the TH-ir neurons in 10N function as parasympathetic effectors, since no study of double-labeling of TH with cholinergic or HRP immunohistochemistry in humans is possible. However, colocalization of TH and choline acetyltransferase (ChAT) was revealed in the rodent 10N. This double-labeling shows that neurons containing TH belong to efferent vagal preganglionic neurons (Armstrong et al., 1990). TH-ir neurons in 10N were also shown to contribute to the vagal projection to the stomach in the rat (Hayakawa et al., 2004). Therefore, it is highly probable that TH-ir neurons in human 10N are involved in parasympathetic preganglionic functions.

Immunolocalization of GAP-43 in 10N was briefly reported in adult opossums (*Didelphis virginiana*)(Zou and Martin, 1995) as well as human fetuses (Kinney et al., 1993). In the present study, intensive GAP-43 immunoreactivity was found in the neuropil in 10N as early as 13 weeks. Since GAP-43 is closely related to the growth and remodeling of the nervous system (Gordon-Weeks, 1989; Kinney et al., 1993; Zou and Martin, 1995), strong immunoreactivity in 10N suggests highly active axonal growth in the vicinity of 10N neurons. Immunoreactivity for GAP-43 was reduced by 21 weeks but remained strong in 10N compared with surrounding structures; an observation which suggests persistence of synaptic reorganization in axons of afferents to 10N throughout development (Kinney et al., 1993).

In the present study, SP-ir neurons were identified in various subnuclei of 10N at 21

weeks. Unlike TH-ir neurons, which were mainly located at the ventromedial part of 10N, SP-ir neurons in 10N were distributed evenly in the principal subnuclei of 10N, with 10CeI containing slightly higher numbers of SP-ir neurons. SP immunoreactivity was reported to be present in human fetal 10N as early as 13 to 16 weeks by other authors (Nomura et al., 1982; Wang et al., 1993), which is consistent with the present study. However, neither of those authors has described the morphology of SP-ir neurons in fetal 10N. According to Huang et al. (Huang et al., 1993a), SP-ir neurons in the adult 10N are mainly distributed in the intermediate-to-caudal segments of 10N, and are comprised of three types of cells. In the present study, a similar distribution of SP-ir was present in the fetal 10N. However, it was not possible at this age to differentiate the subtypes of SP-ir neurons, because they were still in a immature state compared with adult neurons. Physiological studies on the role of SP in 10N have shown that this neurotransmitter is mainly involved in regulating gastrointestinal movement (Lewis and Travagli, 2001; Saito et al., 2003). The receptor for SP (neurokinin 1 receptor, NK1) found on 10N neurons, plays an important role in reducing gastric motility and evoking gastric relaxation (Krowicki and Hornby, 1996; Krowicki and Hornby, 2000) and is the major factor in controlling major types of vomiting (Saito et al., 2003). Therefore, emergence of SP-ir neurons in 10N at mid-gestation in the present study may be suggestive of early establishment of a controlling mechanism on gastrointestinal motility during fetal life.

4.3.2 Development of Vagal Functions Involving the Dorsal Motor Nucleus of Vagus

Preganglionic parasympathetic motor neurons located in 10N innervate the

subdiaphragmatic viscera via 10n (Fox and Powley, 1992). Neurons within 10N projecting to various subdiaphragmatic organs are arranged in longitudinal columns parallel to each other on either side of medulla(Fox and Powley, 1985). The medial column contributes to the gastric branches of the vagus nerve (left 10N to anterior and right to posterior gastric branch), while the lateral column contributes to the celiac plexus branches of the vagus nerve (left 10N to accessory celiac and right to main celiac branch). Another diffuse column, which is coextensive with the left medial column, represents the hepatic branch of the vagus nerve (Fox and Powley, 1985). Although the present study was not able to decipher the columnar arrangement of neuronal groups, since these are only visible in horizontal sections, it is possible to interpret the columnar organization of Fox and Powley (Fox and Powley, 1985) in the context of the anatomical subnuclei described in the present study. It is probable that the dorsomedially located 10DI and 10CeI are mainly involved in gastric functions, while the ventrolaterally located 10VI and 10CaI are involved in intestinal (celiac) functions. Since only the right side 10N was studied in the present report, strictly speaking the hepatic representation should not be present (Fox and Powley, 1985), but there were no cytoarchitectonic differences between the two sides; thus, a substrate for functional lateralization proposed by Fox and Powley (Fox and Powley, 1985) was not detected in this study.

In the human, ultrasonographic images have shown that gastric peristalsis appears as early as 14 weeks of gestation. The peristaltic waves occur sporadically during early pregnancy and increase and consolidate into prolonged clusters of peristaltic waves by 24 weeks (Sase et al., 2005). Such movement is coincidental with increasing vagal innervation

of the stomach during the second trimester (Abel et al., 1998) and is associated with increasing exchange of fluid between the stomach and amniotic sac (Sase et al., 2005). This exchange is critical to fetal developmental processes such as regulation of amniotic fluid volume and composition, and contributes to recirculation of amniotic proteins and growth factors to the fetus (Sase et al., 2005). In the present study 10N, which is mainly involved in regulation of gastric motility via the vagus nerve, appeared as a distinctive neuronal group by 13 weeks, and approached the adult appearance in cyto- and chemoarchitecture by 21 to 25 weeks. Thus the time-course of the development of 10N occurs in parallel with the functional maturation of the gastrointestinal system (Sase et al., 2005; Sase et al., 1999). These findings suggest that the anatomical development of 10N mirrors the functional development of its target organs and, therefore, provides a foundation for functional investigations of the control of the developing human viscera by 10N.

In addition to the gastrointestinal projections, 10N has been reported to be involved in cardiovascular functions (Cheng et al., 1999; Kalia and Mesulam, 1980a; Kalia and Mesulam, 1980b). In the rat, 10N sends efferent projections to all three major ganglionic plexuses located in the epicardium and the axons form dense basket terminals around principal cardiac neurons. Like the 10N projections to the gastrointestinal tract, the vagal preganglionic projections from 10N to the cardiac plexus also exhibit lateralization, with the right 10N sending more efferent fibers to surround the principal neurons embedded within the sinoatrial plexus, whereas the left 10N preferentially projects to the principal neurons in the atrioventricular plexus (Cheng et al., 1999). At present, the functional

question of whether 10N neurons belong to the cardiac chronotropic (affecting rate), dromotropic (affecting conduction velocity) or inotropic (affecting force of contraction) centres has not been clearly answered, although physiological studies have revealed that electrical stimulation of 10N may produce either negative chronotropic or negative inotropic effects (Geis and Wurster, 1980; Gunn et al., 1968). In the human fetus, the first echocardiographic recordings of cardiac movement have been obtained in early second trimester (Allan et al., 1981; Allan et al., 1980), although cardiac function must occur as early as 18 days of gestation (Moore, 1977). The early development of the cyto- and chemoarchitecture of 10N during the second trimester as seen in the present study, together with the establishment of a contribution from 10N to the vagal projection by 13 weeks (Cheng et al., 2004, Chapter 5), implies the early development of anatomical substrates for cardiac functional regulation in the human fetal CNS.

4.4 Concluding Remarks

In conclusion, the present study has revealed that 10N, the major parasympathetic preganglionic nucleus in the brain, begins its development as early as 9 weeks and appears as a distinctive neuronal group both cyto- and chemoarchitectonically as early as 13 weeks. Subnuclear divisions within 10N appear at 15 weeks and approach a mature organization during the period from 21 to 25 weeks. The structural development of 10N appears to occur in parallel with functional maturation of the cardiovascular and gastric movements (Cheng et al., 1999; Sase et al., 2005) which 10N controls.

Figure 4.1 Photomicrographs of Nissl stained section of fetal 10N at 9 weeks: (a) low power image showing 10N with its surroundings; the rectangle indicates the area which (b) was taken; (b) high power image showing cellular morphology of 10N.

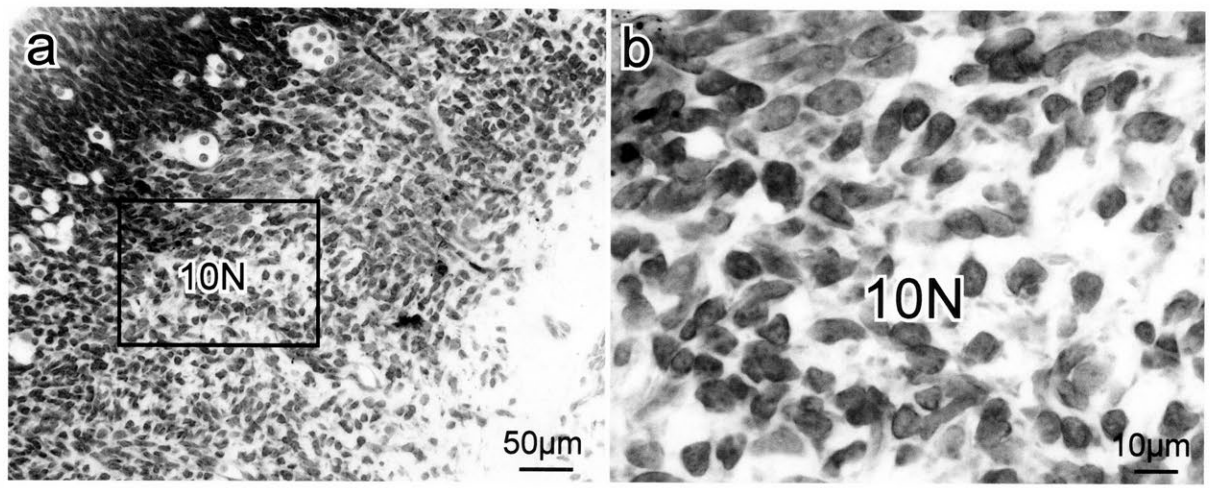

Figure 4.1

Figure 4.2 Photomicrographs of low and high power images of Nissl stained sections at 13 weeks. (a) Low power image at level of open medulla at the rostral limit of 12N; (b) Low power image at the level of area postrema at the rostral limit of the gracile nucleus (Gr); (c) Low power image at the level caudal to the obex close to the medulla-spinal cord junction. (d)-(g) High power images of subnuclei in 10N, arrows in (f) indicates the large, darkly stained neurons in 10CaI.

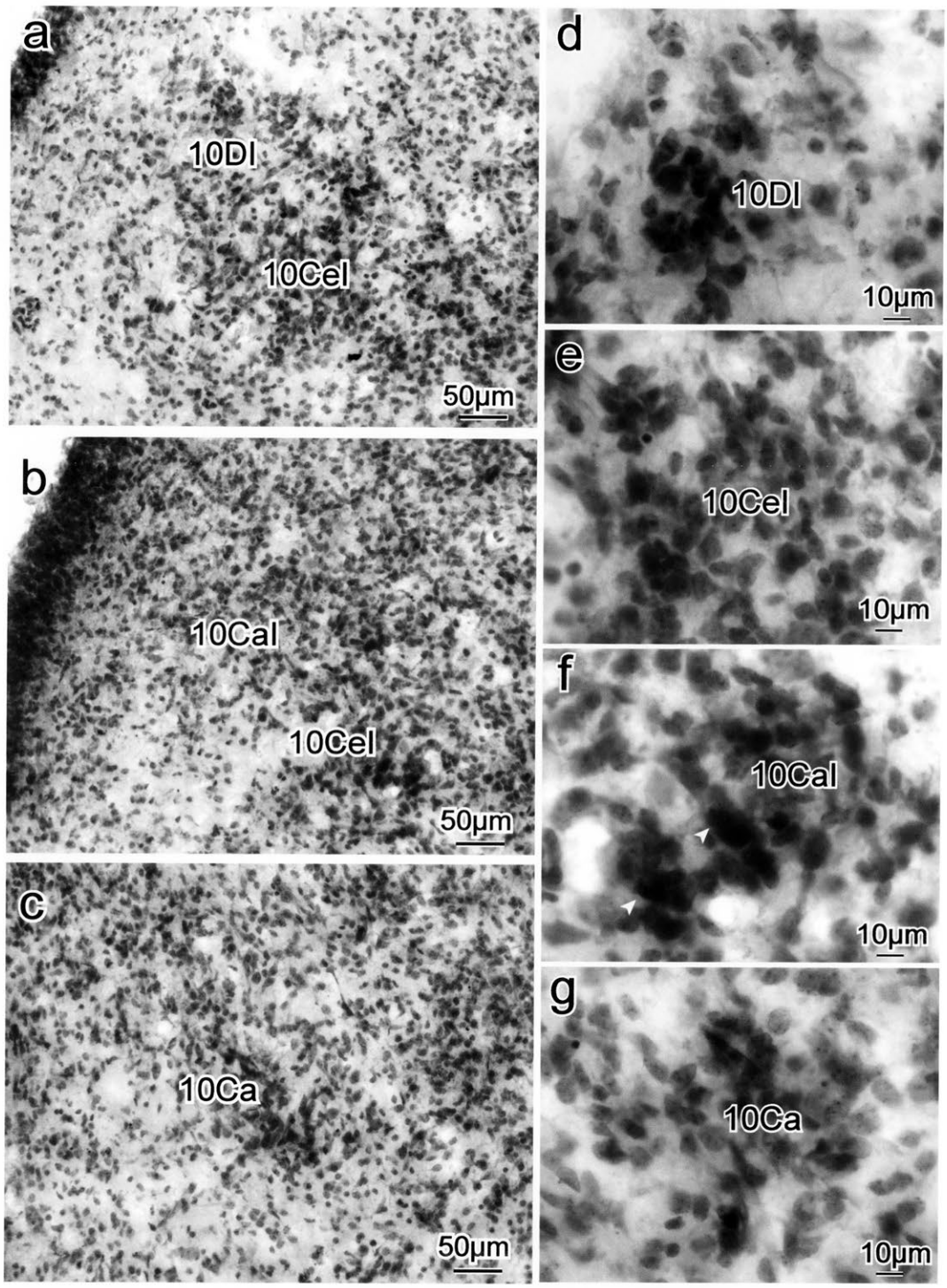
a
10DI
10CeI
50μm
b
10CaI
10CeI
50μm
c
10Ca
50μm
d
10DI
10μm
e
10CeI
10μm
f
10CaI
10μm
g
10Ca
10μm

Figure 4.2

Figure 4.3 Photomicrographs of low and high power images of Nissl stained sections at 15 weeks. (a)-(c) Low power images of 10N, levels chosen in accordance with Figure 4.2. (d)-(h) High power images of neurons in 10N subnuclei. It is noted that the ventrally and caudally located subnuclei (10VI, 10CeI and 10Ca) contained more large neurons than the dorsally located subnuclei (10DI and 10CaI).

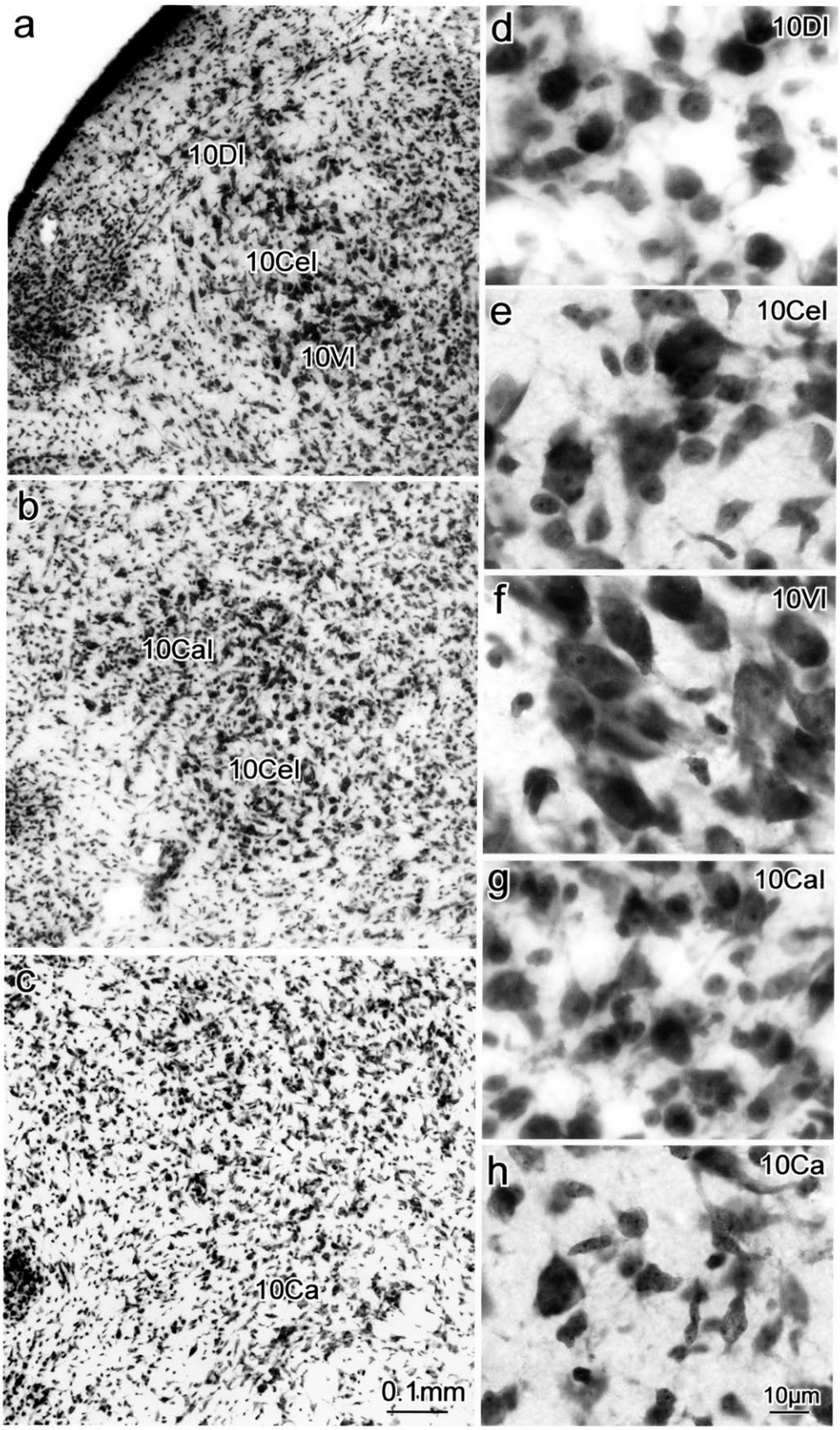
a
10DI
10CeI
10VI
b
10CaI
10CeI
c
10Ca
0.1mm
d
10DI
e
10CeI
f
10VI
g
10CaI
h
10Ca
10μm

Figure 4.3

Figure 4.4 Photomicrographs of low and high power images of Nissl stained sections at 21 weeks. (a)-(c) Low power images of 10N, levels chosen in accordance with Figure 4.2. (d)-(h) High power images of neurons in 10N subnuclei. More large neurons now appear in (d) 10DI and (g) 10CaI, while (e) 10CeI, (f) 10VI and (h) 10Ca continue to contain higher density of large neurons than 10DI and 10CaI.

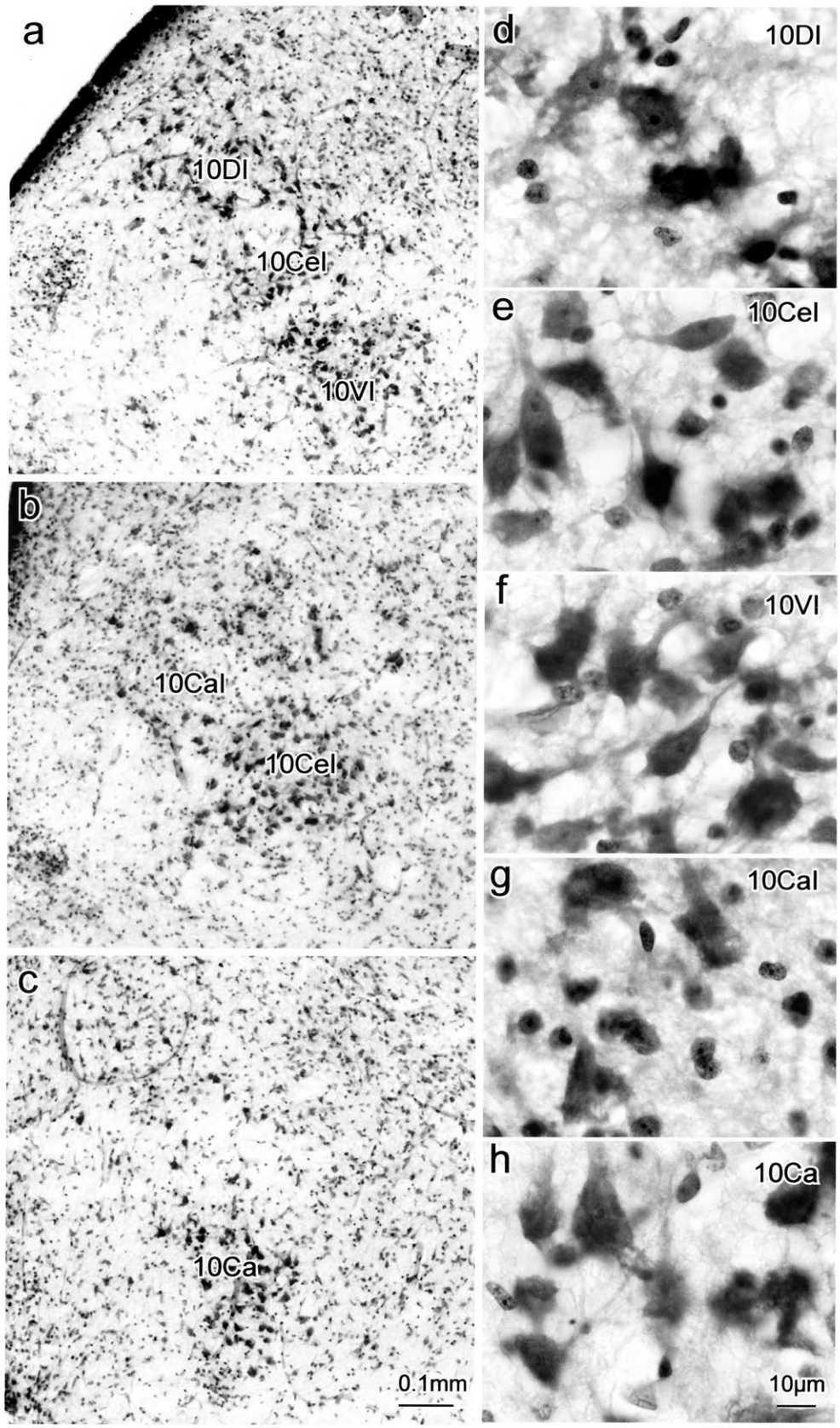
a
10DI
10CeI
10VI
b
10CaI
10CeI
c
10Ca
0.1mm
d
10DI
e
10CeI
f
10VI
g
10CaI
h
10Ca
10μm

Figure 4.4

Figure 4.5 Photomicrographs of low and high power images of Nissl stained sections at 25 weeks. (a)-(c) Low power images of 10N, levels chosen in accordance with Figure 4.2. (d)-(h) High power images of 10N subnuclei. Appearance of neurons in 10N at 25 weeks is similar to that of 21 weeks but neurons are larger in size.

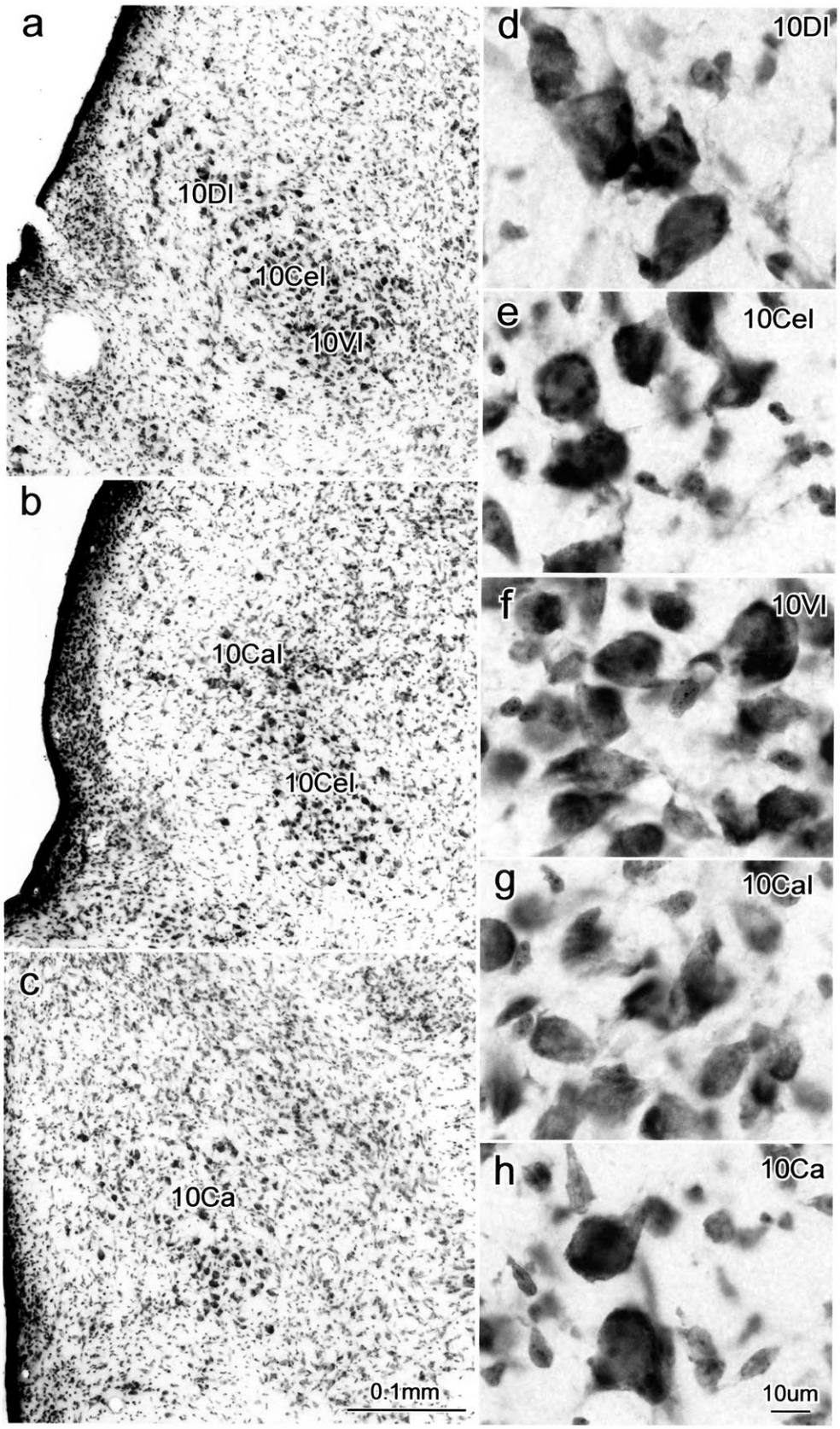
a
10DI
10CeI
10VI
b
10CaI
10CeI
c
10Ca
0.1mm
d
10DI
e
10CeI
f
10VI
g
10CaI
h
10Ca
10um

Figure 4.5

Figure 4.6 Photomicrographs of Cb-ir somata in 10N subnuclei at various ages. (a) Low power image showing Cb immunoreactivity in 10N at 13 weeks; (b) High power image of Cb-ir somata in 10CeI at 13 weeks; (c) Low power image of Cb immunoreactivity in 10N at 15 weeks; (d) (e) High power image of Cb-ir somata in 10CeI and 10VI at 15 weeks; (f) Low power image of Cb immunoreactivity in 10N at 21 weeks; (g) (h) High power image of Cb-ir somata in 10CeI and 10VI at 21 weeks; (i) Low power image of Cb immunoreactivity at 25 weeks; (j) (k) High power image Cb-ir somata in 10CeI and 10VI at 25 weeks.

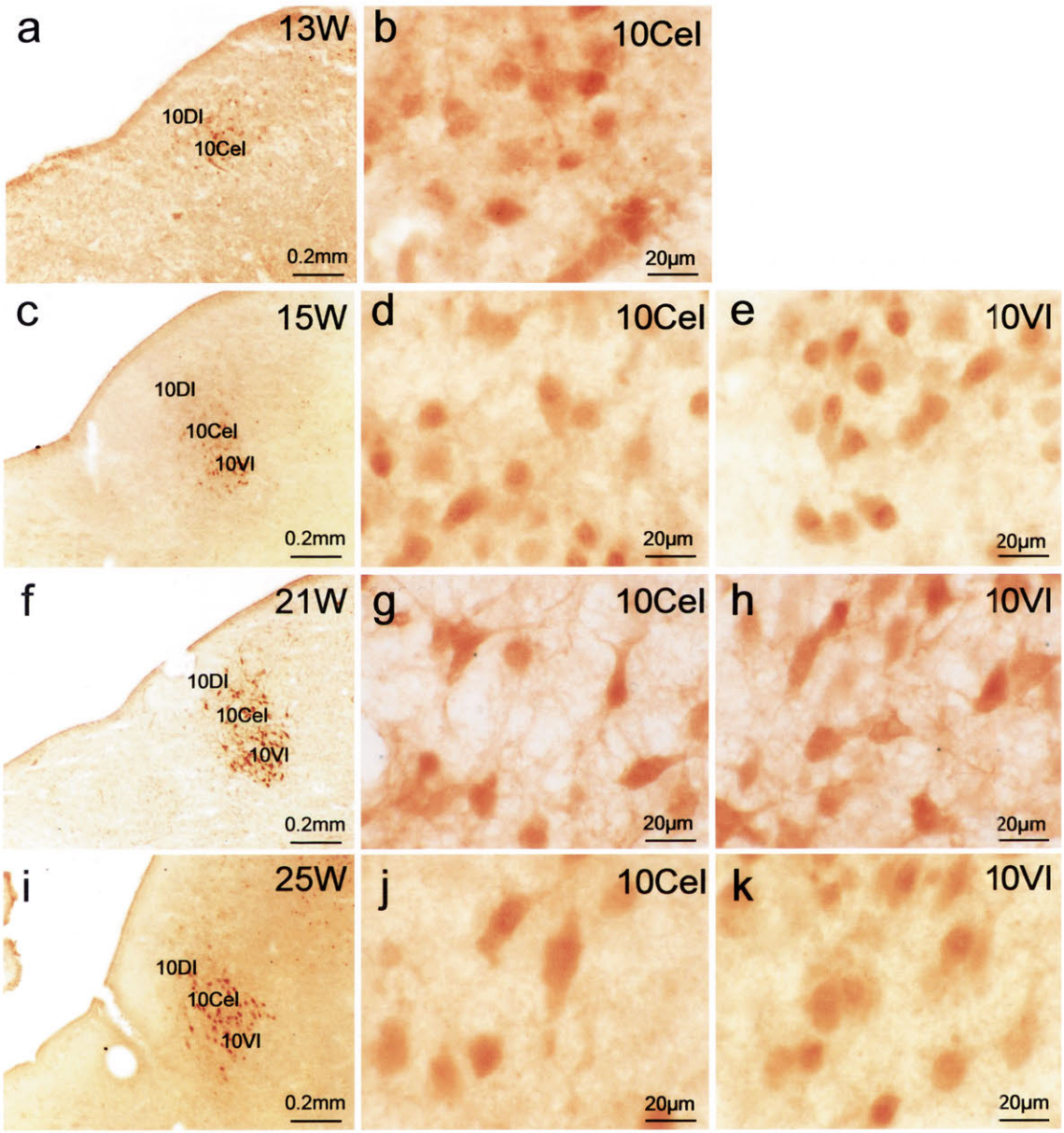
a
13W
10DI
10CeI
0.2mm
b
10CeI
20μm
c
15W
10DI
10CeI
10VI
0.2mm
d
10CeI
20μm
e
10VI
20μm
f
21W
10DI
10CeI
10VI
0.2mm
g
10CeI
20μm
h
10VI
20μm
i
25W
10DI
10CeI
10VI
0.2mm
j
10CeI
20μm
k
10VI
20μm

Figure 4.6

Figure 4.7 Photomicrographs of low and high power images of TH immunoreactivity in 10N at 13 weeks. (a) Low power image at the level of open medulla, both 10DI and 10CeI contains TH-ir neurons; High power images of TH-ir neurons in 10DI and 10CeI are shown in (d) and (e); (b) Low power image at the level of area postrema, most TH-ir neurons are in 10CeI; (c) Low power image at the caudal level, TH-ir neurons in 10Ca are shown at high power in (f).

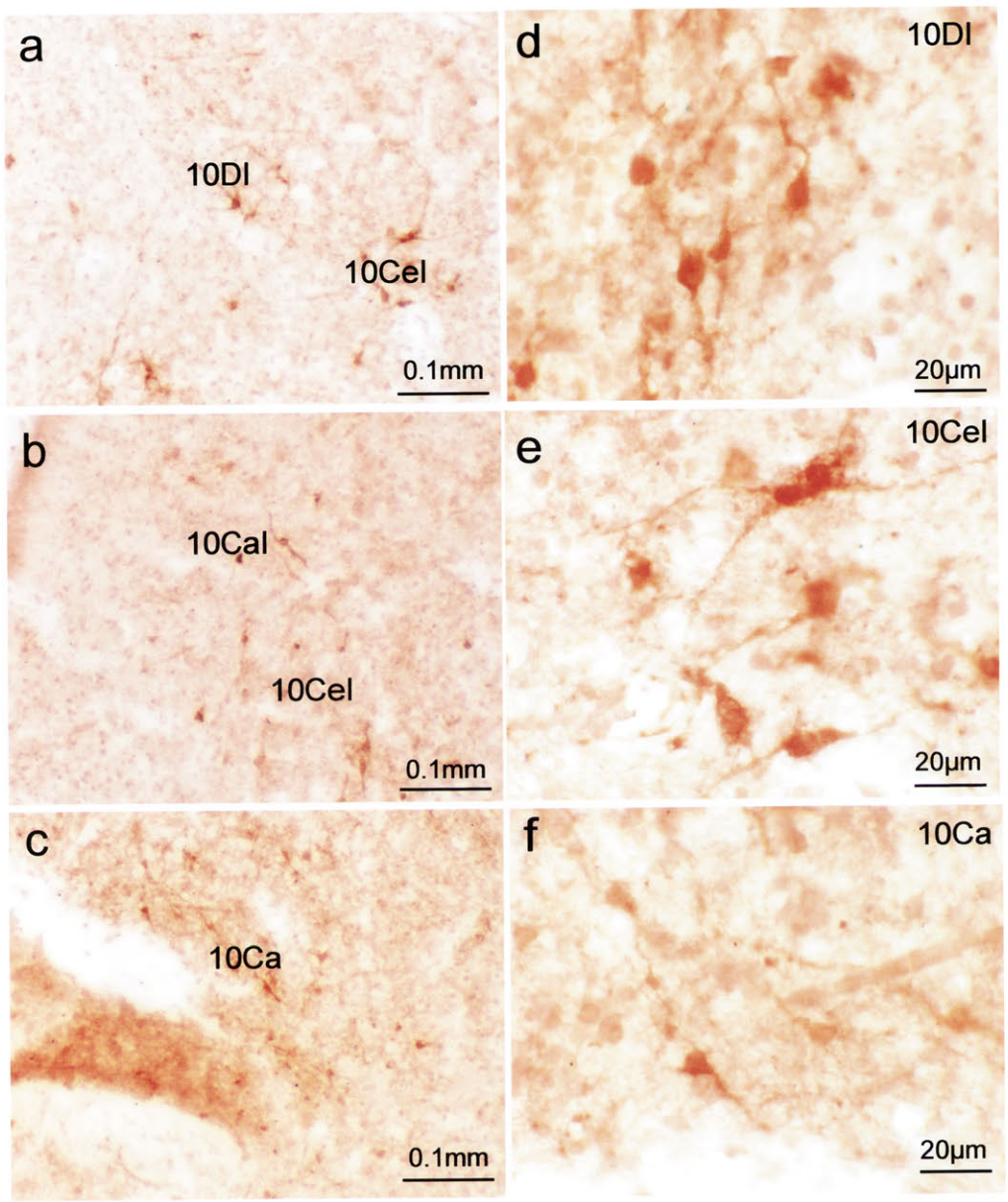
a
10DI
10CeI
0.1mm
d
10DI
20µm
b
10CaI
10CeI
0.1mm
e
10CeI
20µm
c
10Ca
0.1mm
f
10Ca
20µm

Figure 4.7

Figure 4.8 Photomicrographs of low and high power images of TH immunoreactivity in 10N at 15 weeks. (a)-(c) Low power images at three selected rostrocaudal levels in accordance with Figure 4.2; (d)-(g) High power images of TH-ir neurons in 10DI, 10VI, 10CeI and 10Ca.

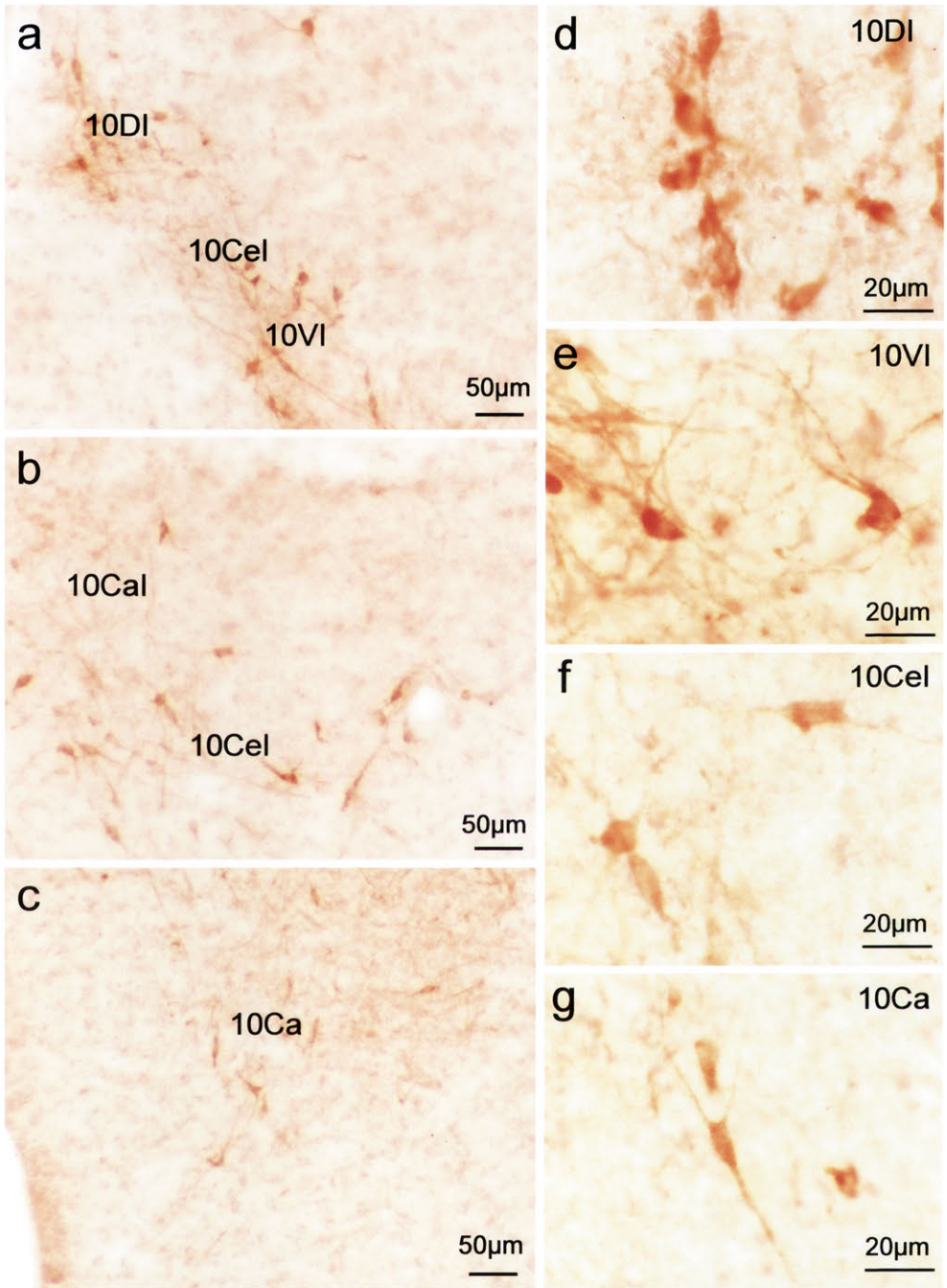
a
10DI
10CeI
10VI
50µm
b
10CaI
10CeI
50µm
c
10Ca
50µm
d
10DI
20µm
e
10VI
20µm
f
10CeI
20µm
g
10Ca
20µm

Figure 4.8

Figure 4.9 Photomicrographs of low and high power images of TH immunoreactivity in 10N at 21 weeks. (a)-(c) Low power images at three selected rostrocaudal levels in accordance with Figure 4.2; (d)-(g) High power images of TH-ir neurons in 10DI, 10CeI, 10VI and 10Ca.

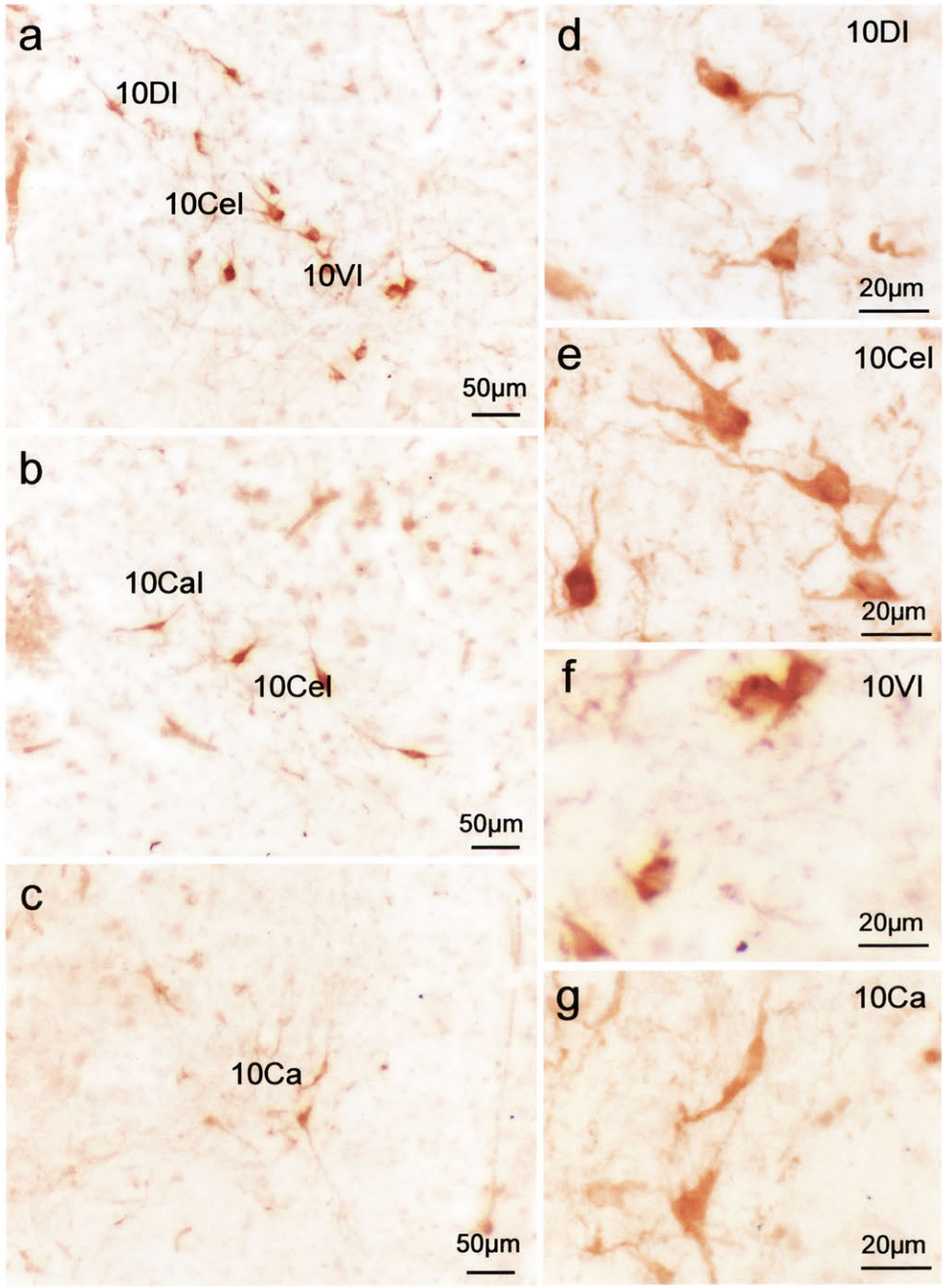
a
10DI
10CeI
10VI
50μm
b
10CaI
10CeI
50μm
c
10Ca
50μm
d
10DI
20μm
e
10CeI
20μm
f
10VI
20μm
g
10Ca
20μm

Figure 4.9

Figure 4.10 Photomicrographs of low and high power images of TH immunoreactivity in 10N at 25 weeks. (a)-(c) Low power images at three selected rostrocaudal levels in accordance with Figure 4.2; (d)-(g) High power images of TH-ir neurons in 10DI, 10CeI, 10VI and 10Ca.

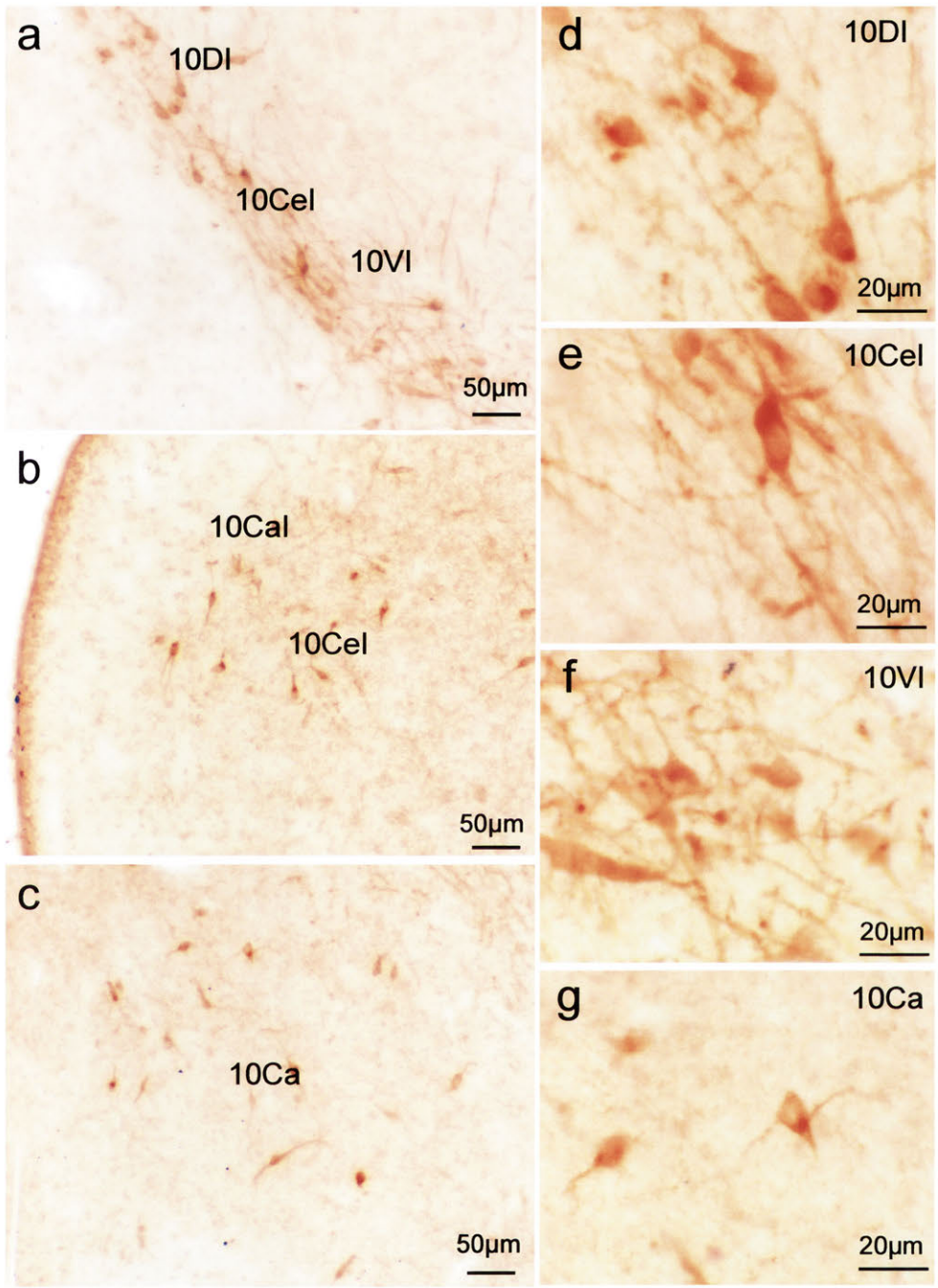
a
10DI
10CeI
10VI
50µm
b
10CaI
10CeI
50µm
c
10Ca
50µm
d
10DI
20µm
e
10CeI
20µm
f
10VI
20µm
g
10Ca
20µm

Figure 4.10

Figure 4.11 Photomicrographs of GAP-43 immunoreactivity in 10N at (a)-(c) 13 weeks and (d)-(f) 21 weeks. Note the stronger GAP-43 expression in 10N compared with the surrounding structures and the global decline of GAP-43 immunoreactivity from 13 to 21 weeks.

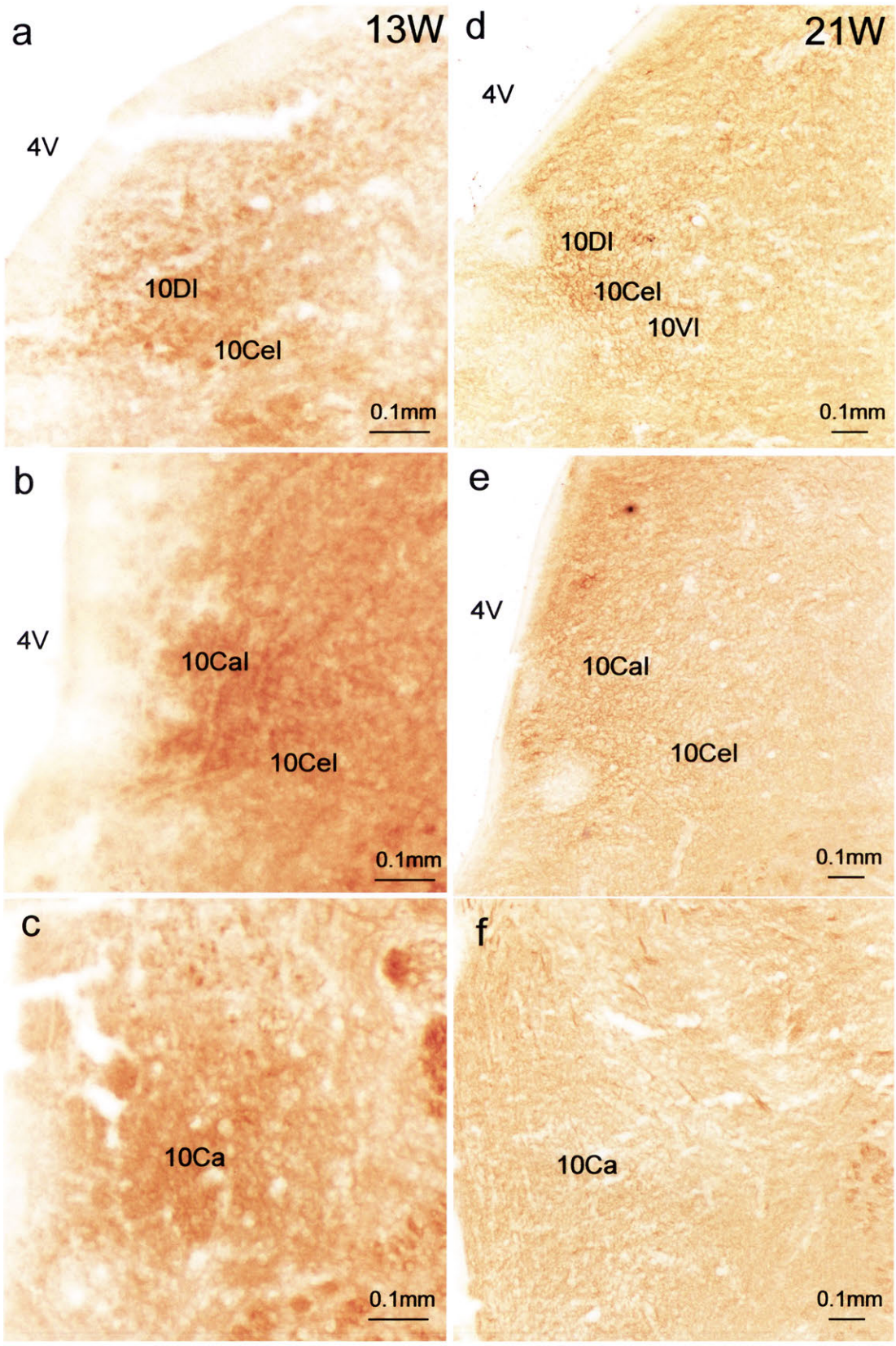
a
13W
4V
10Dl
10Cel
0.1mm
d
21W
4V
10Dl
10Cel
10Vl
0.1mm
b
4V
10Cal
10Cel
0.1mm
e
4V
10Cal
10Cel
0.1mm
c
10Ca
0.1mm
f
10Ca
0.1mm

Figure 4.11

Figure 4.12 Photomicrographs of SP immunoreactivity in 10N at 21 weeks. (a)-(c) Low power images showing SP immunoreactivity in subnuclei of 10N at different levels. (d)-(h) High power images of SP-ir neurons and neuropil in 10DI, 10CeI, 10VI, 10CaI and 10Ca, respectively.

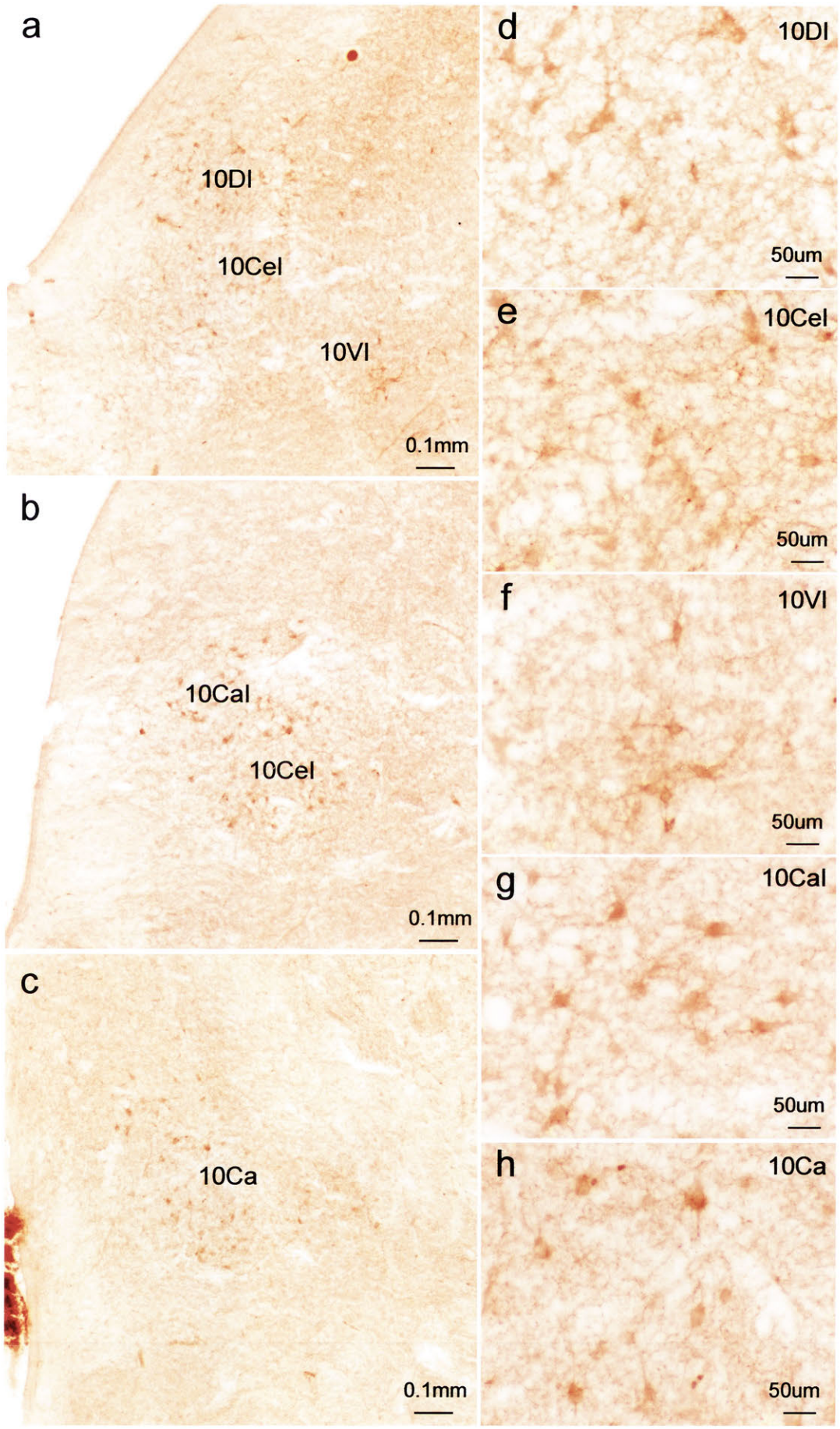
a
10DI
10CeI
10VI
0.1mm
b
10CaI
10CeI
0.1mm
c
10Ca
0.1mm
d
10DI
50um
e
10CeI
50um
f
10VI
50um
g
10CaI
50um
h
10Ca
50um

Figure 4.12

Chapter 5 Development of Central Vagal Sensory and Motor Connections in the Human

5.1 Introduction

The vagus nerve (10n) is the major visceral cranial nerve containing (a) afferent fibers that conduct visceral sensory input from the pharynx, larynx, trachea, the thoracic and abdominal viscera, and a few scattered taste buds in the region of the epiglottis, and (b) efferent fibers from preganglionic motoneurons in the medulla that project to the cardiovascular, respiratory and gastrointestinal viscera in the thorax and abdomen (Altman and Bayer, 1982; Bieger and Hopkins, 1987; Blessing, 1997; Broussard and Altschuler, 2000a; Cheng and Powley, 2000; Cheng et al., 1997; Cheng et al., 1999; Kalia and Mesulam, 1980a; Kalia and Mesulam, 1980b; Rinaman and Levitt, 1993).

The termination field of the sensory vagus nerve is mainly located in the solitary nucleus (Sol), which is a complex of as many as ten subnuclei located in the dorsomedial medulla between the dorsal motor nucleus of vagus (10N) ventromedially, the area postrema (AP) dorsally and the cuneate nucleus (Cu) laterally. Its organization has been studied in many mammalian species including humans (Altman and Bayer, 1982; Cheng and Powley, 2000; Cheng et al., 1997; Cheng et al., 1999; Kalia and Mesulam, 1980a; Kalia and Mesulam, 1980b; Loewy, 1990; McRitchie and Tork, 1993; Saper, 1995; Tork et al., 1990).

The visceral effector neurons which send axons to upper gastrointestinal, cardiovascular and respiratory organs are mainly located in the ambiguus nucleus (Amb) and 10N (Huang et al., 1993a; Kitamura et al., 1993; Lawn, 1966). Neurons of both nuclei possess extensive dendrites that receive input from the Sol. This close connection between the sensory and motor neurons of the vagus nerve implies the presence of an

integrated neuronal circuit controlling the autonomic reflexes of the thoracic and abdominal viscera (Cunningham and Sawchenko, 1989).

Although the connections of the vagus nerve have been studied extensively in adult experimental species both morphologically and functionally (Barraco and Robin, 1994; Broussard and Altschuler, 2000a; Loewy, 1990; Ritter et al., 1992), the development of central vagal sensory and motor connections has received much less attention and none so far in humans. Rinaman and Levitt (Rinaman and Levitt, 1993) used carbocyanine dye tracing techniques to study the establishment of vagal connections of the Sol, 10N and Amb in embryonic and fetal rats. Zhang and Ashwell (Zhang and Ashwell, 2001a) examined in more detail the development of the distribution of vagal afferents to the rat Sol and revealed the viscerotopic pattern of cranial afferent fibers in the different subdivisions of the developing Sol. However, no carbocyanine dye studies have been made of vagal afferents and efferents in either adult or developing human brainstem.

Establishment of vagal connections is clearly of major significance for visceromotor and respiratory function because the vagus provides the afferent limb of respiratory reflexes and afferent and effector pathways in control of cardiovascular and digestive function. In the human, the cardiorespiratory and gastrointestinal organs develop at an early embryonic stage and achieve morphological and functional maturity long before the end of gestation. However, it remains unclear at what developmental stage the neural circuits which control the functions of these visceral organs achieve maturity in humans. The present study set out to determine the time-course of maturation of the distribution of vagal afferents within the subnuclei of the solitary nuclear complex and the

morphological development of the vagal efferent neurons in 10N.

5.2 Results

Analysis of the cyto- and chemoarchitecture of the development of Sol and 10N was carried out in the previous chapters. These have provided a comprehensive subnuclear topography of these structures for the study of the distribution of DiI labeled afferents and efferents described below.

5.2.1 DiI Labeling of Vagal Afferents and Central Projections at 8 to 9 Weeks of Development

Figure 5.1 shows labeling of sensory neurons of the inferior vagal ganglion (10Gn) at 7 to 8 weeks of gestation (head length 7.5 mm; crown-rump length 16.5 mm, Fig. 5.1a) identified after application of DiI to the vagus nerve at the level of the aortic arch. Labeling was also seen in the mantle layer of developing myelencephalon (Fig 5.1b) at the same developmental stage, apparently in rootlets and processes of the vagus nerve as it entered the brainstem. At this point in development, no labeling of radial glia (as reported following labeling of rodent vagus nerve with DiI (Zhang and Ashwell, 2001a) was seen, and labeled cells were confined to the region near the attachment of the vagus nerve along the lateral myelencephalon.

About a week later (approximately 61 days since last menstrual period (LMP), head length 10.5 mm; crown-rump length 19 mm as shown in Fig. 5.1c-e), numerous labeled cells were found in the vicinity of the sulcus limitans (Fig. 5.1c), although occasional presumptive labeled radial glia were also found in the medial basal plate of the

myelencephalon (Fig. 5.1d). All labeled somata were found within 100 to 200 μm of the ventricular lining, indicating that dispersal to the site of 10N had not yet occurred. The labeled cells were all of bipolar morphology with soma diameters of the order of 7 to 9 μm (short axis) by 12 to 15 μm (long axis). Many labeled cells showed processes connecting the soma to the ventricular surface.

5.2.2 DiI Labeling of Afferents and Neurons at 13 Weeks of Gestation

Figures 5.2 and 5.3 show examples of DiI labeled afferent terminal fields and retrogradely labeled neurons following insertion of DiI into the vagal nerve rootlets at 13 weeks of gestation. A line diagram shows the labeled area in coronal sections (Fig. 5.2a). Figures 5.2b to 5.2g show termination patterns (Fig. 5.2b-d) and occasional labeled neurons (Fig. 5.2d-g).

Very strong label was found in fascicles of the vagus nerve and associated glial fibers projecting from the ventricular surface immediately lateral to the sulcus limitans (Fig. 5.2a, b). These radial glia fibers coursed through the dorsolateral parts of 10N. Putative commissural axons were also seen arising from the dense mass of labeled vagal fibers adjacent to 10N, and could be followed as they coursed ventral to the intercalated nucleus (In) and nucleus 12 (12N) towards the midline. It was not possible to trace these fibres much further than the midline because they became too faint to follow. The solitary tract itself was also strongly labeled and axons from the solitary tract were distributed predominantly to dorsomedial subnuclei of Sol. As shown in Figure 5.2b, c, SolG, which is located dorsal to the sol, contained a particularly dense patch of afferent terminals in its

center thereby forming a compartment which could be clearly distinguished from the surrounding structures. Ventral to SolG, the SolM was traversed by fascicles of labeled axons streaming out of the sol. SolDL and SolVL contained very few afferent terminals but did have occasional small multipolar or bipolar neurons (11 to 15 μm soma diameter) (Fig. 5.2d, e and g). Occasional small labeled neurons (10 to 12 μm soma diameter) were also found in the SolIM (Fig. 5.2d, f).

Figure 5.3a and b show retrograde DiI labeling of 10N at the level of the open medulla. Clear demarcation of 10DI, 10CeI and 10VI was visible at this age consistent with my observations in Nissl-stained material (see previous chapters), with the commissural fiber bundle of the vagus coursing through the ventral edge of 10VI. Labeling was so intense and cells so densely clustered that the extent of the dendritic trees of individual neurons was difficult to follow. Nevertheless, it was clear for some isolated neurons that at this stage the dendritic trees do not all extend as far as the nucleus of the solitary tract, so that vagal afferents could be seen to be clearly separated from the dendrites of the motoneurons in 10N. Cells in 10N at this age were approximately 15 to 17 μm in diameter. Dendrites of 10N motoneurons were approximately 2 μm in diameter and were free of spines, although many showed occasional varicosities of up to 3 μm diameter along their length.

5.2.3 DiI Labeling of Afferents and Neurons at 20 Weeks of Gestation

Figure 5.4 shows the distribution of DiI labeling at 20 weeks. At this age, labeling of radial glia fibers was less intense than that seen in 13 weeks, but some radial glia fibers

nevertheless were seen to course through the solitary complex and 10DI, with labeled cell bodies (presumably radial glia) at the ventricular floor (Fig. 5.4c). As seen in the previous age, most labeled afferent terminals were in the medial part of the solitary nuclear complex (i.e. the subnuclei SolG, SolIM, SolM and medial parts of SolDL). Figure 5.5 shows examples of the occasional labeled cell bodies also seen. These were particularly common in the medial parts of the solitary complex adjacent to the 10N (SolG, SolM and SolIM, Fig. 5.5a-c) and in the ventrolateral subnucleus (SolVL, Fig. 5.5d). These cells were bipolar or multipolar in morphology with long primary dendrites (i.e. more than 120 μm in length) extending into parts of 10N (lateral edges of 10VI and 10CeI) in some cases.

Figure 5.6 shows the distribution and morphology of labeled neurons in the 10N at this age. All four magnocellular divisions of 10N could be distinguished at the appropriate levels, but the parvicellular medial fringe (MeF) remained unlabeled. The neurons within the magnocellular divisions of 10N (10DI, 10CeI, 10VI and 10CaI) were found to be large multipolar cells with somata diameters greater than 25 μm. There was some evidence of differences in morphology between the different subnuclei of 10N at this age, in that neurons of 10DI had a more elongated soma shape compared to the more circular or polygonal soma shape of neurons in the more densely packed 10CeI (Fig. 5.6c).

5.2.4 DiI Labeling of Afferents and Neurons at 24 Weeks of Gestation

In many respects, the pattern of vagal afferent termination fields and the morphology of 10N neurons was similar at this age to that seen at 20 weeks. For example, the pattern of the termination of the vagal afferents in the solitary nuclear complex was

largely confined to subnuclei in the dorsomedial part of the complex, e.g., SolG, SolM and SolIM (Fig. 5.7a). On the other hand, one aspect of vagal afferent termination was particularly striking at this age. This was the presence of large fascicles of afferents arising from the sol and coursing through SolM and SolIM to terminate in 10N (Fig. 5.7b), with the highest density of terminations seen in the caudointermediate part (10CaI) and some labeling in the centrointermediate part (10CeI). Unlike previous stages, no radial glia fiber labeling was seen at this age.

5.2.5 DiI Labeling of Afferents and Neurons at 27 Weeks Development

Figure 5.8 illustrates selected views of labeled vagal afferents and efferent neurons at this age. The only available specimen at this age showed labeling of afferents sequestered in the ventral and medial parts of the solitary tract despite extensive application of DiI to all vagal rootlets alongside the olive. This was in contrast to previous ages, where afferents were distributed throughout the solitary tract, and may signify improved spatial segregation within the tract. Figure 5.8c to f show a variety of neurons occasionally labeled within the subnuclei of the Sol. Labeled neurons were found in the dorsomedial parts of the nucleus (SolIM, SolM and medial SolDL) with occasional neurons found in the ventrolateral area (SolVL). Somata were of 20 μm diameter or less. The majority of neurons (SolIM, SolM and SolVL) had fusiform or elliptical somata with usually two, but occasionally three, primary dendrites and with most cells having their primary dendrites arranged circumferentially around the periphery of the solitary tract. Where dendritic trees of these neurons could be traced along the plane of section, they extended for up to

250μm from the soma. Both primary and secondary dendrites in these neurons were smooth with only very occasional dendritic appendages seen. In contrast to this, neurons in SolDL had a slightly different morphology with most somata being round or slightly ovoid and being 20 μm or more in diameter. Labeled neurons in SolDL appeared to have up to 5 primary dendrites, with the total dendritic tree ramifying within 200 μm of the soma. Both primary and secondary dendrites were more irregular than that seen for neurons from other parts of the Sol.

Figure 5.9 shows retrogradely labeled neurons in 10N at 27 weeks. As at previous ages, most retrogradely labeled neurons in 10N were concentrated in 10CeI. These neurons had round somata 20 to 30 μm in diameter with 2 or occasionally 3 short (20 to 40 μm long) primary dendrites and dendritic trees that could be traced for about 250 μm, but appeared to be confined to 10CeI. This nucleus was also penetrated by what appeared to beaded afferents entering from the direction of SolM. A second major cluster of retrogradely labeled neurons was seen in 10VI. There the neurons were less intensely labeled than those seen in 10CeI and were smaller (somata usually less than 20 μm in diameter).

5.3 Discussion

5.3.1 Distribution of the Vagal Projection to the Human Solitary Nucleus

The solitary nucleus is the principal recipient of visceral sensory afferents in the brain. It has been shown in experimental animals that Sol not only receives afferent fibers via the vagus nerve, but also receives gustatory afferents via facial and glossopharyngeal

nerves (Hamilton and Norgren, 1984). The caudal two thirds of the Sol is concerned with visceral sensory reception, and thus possesses connections with the vagus nerve (Hyde and Miselis, 1992; Kalia and Mesulam, 1980a; Kalia and Mesulam, 1980b; Kalia and Sullivan, 1982). As a whole, the distribution of visceral nerves terminating in adult Sol represents a complex topographic pattern, with the gustatory afferents occupying the most rostral portion and gastrointestinal afferents synapsing in the intermediate portion of the nucleus, including the central and gelatinous subnuclei (Kalia and Mesulam, 1980a; Kalia and Mesulam, 1980b; Lundy and Norgren, 2004; Zhang and Ashwell, 2001a). Cardiovascular afferents terminate in the caudal half of the nucleus (i.e. within the dorsomedial, medial, parvicellular and commissural subnuclei, as well as in the area postrema in the rat) (Cheng and Powley, 2000), while respiratory afferents end mainly in the ventrolateral, intermediate and commissural subnuclei in the rat. Therefore, it is assumed that human vagal afferents, carrying visceral sensory signals from gastrointestinal, cardiovascular and respiratory systems, mainly input into the intermediate to caudal levels of the nucleus, including central, gelatinosus, dorsomedial, parvicellular, commissural, ventrolateral, intermediate subnuclei of Sol, as well as the area postrema.

In the present study, I found that labeled vagal afferents were distributed mainly to the dorsomedial subnuclei (SolG, SolM, SolIM, and medial part of the SolDL) of the Sol in the middle and caudal parts of its rostro-caudal extent. Lundy and Norgren (Lundy and Norgren, 2004) argued on the basis of findings in rodent Sol that the gustatory afferents in mammals in general should be distributed to the rostral tip and the lateral subnuclei of Sol, which in humans would correspond to rostral Sol, SolI, SolDL and SolVL. Therefore,

the present findings are consistent with the proposed schema of Lundy and Norgren (Lundy and Norgren, 2004).

I also observed carbocyanine dye labeling of putative commissural fibres seen arising from the dense mass of vagal fibers adjacent to 10N. These could be followed as they coursed ventral to In and 12N towards the midline. It was difficult to follow these fibres any further than the midline because of the limited extent to which DiI will diffuse in the large human brainstem, but they may represent contralaterally projecting vagal afferents. Bundles of vagal afferent fibres with a similar trajectory can be seen in the illustrations of the results of tracing studies performed in experimental animals (Hopkins et al., 1984). I am confident that these are true vagal afferent bundles because previous studies with carbocyanine dye tracing in the rodent vagal sensory motor system have shown that DiI is confined to vagal afferents and does not appear to spread to other axons (Zhang and Ashwell, 2001a). The labeled putative vagal commissural fibres which I saw in the developing human brainstem can be traced in continuity with labeled vagal rootlets. They are also quite separate from the radial glial cells sometimes seen to be labeled in my early fetal material (as well as in rodent fetal material labeled from the peripheral vagus nerve, (Zhang and Ashwell, 2001a) and were seen consistently at 13, 20 and 27 weeks.

5.3.2 Development of Human Solitary Nucleus

There are very few studies which have examined the pre- and perinatal development of the Sol in humans. Two studies have examined the development of substance P immunoreactivity in prenatal and early postnatal human. The first of these was by Rikard

Bell and co-workers (Rikard-Bell et al., 1990) who examined the distribution of substance P immunoreactivity in Sol shortly after birth. They found that very dense substance P immunoreactivity was present in the paracommissural subnucleus of the Sol at this age, while dense immunoreactivity was also present in commissural, medial, dorsal, dorsolateral, ventral and ventrolateral subnuclei. By contrast, only moderate substance P immunoreactivity was present within the gelatinosus subnucleus. Wang et al. (Wang et al., 1993) reported that SP-ir fibers first appeared in the Sol between 11.5 and 16 weeks gestation. These initial fibers were distributed in the dorsalis subnucleus and, as the fetus grew, density and intensity of SP-ir fibers increased gradually.

Studies in rodents (Rinaman and Levitt, 1993; Zhang and Ashwell, 2001a) have reported that vagal afferents are initially confined to the solitary tract until about E15, before emerging to project medially through the developing Sol and ending in the ventricular zone. In the present study on human fetuses, I noted labeling of putative radial glial fibres and some processes extending into the ventricular zone at the earliest age examined (8 to 9 weeks) as well as some putative radial glia labeling at later ages (13 weeks). Rinaman and Levitt (Rinaman and Levitt, 1993) suggested that vagal afferents might be unlike other sensory afferents (e.g. in dorsal horn) in that they make an initial projection into the ventricular zone. On the other hand, Zhang and Ashwell (Zhang and Ashwell, 2001a) noted that afferents derived from both facial and trigeminal nerves and distributed within the sol also extended into the ventricular zone during the period from E13 to E15. In any event, my finding of labeling in the ventricular zone following insertion of DiI into peripheral vagal nerve fibres is entirely consistent with findings in

experimental animals.

One possible difference in the distribution of vagal afferents between human and rodent Sol concerns the invasion of the dendritic domain of 10N by these afferents. In the rodent (Rinaman and Levitt, 1993), the solitary tract and 10N are separated by only 100 to 130 μm at E16, and it is clear that vagal afferents can readily enter the region of the dendritic fields of the motoneurons of 10N. This appears to occur well before vagal afferent distribution in the medial parts of Sol approaches its mature appearance. On the other hand, the Sol and 10N in the human brainstem are separated by between 200 and 300 μm and vagal afferents cannot be clearly seen to enter the dendritic domains of the neurons in 10N until 20 weeks, and these projections do not appear to be well-developed until 24 weeks. It is also noticeable that, in human Sol, a relatively mature pattern of vagal afferent distribution, with patches in the gelatinosus subnucleus some 500 μm away from the solitary tract occurs before clear vagal afferent distribution to the much closer 10N can be seen. The early invasion of 10N by vagal afferents in rodents may simply reflect the overall smaller size of the rodent brainstem, but this cannot explain the delay of this invasion of 10N relative to the development of mature afferent distribution to more dorsal and distant subnuclei of Sol (i.e. SolG). If the invasion of 10N by vagal afferents or interneuron axons from medial Sol is a significant developmental event in the origin of vagal sensorimotor reflexes, then these findings set an early limit of about 20 weeks development for acquisition of this circuitry.

In the present study I found occasional neurons within the Sol, which were retrogradely labeled after insertion of DiI into the vagal rootlets. Preganglionic effector

neurons and motoneurons retrogradely labeled after insertion of tracers into the cervical vagus are mainly located within 10N and Amb, respectively (Fryscak et al., 1984; Hopkins et al., 1984; Kalia and Sullivan, 1982). The retrogradely labeled neurons which I observed in Sol may represent transient developmental projections of Sol neurons into the cervical vagus nerve, but I did not observe any age-related changes in the frequency with which these neurons were encountered. In other words, retrogradely labeled Sol neurons were encountered just as often in the 24 or 27 weeks specimens as in the 13 week specimens. On the other hand, occasional labeled neurons have been found in the Sol of experimental animals following injections of horseradish peroxidase into the cervical vagus nerve of the cat (Todo, 1977) and developing pig (Hopkins et al., 1984). The latter authors also noted that these neurons in Sol were seen just as frequently in newborn and 60 day old pigs. Therefore, the occasional retrogradely labeled neurons which I noted in human Sol may represent a true and long-standing population of vagally projecting efferent neurons. Further studies in the adult human brainstem may help to clarify this.

5.3.3 Development of Human Dorsal Motor Nucleus of Vagus

The cyto- and chemoarchitecture of the adult human 10N has been examined by Huang et al. (Huang et al., 1993a; Huang et al., 1993b) and the nucleus has been delineated by Paxinos and Huang (Paxinos and Huang, 1995). An ultrastructural study by Ling et al (Ling et al., 1987) in hamsters identified two types of neurons within 10N: large neurons (averaging 20 x 12 μm in soma diameter) rich in cytoplasmic organelles which contributed axons to the vagus nerve; and smaller neurons (averaging 15 x 9 μm in soma

diameter) which did not project into the vagus nerve and typically had infolded nuclei and organelles not as well developed as in the larger neurons.

The only previous study of the developing human 10N was by Nara et al. (Nara et al., 1991), who identified three subnuclei (caudal, dorsal and ventral) in human brainstem specimens ranging in age from 16 weeks of gestation to 63 years of age. They noted that during fetal life, neurons of rostral 10N were arranged in two or more distinct groups with dorsal and ventral subnuclei, while caudally this nucleus was reported to have a single caudal subnucleus. The caudal subnucleus was generally continuous orally with the dorsal subnucleus.

In the present study, carbocyanine dye tracing experiments showed differential labeling in the subdivisions of 10N as early as 13 weeks, consistent with the findings from Nissl stained material at that age. This labeling was confined to the 10DI, 10CeI, 10VI and 10CaI. No apparent retrograde labeling of somata was found in the parvicellular MeF. This is consistent with findings of retrograde labeling from injection of tracer into the cervical vagus nerve of experimental animals (Hopkins et al., 1984) in which the medial fringe is unlabeled. The pattern of retrograde labeling with carbocyanine dye even at 13 weeks closely reflected that seen with Nissl staining. In other words, there was a pronounced clustering of labeled neurons in the centrointermediate subnucleus. This means that the basic compartmental organization of 10N is already developed by 13 weeks and that subsequent maturation of this nucleus mainly provides a refinement of this organization. This is consistent with observations of 10N development in the rat (Rinaman and Levitt, 1993), where it was noted that DiI labeled motoneurons of 10N

formed a discrete group even before the nucleus was discernable in Nissl stained sections. At present it is unclear as to what is the functional significance of this compartmentalization of 10N. In other mammals, no particular segregation of neurons supplying different visceral organs has been reported (Kalia and Mesulam, 1980a; Kalia and Mesulam, 1980b; Zhang and Ashwell, 2001a).

It is also noteworthy that the dendritic development of retrogradely labeled 10N neurons was well advanced by 13 weeks. This is consistent with the observations of Rinaman and Levitt (Rinaman and Levitt, 1993) in the rat, where dendritic development occurs as early as E15. On the other hand, dendritic fields of neurons in the human 10N did not extend into the terminal field of the solitary tract afferents as extensively as they were noted to do at early ages in the rat. The dendritic trees of the neurons in human 10N were largely confined to the boundaries of the nucleus until 20 weeks of development. This may indicate that the co-distribution of vagal sensory afferents and motoneuron dendrities of 10N may be relatively delayed in the human brainstem compared to rodents, with further significance for the development of visceral vagal reflexes.

A further similarity between my observations and the findings of Rinaman and Levitt (Rinaman and Levitt, 1993) and Zhang and Ashwell (Zhang and Ashwell, 2001a) is that in both species, there was no evidence of grossly exuberant projections within the caudal medulla as vagal sensory afferents and 10N motoneuron dendrites develop, supporting the notion that the development of vago-vagal connections in the visceral sensorimotor complex occurs by a highly ordered, progressive series of developmental events. This is in

contrast to the reported exuberance during development of sensory input in visual and somatosensory pathways (Callaway and Katz, 1990; Frost, 1984; Waite et al., 1995).

5.3.4 Functional Significance of the Developmental Time Course of the Vagal Sensorimotor Circuits

The developing Amb has been shown to make contributions to the developing glossopharyngeal and vagal nerves as early as 6 weeks of gestation. The earliest overt evidence of swallowing in the human fetus has been reported in response to perioral stimulation at 12 weeks of gestation (Brown, 1990), while at 14 weeks, swallowing is a consistent consequence of perioral stimulation (Humphrey, 1968; Muller et al., 1981). The motor sequence of swallowing is believed to be centrally programmed by a neuronal network divided into three levels: (1) an afferent level corresponding to the solitary tract; (2) an efferent level involving different pools of motoneurons within the trigeminal and hypoglossal nuclei and in the ambiguus nucleus; (3) an interneuron network which programs the swallowing motor sequence (Jean, 1984). During the buccopharyngeal phase of swallowing, vagal afferents from the pharynx and larynx terminate in the intermediate and interstitial subnuclei of the Sol (Broussard and Altschuler, 2000b). In my study, I found that by 13 weeks, the time by which Humphery (Humphrey, 1968) observed consistent swallowing in response to perioral stimulation, vagal afferents had a quite mature distribution.

The importance of the vagus nerve in carrying information vital to pulmonary reflexes has prompted several studies of development of that nerve. Myelination of the human vagus nerve begins between 14 and 17 weeks of development (Wozniak and

O'Rahilly, 1981). Total numbers of myelinated fibres in the vagus increase linearly from about 5,000 at 26 weeks of gestation to as many as 40,000, the adult value, at 10 weeks after birth (Sachis et al., 1982). Immaturity of the vagus may be responsible for the unstable breathing patterns in preterm infants. Indeed, the Hering-Breuer inspiration inhibiting reflex, which is mediated by large myelinated vagus fibres, is reported to be weak in infants of 32 weeks of gestation, but increases in strength until 38 weeks of gestation (Bodegard et al., 1969). After birth, the number of myelinated axons in the vagus remains fairly constant (Sachis et al., 1982), and a multimodal distribution of fibre size begins to appear at about 3 months after birth (Pereyra et al., 1992).

Windle (Windle and Fitzgerald, 1937) has argued that the component movements needed for breathing develop very early, and Humphery (Humphrey, 1968) has reported that respiratory gasps occur as early as 88.5 mm CRL. Respiratory movements take place as early as 13 weeks gestation (Dawes, 1974) and perhaps even as early as 11 weeks of gestation (Windle and Fitzgerald, 1937).

Vagal innervation of human fetal viscera has received some attention, although the data set is thin. Palatine and pharyngeal muscles begin to appear at about 5 to 6 weeks of gestation and receive their innervation (from trigeminal, glossopharyngeal and vagal nerves) from about 8 weeks of gestation (Domenech-Ratto, 1977). In the developing larynx (Muller and O'Rahilly, 1985; Muller et al., 1981), the adult pattern of motor innervation is present from stage 23 (about 52 days of development) although sensory innervation is not complete at this stage. Inferior vagal ganglion cells can be retrogradely labelled by carbocyanine dye insertion into the pylorus from 12 weeks of gestation (Abel

et al., 1998). In the present study, I found that vagal afferents form a distinct patch in SolG as early as 13 weeks. This nucleus appears to be homologous to SolG in the rat, which is known to receive afferents from esophageal and stomach wall (Altschuler et al., 1989). My findings therefore suggest that the afferent terminal field from the developing human foregut is spatially segregated as early as 13 weeks.

5.4 Conclusion

In conclusion, the present study established the time course of development of central vagal sensory and preganglionic connections in human embryos and fetuses. In the human, there is a dorsomedial distribution of vagal afferents within the Sol, as has been seen in other mammals (Kalia and Mesulam, 1980a; Kalia and Mesulam, 1980b; Lundy and Norgren, 2004). Subnuclear organization as revealed by both Nissl staining and carbocyanine dye tracing is advanced at a relatively early fetal age, with afferent segregation in the Sol apparent at 13 weeks and subnuclear organization of efferent magnocellular divisions of 10N noticeable at the same stage. On the other hand, the first suggestion of vagal afferents invading 10N from the medial Sol was not seen until 20 weeks and was not well developed until 24 weeks. The early maturation of structures involved in vagal sensorimotor circuits implies that in humans, as in rats, neural control of the movements and reflexes of visceral organs, such as the upper gastrointestinal and respiratory tracts, attains functional potential long before birth (Humphrey, 1968).

Figure 5.1 Confocal microscopic images of DiI labeled cells in vagal ganglia and the developing vagal sensory motor complex in fetuses of 8 (a and b) to 9 (c, d and e) weeks of gestational age: (a) labeled cells in the inferior ganglion of the vagus nerve (10Gn); (b) labeled cells in the mantle zone (MZ) of the developing myelencephalon; (c) low power view of labeled cells in the vicinity of the sulcus limitans; (d) high power view of labeled ventricular zone cells in the medial floor of the 4^{th} ventricle; (e) labeled cells with assorted morphologies, some with somata lying close to the ventricular floor and with processes in direct contact with the ventricular surface (suggestive of radial glia) and some with no apparent connection with the ventricular floor (presumptive 10N neurons migrating from the ventricular germinal zone). Dorsal is to the top in all photomicrographs.

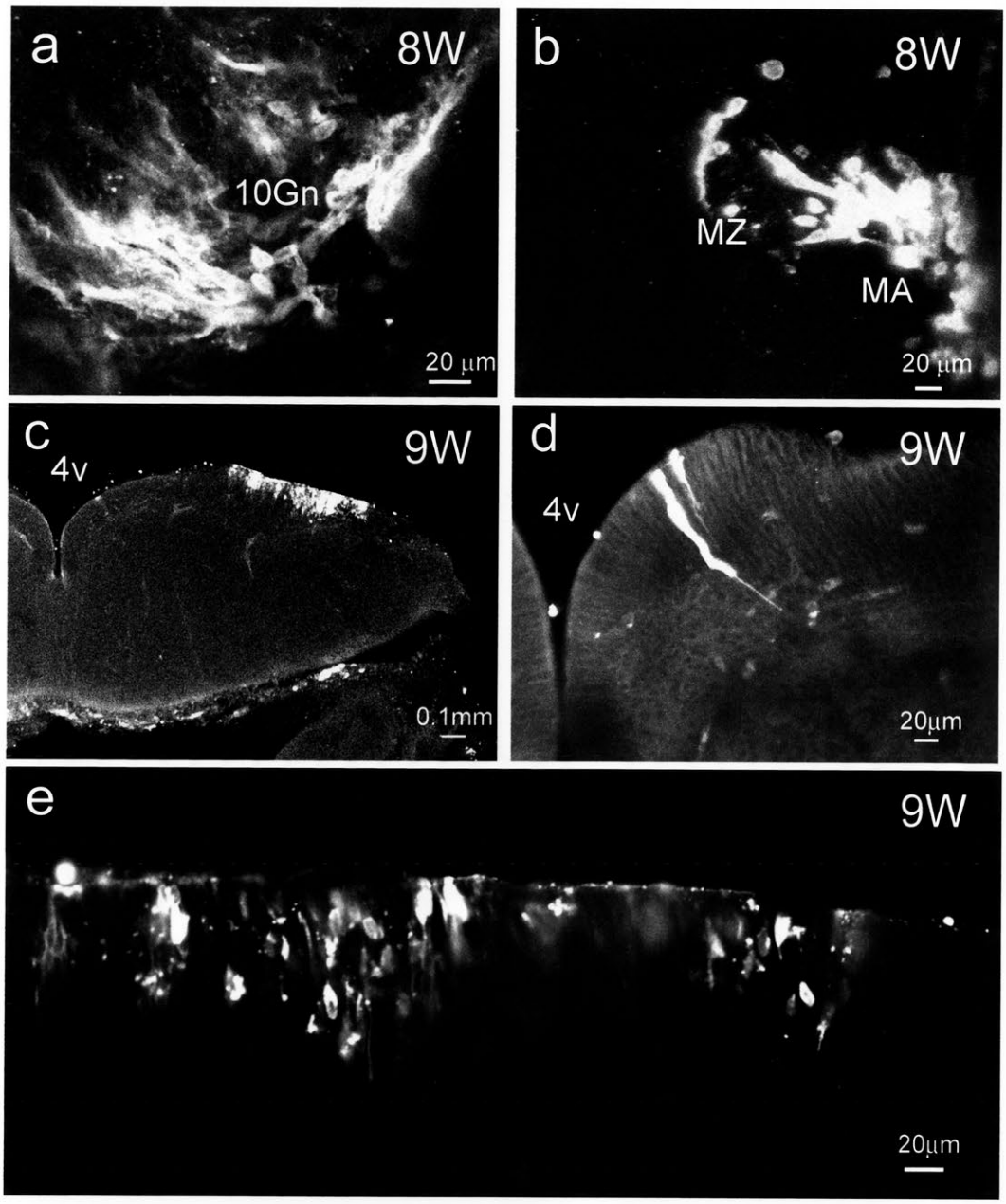

Figure 5.1

Figure 5.2 (a) Line diagram summarizing DiI insertion site and labeled regions, and (b-f) confocal microscopic images of DiI labeled afferent terminal fields and occasional neurons found in various subnuclei of the Sol at 13 weeks of gestation. Figure (c) shows a higher power view of (b). Labeled axons were noted in the solitary tract, vagal commissural bundle and efferent fibers from Amb. Even at this early age, differential subnuclear labeling of vagal afferents could be seen, with most vagal afferents distributed to the medial subnuclei of Sol and a distinct terminal patch in presumptive SolG. Figure (d) shows the disposition of the major subnuclei around the sol and labeled neurons in those subnuclei. Figures (e), (f) and (g) show examples of the occasional labeled somata seen in some of the subnuclei of Sol.

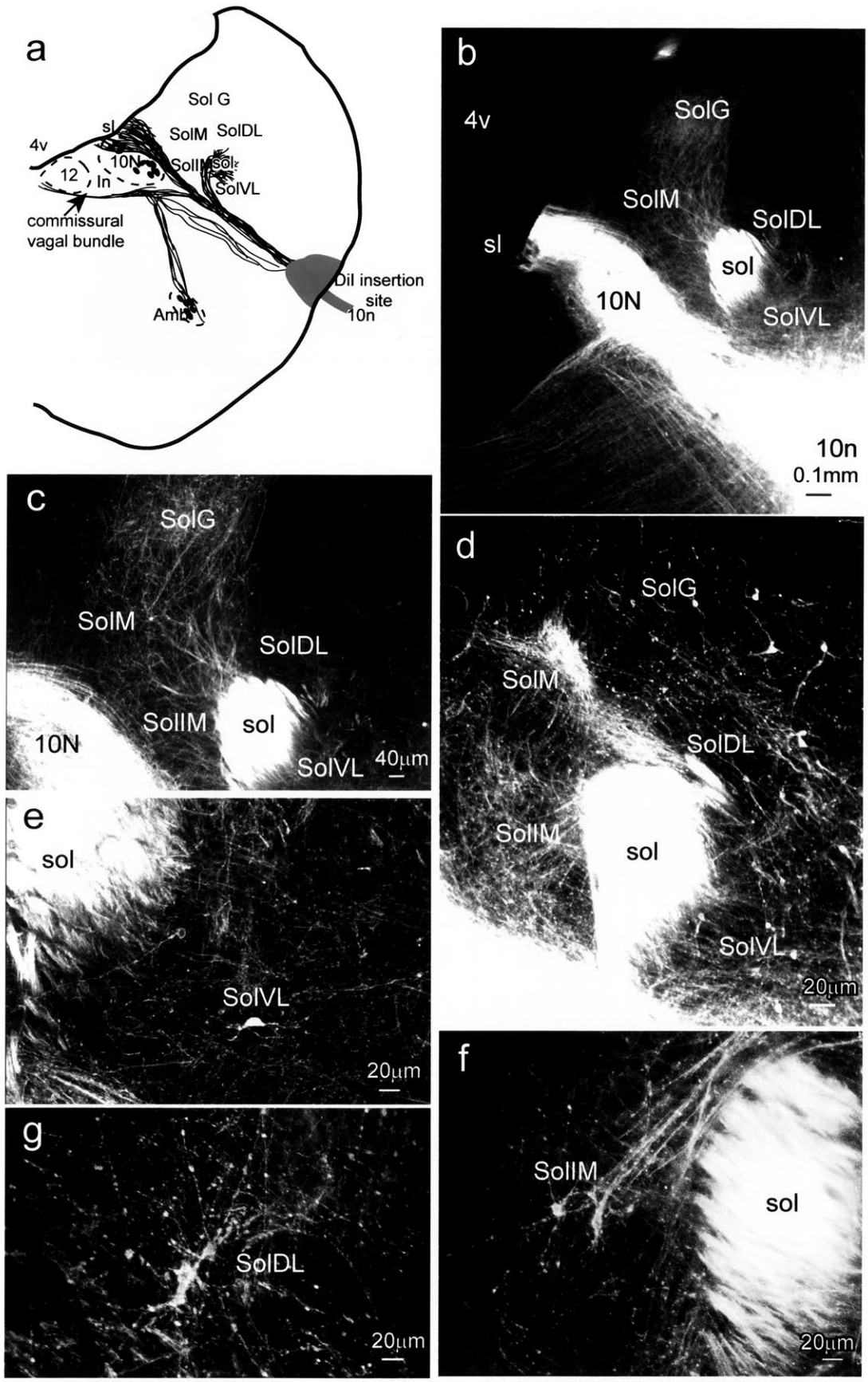
a
Sol G
sl
SolM
SolDL
4v
10N
SolIM
Sol
12
In
SolVL
commissural
vagal bundle
DiI insertion
site
10n
Amb
b
4v
SolG
SolM
SolDL
sl
sol
10N
SolVL
10n
0.1mm
c
SolG
SolM
SolDL
SolIM
sol
10N
SolVL
40μm
d
SolG
SolM
SolDL
SolIM
sol
SolVL
20μm
e
sol
SolVL
20μm
f
SolIM
sol
20μm
g
SolDL
20μm

Figure 5.2

Figure 5.3 Confocal microscopic images of DiI labeled cells and fibers in the fetal 10N at 13 weeks of gestation: (a), (b) low and high power images, respectively, of labeled neurons and dendritic branches in 10N. Note that even at this age, there was clear differentiation between 10CeI centrally, and 10DI and 10VI on each side.

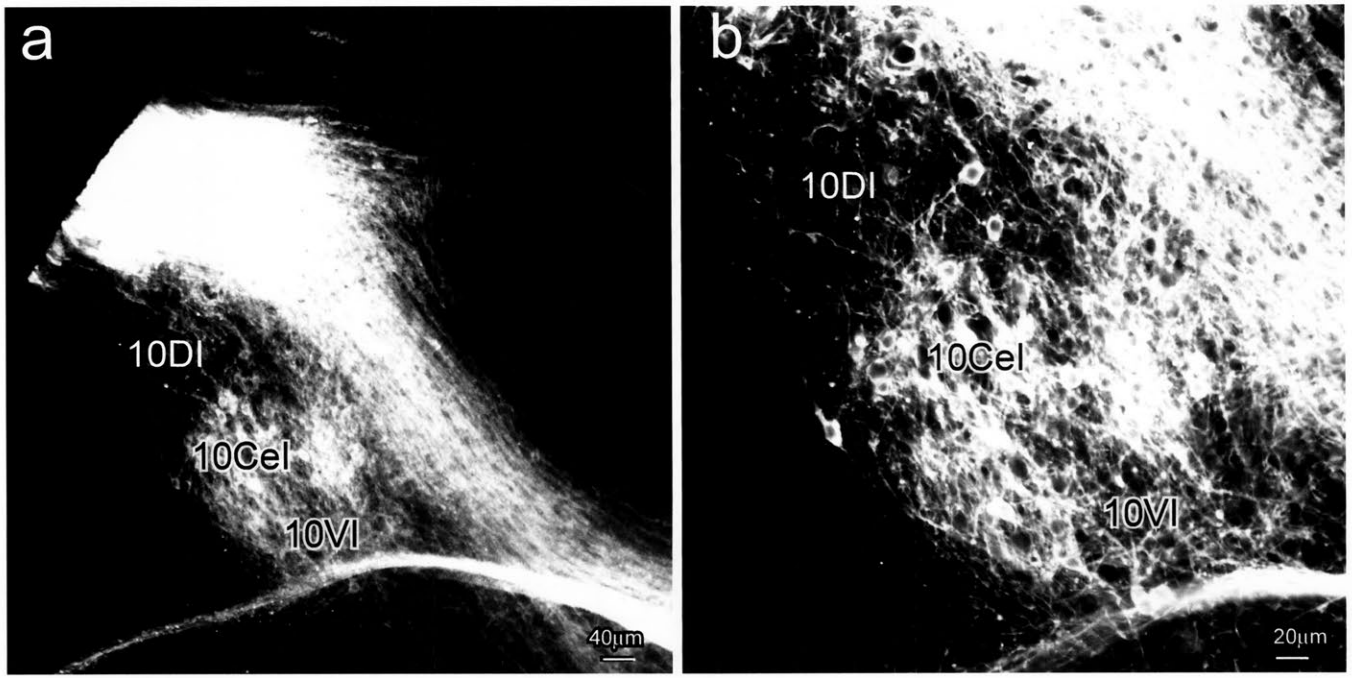

Figure 5.3

Figure 5.4 (a) Line diagram summarizing major nuclear groups and patterns of DiI labeling of vagal afferents and efferents at 20 weeks. Confocal microscopic images of DiI labeled cells and fibers in the fetal ventral Sol (b), medial Sol and 10N (c). Labeling of ventricular zone processes is still visible at this age (arrow in c), but less pronounced than at 13 weeks.

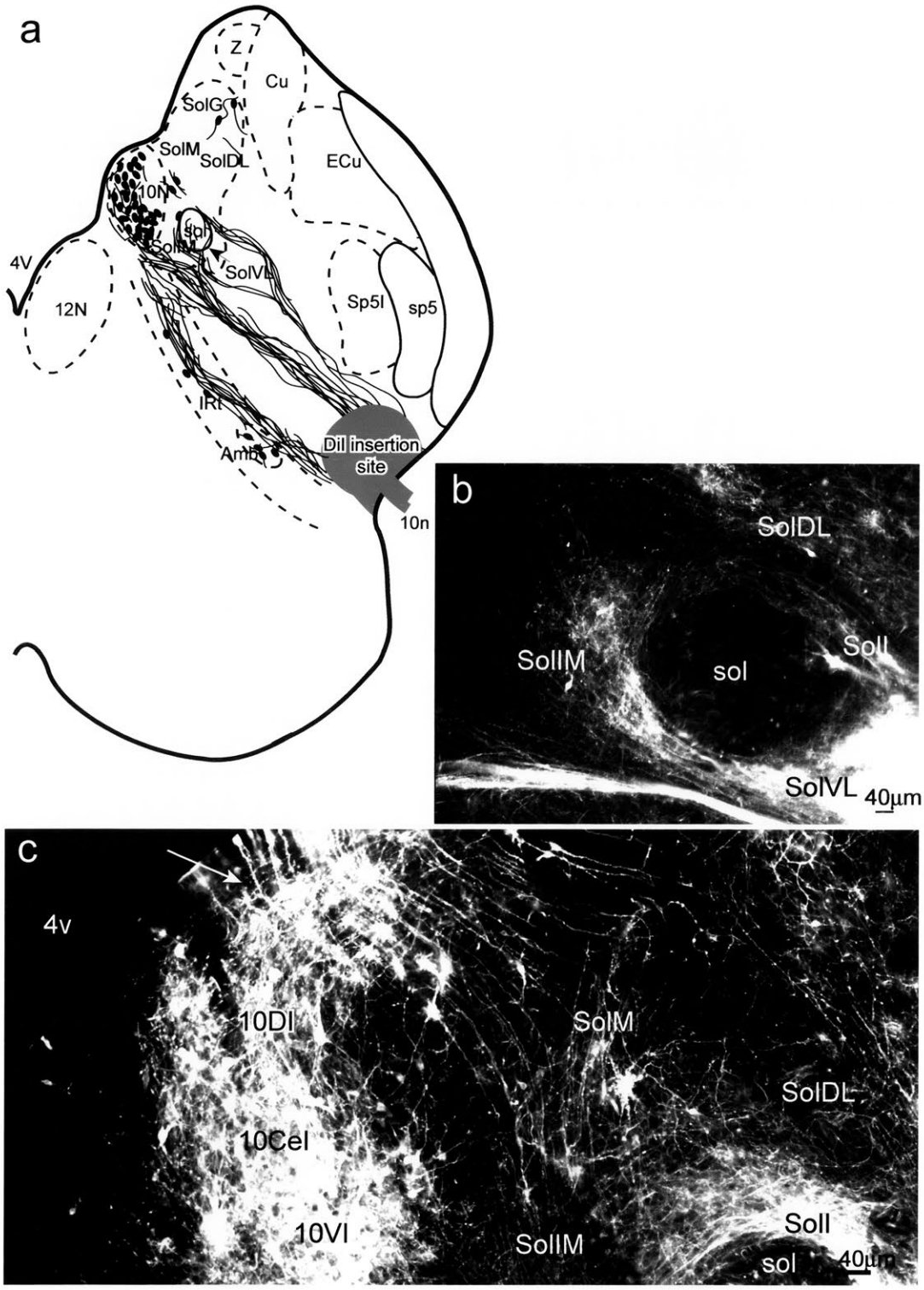
a
Z
Cu
SolG
SolM
SolDL
ECu
10N
spl
SolL
4V
SolVL
12N
Sp5I
sp5
IRt
Amb
Dil insertion site
10n
b
SolDL
SolIM
sol
SolI
SolVL
40µm
c
4v
10DI
SolM
SolDL
10CeI
10VI
SolIM
SolI
sol
40µm

Figure 5.4

Figure 5.5 High power confocal microscopic images of DiI labeled cells and dendrites in the fetal Sol at 20 weeks of gestation: (a) in SolG and SolM; (b) in SolM and 10CaI; (c) in SolM; (d) in SolVL. Note the close proximity between SolIM and 10CaI, and invasion of 10CaI by processes from SolIM.

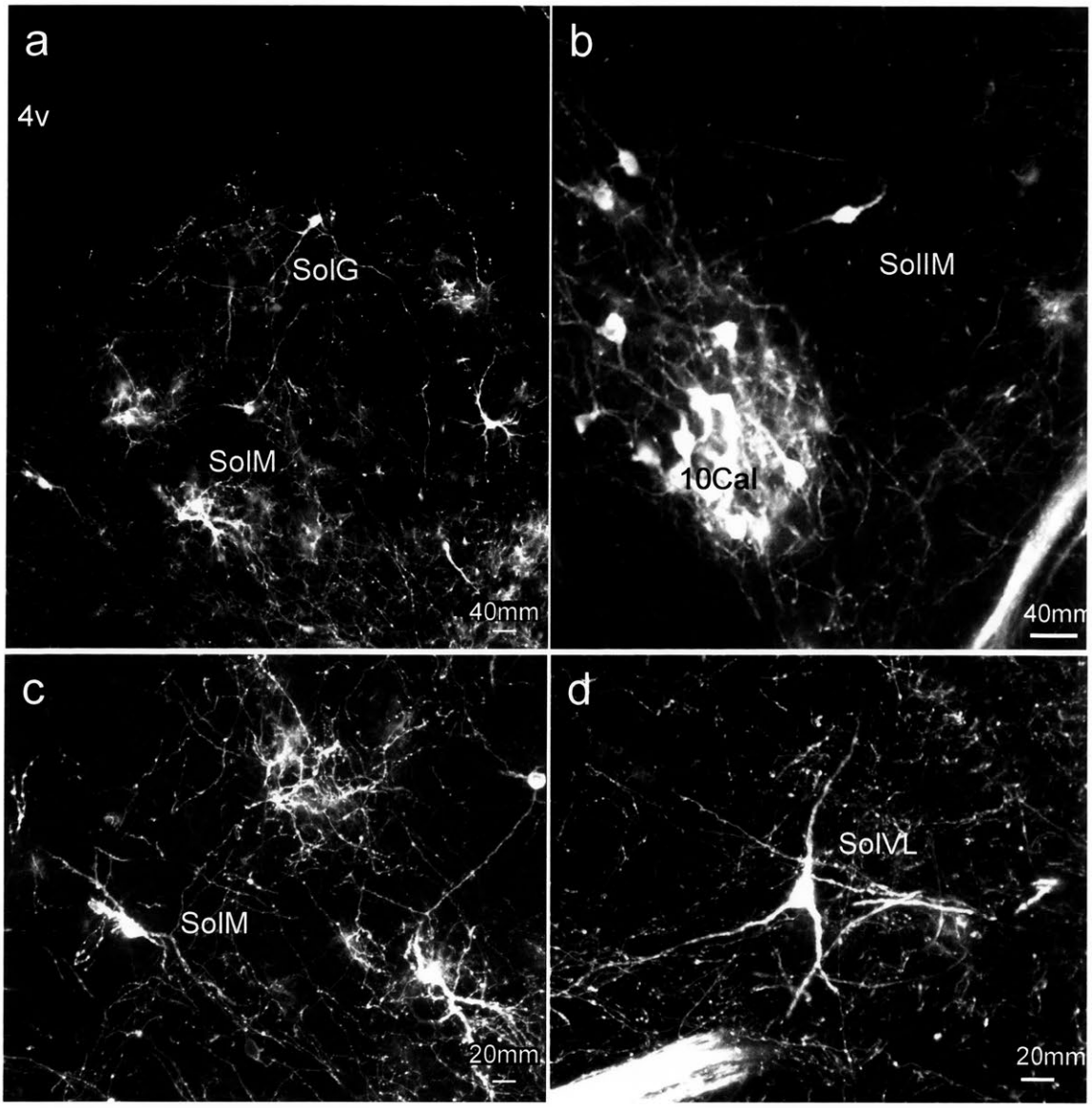

Figure 5.5

Figure 5.6 Low and high power confocal microscopic images of DiI labeled cells and dendrites in the fetal 10N at 20 weeks of gestation: (a) low power image of 10DI, 10CeI and 10VI; (b) high power images of 10DI, 10CeI and 10CaI; (c) high power images of 10DI, and 10CeI.

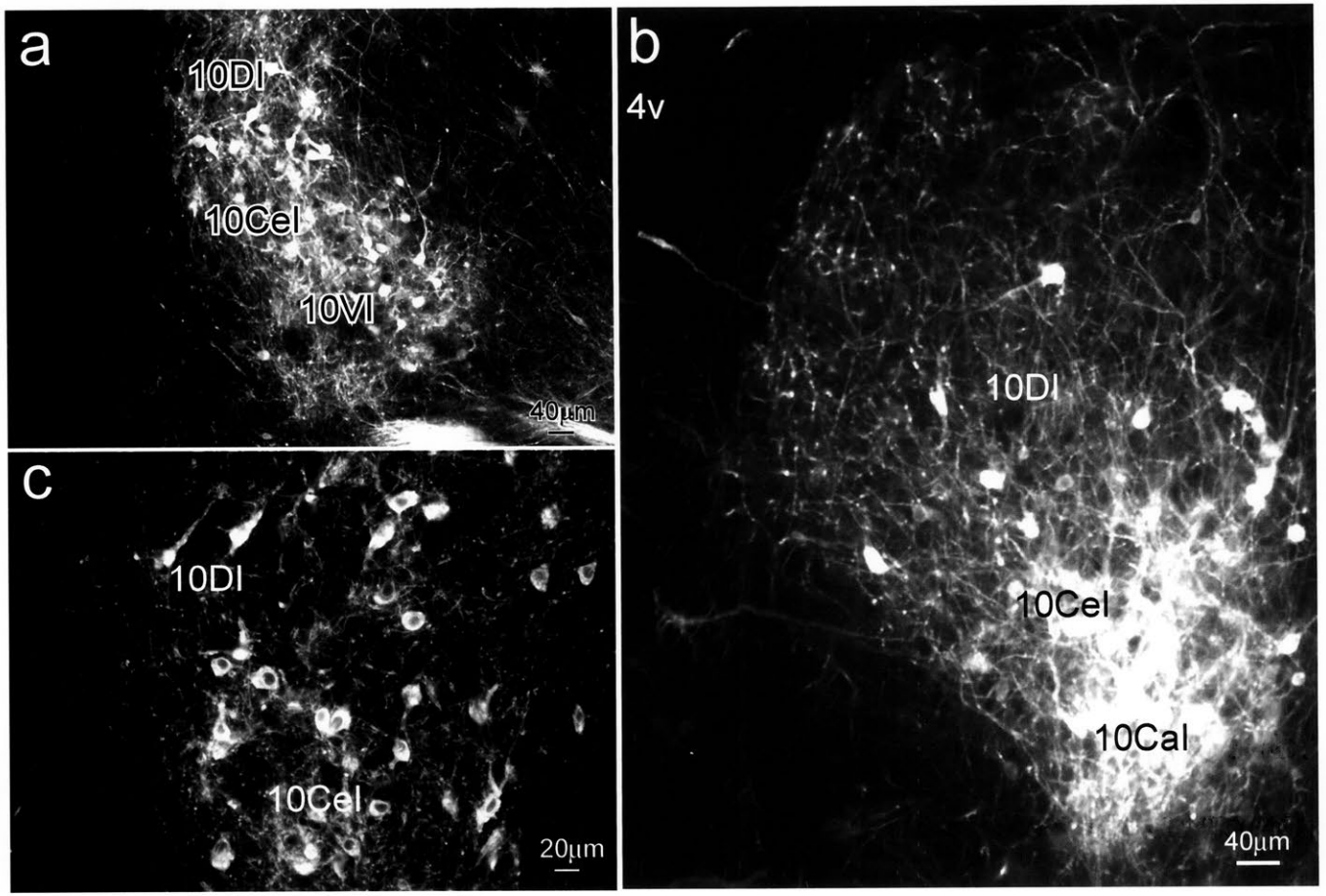
a
10DI
10CeI
10VI
40μm
b
4v
10DI
10CeI
10CaI
40μm
c
10DI
10CeI
20μm

Figure 5.6

Figure 5.7 Confocal microscopic images of DiI labeled cells and afferent terminal fields in fetal vagal nuclei at 24 weeks of gestation: (a) low power view of labeled dendritic fields of Sol and 10N; (b) high power view of labeled cells and dendrites of subnuclei of 10N. Note that vagal afferent terminals are segregated in medial parts of the solitary nuclear complex (SolG and SolM) and that there are afferent bundles (arrowheads in b) coursing from medial Sol into nucleus 10N (mainly into the subnuclei 10CeI and 10CaI).

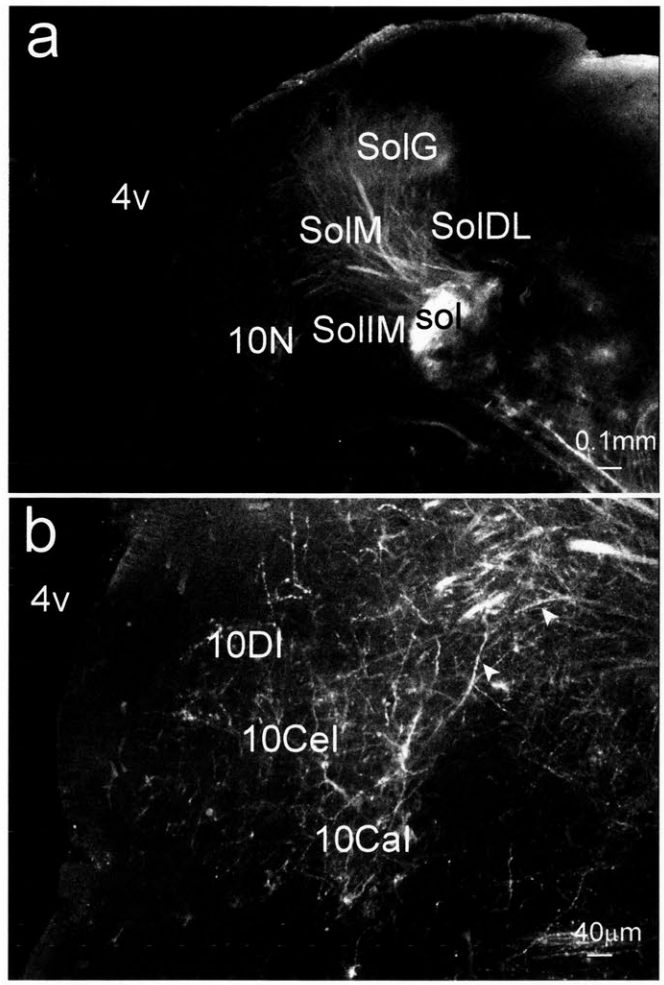
a
4v
SolG
SolM
SolDL
10N
SolIM
sol
0.1mm
b
4v
10DI
10CeI
10CaI
40μm

Figure 5.7

Figure 5.8 Line diagram and confocal microscopic images of DiI labeled neurons and terminal fields in the fetal medulla at 27 weeks of gestation: (a) line diagram of the labeled area as well as the DiI insertion site in a representative transverse section; (b) low power image of labeled cells and dendritic fields in 10N and Sol; (c) to (f) high power images of labeled neurons and dendrites in the various subnuclei of Sol.

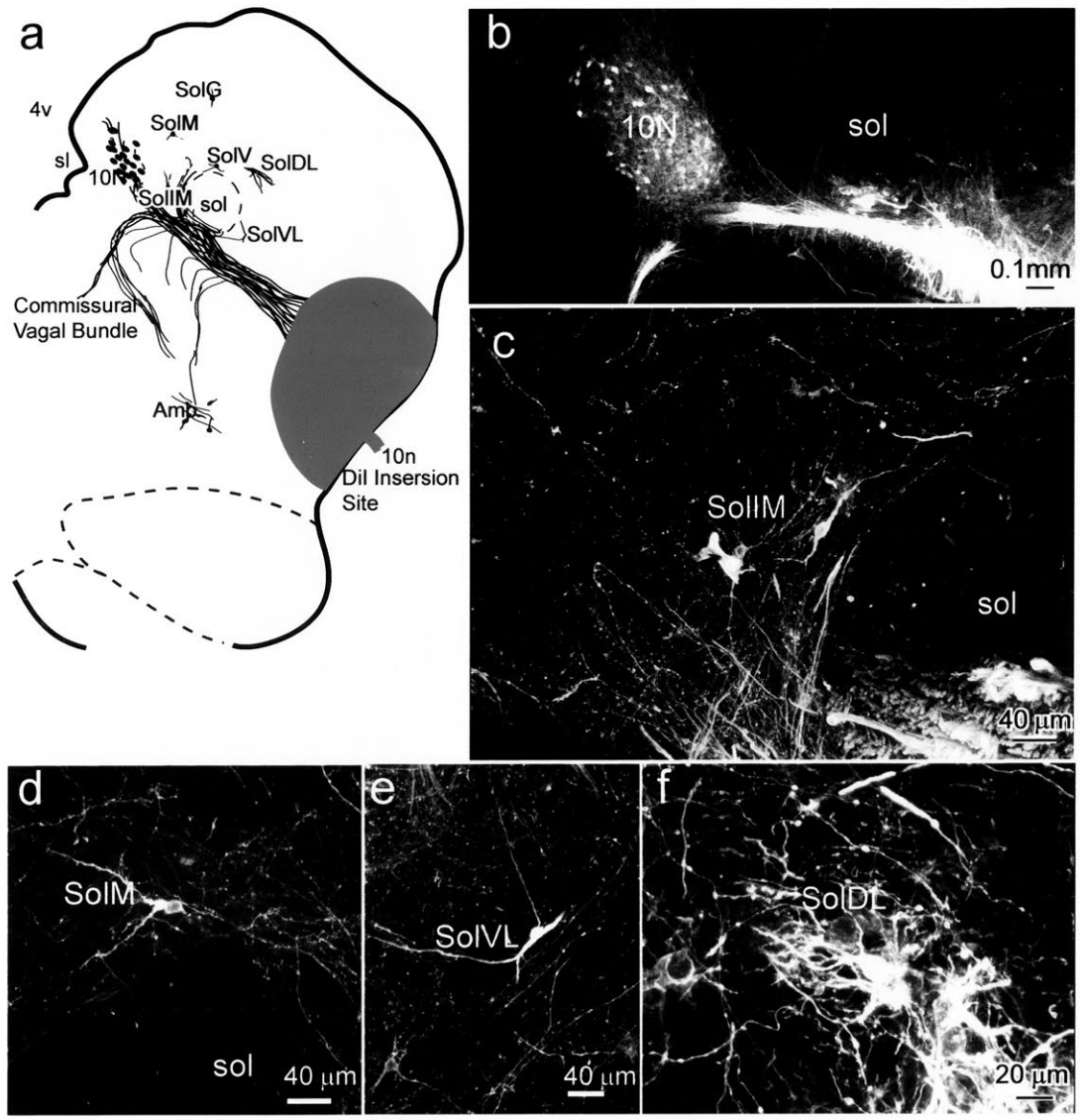
a
4v
SolG
SolM
sl
SolV
SolDL
10N
SolIM
sol
SolVL
Commissural
Vagal Bundle
Amb
10n
DiI Insersion
Site
b
10N
sol
0.1mm
c
SolIM
sol
40 μm
d
SolM
sol
40 μm
e
SolVL
40 μm
f
SolDL
20 μm

Figure 5.8

Figure 5.9 Confocal microscopic images of DiI labeled neurons and dendrites in fetal 10N at 27 weeks of gestation: (a) low power image of labeled neurons and dendrites in subnuclei of 10N; (b) high power image of labeled neurons and dendrites in 10CeI. Note the tight clustering of neurons in 10CeI with pronounced intermingling of dendrites.

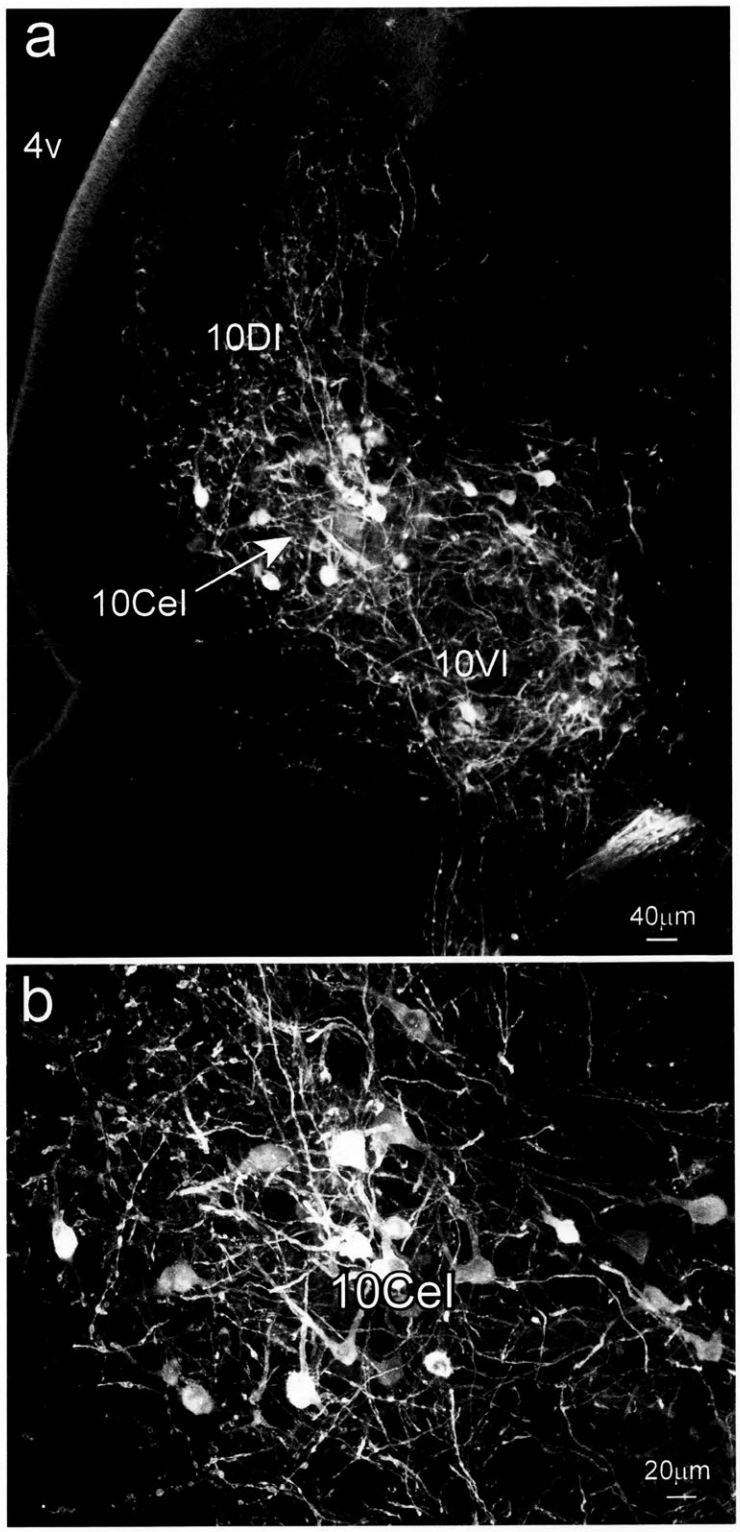

Figure 5.9

Chapter 6 General Discussion

In the present study, the development of the dorsomedial medullary nuclei of the vagus nerve, the solitary nucleus (Sol) and dorsal motor nucleus of vagus (10N), has been examined in human fetuses from the end of embryonic stage 23 (approximately 8 weeks of development) to the beginning of the third trimester (28 weeks of development). The study was focused on the establishment of the organization (both cyto- and chemoarchitectonic) and neural connectivity (DiI tract tracing) of these two nuclei. In the previous chapters, specific issues concerning the development of each nucleus have been discussed. Therefore this chapter will focus on consideration of those general aspects of fetal development which are relevant to the present study and the broader implication of the present findings.

6.1 Limitations of the Present Study

The present work has relied on analysis of fixed postmortem material obtained from terminations of pregnancy. A strong effort was made to minimize postmortem delay: all fetuses were perfused as soon as possible, usually within 20 minutes and always within 2 hours of termination. The nature and history of such tissue naturally places considerable limitations on the type of analysis that can be performed and the data obtained. Tissue of this kind is eminently suited to use of carbocyanine dye tracing techniques, but such methods only allow tracing of pathways over limited distances (usually less than 1 cm). This means that tracing of complete vagal pathways in human fetuses is essentially impossible with present technology and any investigation must be confined to study of vagal (or other cranial nerve) rootlet distribution. This in turn makes it difficult to

distinguish sensory from motor roots in mixed nerves like the vagus, but fortunately this has not interfered with the major connectional aim of the present study – namely the analysis of connections between sensory and motor elements of the autonomic centres in the dorsomedial medulla.

Fixed postmortem human fetal material is also suitable for immunohistochemistry provided appropriate antigen retrieval techniques are available. Naturally antibodies against less robust antigens than the calcium binding proteins and tyrosine hydroxylase are difficult to apply in such tissue and it was clear in the present study that success with antibodies against SP was quite variable.

Trial experiments also have made it clear that this material is quite unsuited for electron microscopy, which means that it is not possible to establish that important ultrastructural correlate of functional maturation in this system as has been done for rodent Sol (Zhang and Ashwell, 2001b). One alternative to electron microscopy might be to use synaptophysin immunohistochemistry, but this does not provide the necessary resolution to determine whether connections with particular neurons have been formed.

6.2 The Time-Course of Development of Sol and 10N in the Human Fetus

Unlike the rat, in which direct evidence of time of origin of neurons in Sol and 10N is readily available by ^{3}H thymidine autoradiaographic techniques (Altman and Bayer, 1980), study of embryonic human Sol and 10N does not provide the definitive time of origin of each nucleus. However, it has been reported that both nuclei complete cellular migration as early as 6 to 7 weeks of development (Muller and O'Rahilly, 1990). The

present study demonstrated that at 9 weeks Sol and 10N still showed immature cytoarchitecture with no subdivisional differentiation.

In the present thesis, the period between 9 and 13 weeks was found to be a time of accelerated growth for Sol. By the end of 13 weeks, most subnuclei of Sol have appeared, although the neuronal morphology is far from well differentiated. Over a similar period, 10N has also appeared as a densely packed neuronal group distinct from the surrounding structures. The most significant changes of Sol and 10N take place between 13 and 15 weeks. During this period, Sol subnuclei were becoming clearly discerned and neurons began to differentiate into various shapes and sizes. The speed of subnuclear differentiation in Sol and 10N decreased after 15 weeks, and the only changes in cytoarchitecture between 15 and 25 weeks were in the volume of the nucleus and the increasing concentration of putative glial cells.

Subdivisional differentiation of Sol occurred in parallel with that of 10N. The period between 13 and 15 weeks was the key period for 10N, during which time it grew from a densely packed group of immature cells to a neuronal pool of various subdivisions, while the period from 15 to 25 weeks did not show dramatic alteration of the subdivisional patterns. There has not been a published systemic study of the development of cytoarchitecture of the human 10N, although a study by Nara, et al. (Nara et al., 1991) shows that by 16 weeks, three major subdivisions have already developed in 10N: the dorsal, ventral and caudal subnuclei.

One can compare the time-course of development of Sol in the human with that in the rat. Different phases of development have been detected in the rat (Zhang and

Ashwell, 2001b). The rapid period of subnuclear differentiation from E17 to E19 in that rodent appears to be similar to what happened from 13 to 15 weeks in the human (present study). This rapid phase was followed by a steady and slow maturation phase until postnatal stages in the rat. This was similar to that in the human Sol between 21 and 25 weeks, during which time differentiation of subnuclei was succeeded by the expansion of the volume and possible cytological reorganization of the nucleus. Therefore, the time-course of maturation of Sol is comparable in both human and rat, only that in the human, onset of maturation occurs relatively early in fetal life and there is a relatively prolonged slow phase of maturation until birth. Such a developmental difference might reflect the complexity of the human fetal cardiovascular, respiratory and gastrointestinal systems (Harding and Bocking, 2001) rather than significant evolutionary differences between the human and rat.

6.3 Functional Correlations of the Development of Sol and 10N

In addition to identifying the time-course of morphological maturation of Sol and 10N, the present study has provided an initial step in determining the functional implications of these morphological changes, mainly via chemoarchitectonic and connectional studies.

It should be noted that the main purpose of the application of chemoarchitectonic labeling markers is to validate and inform the subdivisional patterns of Sol and 10N drawn from cytoarchitectonic studies. For example, a distinctive group of Cb-ir neurons found in the rostral 10CeI but not the caudal 10CeI implies a heterogeneous

neurochemical feature of this subnucleus. Another example is the different Cr immunoreactivity found in sub-regions of SolM. It is hypothesized that there might be two subdivisions in SolM, something which is not visible in Nissl staining preparations. Besides this main purpose, chemoarchitectonic study is also able to provide hints as to the underlying functional maturation of a given nucleus. In the present study, one example would be the appearance of aggregations of TH-ir neurons in 10N and SolG as early as 13 weeks, which might suggest the maturation of neural control over gastric motility (Hayakawa et al., 2004) at this age.

Clearly, neural control over visceral organs cannot be established without the establishment of connections between them and the CNS. Therefore, connectional studies using DiI tract tracing techniques are important for deducing structural and functional correlations in the development of Sol and 10N. A typical example would be the close relationship between the time of formation of central vagal connections within the brainstem of the human fetus and the emergence of a series of reflexes found in the fetal respiratory system and alimentary canal (Abel et al., 1998; Dawes, 1974; Humphrey, 1968; Windle and Fitzgerald, 1937).

Due to the limitations of descriptive morphological analysis, the functional significance underlying the development of Sol and 10N can still only be inferred indirectly from the present results, but these analyses might well suggest the appropriate time points in the development of Sol and 10N for future investigators to study the maturation of the autonomic functions with which these nuclei are concerned.

6.4 Abnormalities in Development of Human Solitary Nucleus and Dorsal Motor Nucleus of Vagus

There are a few clinical conditions which have some relevance to the development of central vagal connections. These include sudden infant death syndrome (SIDS) (Becker, 1990; Becker and Zhang, 1996; Becker et al., 1993), oesophageal atresia (Qi et al., 1997) and autonomic dysfunction associated with Down's syndrome (Figueroa et al., 2005). Among these, SIDS, which is commonly seen as a condition in which infants die of sudden cardiorespiratory failure without predictable signs, is of particular interest, because it has been suggested that its aetiology involves a subtle defect in the neural circuitry that controls cardiorespiratory function in the new born (Becker and Zhang, 1996). Abnormalities of various centres in the CNS have been detected, mainly in the brainstem (Carey and Foster, 1984; Filiano and Kinney, 1992; O'Kusky and Norman, 1992), though the development of the medullary nuclei of the vagus nerve is of particular importance (Becker and Zhang, 1996). Macchi et al. (Macchi et al., 2002) examined post-mortem specimens from a month old child who died of SIDS and found that 10N, Sol and Amb, showed significant reductions in neuronal numbers, whereas the hypoglossal nucleus (12N) contained increased numbers of neurons. These findings suggested that abnormal cellular migration of vagal neuroblasts during early prenatal development might contribute to the aetiology of SIDS.

Correlations between the abnormal development of particular neurons expressing specific neurotransmitters and SIDS have also been investigated, but the results have been conflicting. In one study, Tolcos et al. (Tolcos et al., 2000) reported that prolonged

exposure to carbon monoxide during fetal life (e.g., in cases of maternal smoking) significantly decreased the number of TH-ir neurons in 10N and Sol, and significantly increased the intensity of ChAT immunoreactivity. On the other hand, immunoreactivity for other neuronal markers, e.g. m2 muscarinic acetylcholine receptor, substance P- or met-enkephalin, was unaffected. The results indicated that abnormal development of catecholaminergic and cholinergic neurons in Sol and 10N may be involved in the etiology of SIDS. However, in another study (Sawaguchi et al., 2003), no significant correlation between TH immunoreactivity and SIDS was found.

Other contributing factors considered in the aetiology of SIDS may involve the development of the vagus nerve itself. Ultrastructural quantitative morphometry of myelinated and unmyelinated fibers in the vagus nerve showed immaturity of vagus nerve fibers in infants dying from SIDS (Becker et al., 1993). However, such alterations are very subtle, and the gross profile of the vagal projections from 10N did not show any trend of reduction or elimination (Loeliger et al., 2000).

In the present study, the time of emergence of those subnuclei of Sol which are involved in the control of cardiorespiratory regulation as well as that of the differentiation of the vagal preganglionic neurons in 10N were shown by cyto- and chemoarchitectonic analysis to be during the early second trimester. Neuronal maturation was coincidentally accompanied by the development of the sensory and motor connections of Sol and 10N with the vagus nerve. Although these findings concerning the normal development of Sol and 10N do not provide direct evidence of causative factors which may underlie SIDS (or any other abnormality of the nuclei), they have identified key time points in the formation

of these autonomic control centres during fetal life. Developmental abnormalities of cardiorespiratory functions would be expected to manifest as changes in cyto- and chemoarchitecture in Sol and 10N during fetal life.

6.4 Future Directions

The present study has focused on development of the medullary vagal nuclei and their cranial nerve connections, but there are many anatomical aspects of the development of this system, which have functional significance and remain unexplored. For example, it is well-known that a variety of hypothalamic and rostral brainstem centres have a strong influence on the function of caudal medullary autonomic nuclei, e.g. projections from the lateral hypothalamic area, bed nucleus of stria terminalis and central amygdaloid nucleus to Sol and 10N are suggested to be important in the modulation of gastrointestinal and cardiovascular functions (Allen and Cechetto, 1992; Berk, 1987; Gray and Magnuson, 1987; Hopkins and Holstege, 1978; Jiang et al., 2003). However, very little is yet known concerning the maturation of those centres and the development of their projections to the Sol or 10N. Although some studies have focused on this area in postnatal rodents (Rinaman, 2003), no investigation on descending projections to 10N and Sol in the developing human has ever been undertaken. A significant future direction for the area of study touched on in the present thesis would be to determine when these "upstream" autonomic centres first make connections with the Sol and 10, thereby defining the first age at which higher centres can influence the medullary autonomic centres. This could readily be achieved by use of carbocyanine dye tracing techniques,

which are applicable to the sort of postmortem material used in the present study (Cheng et al., 2004). Such an analysis would also throw light on the question of when medullary autonomic centres project rostrally to pons, midbrain and hypothalamus.

Naturally carbocyanine dye tracing techniques would have some limitations in that sort of study, in that it would be very difficult to definitively prove that contacts have been made between afferents to a region and the constituent neurons. Double labeling techniques have been applied in fixed postmortem material using different types of carbocyanine dyes with distinct emission spectra (Song et al., 2000) and these may provide a more refined anatomical answer to the question than DiI labeling alone.

Even at the level of the medulla itself, development of the intermediate reticular zone (IRt) and the parasympathetic neurons associated with the nucleus ambiguus have not gained much attention. Brown (Brown, 1990) has investigated the embryonic and early (before 12.5 weeks) fetal development of Amb, and indicates that functions of Amb, manifested by fetal reflex swallowing, occurs after cells migrate into their definitive position. However, the maturation of neurochemical features and the establishment of central and peripheral connections of IRt and Amb remain unknown. The diffuse nature of these autonomic centres makes them difficult subjects of study, particularly in the human fetal brainstem.

6.5 Concluding Remarks

Despite the technical limitations of using fixed human fetal material, the present study has identified some of the milestones in the cyto- and chemoarchitectonic

development of the human fetal Sol and 10N and their afferent and efferent connections via the vagus nerve. The findings indicate that subnuclear differentiation of Sol and 10N takes place mainly between 13 and 15 weeks, and then slows down during the rest of fetal life. The present chemoarchitectonic investigations have mainly confirmed the subnuclear organization revealed by studies in the adult Sol and 10N (Huang et al., 1993a; Huang et al., 1993b; Paxinos and Huang, 1995; Tork et al., 1990), but have also shown neurochemical heterogeneity of cellular groups within particular subnucleus (e.g., Cr-ir neurons in SolM). Development of cyto- and chemoarchitectonic organizations took place in parallel with the establishment of vagal sensory and motor connections to Sol and 10N. Considered jointly, these findings have provided evidence of morphological maturation of the substrates which are important in control over the autonomic functions carried out by the vagus nerve.

References

Abdala, A. P., Haibara, A. S. and Colombari, E. 2003. Cardiovascular responses to substance P in the nucleus tractus solitarii: microinjection study in conscious rats. Am J Physiol Heart Circ Physiol 285:H891-898.

Abel, R. M., Bishop, A. E., Moscoso, G., Spitz, L. and Polak, J. M. 1998. The ontogeny of innervation of the human pylorus. J Pediatr Surg 33:613-618.

Allan, L. D., Tynan, M., Campbell, S. and Anderson, R. H. 1981. Normal fetal cardiac anatomy--a basis for the echocardiographic detection of abnormalities. Prenat Diagn 1:131-139.

Allan, L. D., Tynan, M. J., Campbell, S., Wilkinson, J. L. and Anderson, R. H. 1980. Echocardiographic and anatomical correlates in the fetus. Br Heart J 44:444-451.

Allen, G. V. and Cechetto, D. F. 1992. Functional and anatomical organization of cardiovascular pressor and depressor sites in the lateral hypothalamic area: I. Descending projections. J Comp Neurol 315:313-332.

Allen, W. F. 1923. Origin and distribution of the tractus solitarius in the guinea pig. J Comp Neurol 35:171-204.

Altman, J. and Bayer, S. A. 1980. Development of the brain stem in the rat. I. Thymidine-radiographic study of the time of origin of neurons of the lower medulla. J Comp Neurol 194:1-35.

Altman, J. and Bayer, S. A. 1982. Development of the cranial nerve ganglia and related nuclei in the rat. Adv Anat Embryol Cell Biol 74:1-90.

Altschuler, S., Berthoud, H.-R., Fox, E. and Laughton, W. 1992. Viscerotopic representation of the alimentary tract in the dorsal and ventral vagal complexes in the rat. In: Ritter, S.,Ritter, R. and Barnes, C., editors. Neuroanatomy and Physiology of Abdominal Vagal Afferents. Boca Raton: CRC Press. pp 21-53.

Altschuler, S. M., Bao, X. M., Bieger, D., Hopkins, D. A. and Miselis, R. R. 1989. Viscerotopic representation of the upper alimentary tract in the rat: sensory ganglia and nuclei of the solitary and spinal trigeminal tracts. J Comp Neurol 283:248-268.

Arai, R., Winsky, L., Arai, M. and Jacobowitz, D. M. 1991. Immunohistochemical localization of calretinin in the rat hindbrain. J Comp Neurol 310:21-44.

Arango, V., Ruggiero, D. A., Callaway, J. L., Anwar, M., Mann, J. J. and Reis, D. J. 1988. Catecholaminergic neurons in the ventrolateral medulla and nucleus of the solitary tract in

the human. J Comp Neurol 273:224-240.

Armstrong, D. M., Manley, L., Haycock, J. W. and Hersh, L. B. 1990. Co-localization of choline acetyltransferase and tyrosine hydroxylase within neurons of the dorsal motor nucleus of the vagus. J Chem Neuroanat 3:133-140.

Armstrong, D. M., Pickel, V. M., Joh, T. H., Reis, D. J. and Miller, R. J. 1981. Immunocytochemical localization of catecholamine synthesizing enzymes and neuropeptides in area postrema and medial nucleus tractus solitarius of rat brain. J Comp Neurol 196:505-517.

Astrom, K. 1953. On the central course of afferent fibers in the trigeminal, facial, glossopharyngeal, and vagal nerves and their nuclei in the mouse. Acta Physiol Scand Suppl 29:209-320.

Barraco, I. and Robin, A. 1994. Nucleus of the solitary tract. Boca Raton: CRC Press.

Barraco, R., el-Ridi, M., Ergene, E., Parizon, M. and Bradley, D. 1992. An atlas of the rat subpostremal nucleus tractus solitarius. Brain Res Bull 29:703-765.

Barry, M. A., Halsell, C. B. and Whitehead, M. C. 1993. Organization of the nucleus of the solitary tract in the hamster: acetylcholinesterase, NADH dehydrogenase, and cytochrome oxidase histochemistry. Microsc Res Tech 26:231-244.

Becker, L. E. 1990. Neural maturational delay as a link in the chain of events leading to SIDS. Can J Neurol Sci 17:361-371.

Becker, L. E. and Zhang, W. 1996. Vagal nerve complex in normal development and sudden infant death syndrome. Can J Neurol Sci 23:24-33.

Becker, L. E., Zhang, W. and Pereyra, P. M. 1993. Delayed maturation of the vagus nerve in sudden infant death syndrome. Acta Neuropathol (Berl) 86:617-622.

Beckstead, R. M., Morse, J. R. and Norgren, R. 1980. The nucleus of the solitary tract in the monkey: projections to the thalamus and brain stem nuclei. J Comp Neurol 190:259-282.

Beckstead, R. M. and Norgren, R. 1979. An autoradiographic examination of the central distribution of the trigeminal, facial, glossopharyngeal, and vagal nerves in the monkey. J Comp Neurol 184:455-472.

Belda, M., Covenas, R., Narvaez, J. A., Aguirre, J. A. and Tramu, G. 2003. An immunocytochemical mapping of methionine-enkephalin-Arg6-Gly7-Leu8 in the cat brainstem. Anat Embryol (Berl) 206:399-408.

Berger, A. J. 1979. Distribution of carotid sinus nerve afferent fibers to solitary tract

nuclei of the cat using transganglionic transport of horseradish peroxidase. Neurosci Lett 14:153-158.

Berger, A. J., Averill, D. B. and Cameron, W. E. 1984. Morphology of inspiratory neurons located in the ventrolateral nucleus of the tractus solitarius of the cat. J Comp Neurol 224:60-70.

Berk, M. L. 1987. Projections of the lateral hypothalamus and bed nucleus of the stria terminalis to the dorsal vagal complex in the pigeon. J Comp Neurol 260:140-156.

Bieger, D. 2001. Rhombencephalic pathways and neurotransmitters controlling deglutition. Am J Med 111 Suppl 8A:85S-89S.

Bieger, D. and Hopkins, D. A. 1987. Viscerotopic representation of the upper alimentary tract in the medulla oblongata in the rat: the nucleus ambiguus. J Comp Neurol 262:546-562.

Blessing, W. B. 1997. The Lower Brainstem and Bodily Homeostasis. New York: Oxford Univ. Press.

Boddy, K. and Dawes, G. S. 1975. Fetal breathing. Br Med Bull 31:3-7.

Bodegard, G., Schwieler, G. H., Skoglund, S. and Zetterstrom, R. 1969. Control of respiration in newborn babies. I. The development of the Hering-Breuer inflation reflex. Acta Paediatr Scand 58:567-571.

Bonham, A. C. and Joad, J. P. 1991. Neurones in commissural nucleus tractus solitarii required for full expression of the pulmonary C fibre reflex in rat. J Physiol 441:95-112.

Braak, H. 1972. [Nuclei of the human brain stem. V. The dorsal glossopharyngeus-vagus-complex]. Z Zellforsch Mikrosk Anat 135:415-438.

Bradley, R. M. and Grabauskas, G. 1998. Neural circuits for taste. Excitation, inhibition, and synaptic plasticity in the rostral gustatory zone of the nucleus of the solitary tract. Ann N Y Acad Sci 855:467-474.

Broussard, D. L. and Altschuler, S. M. 2000a. Brainstem viscerotopic organization of afferents and efferents involved in the control of swallowing. Am J Med 108 Suppl 4a:79S-86S.

Broussard, D. L. and Altschuler, S. M. 2000b. Central integration of swallow and airway-protective reflexes. Am J Med 108 Suppl 4a:62S-67S.

Brown, J. W. 1990. Prenatal development of the human nucleus ambiguus during the

embryonic and early fetal periods. Am J Anat 189:267-283.

Browning, K. N., Kalyuzhny, A. E. and Travagli, R. A. 2002. Opioid peptides inhibit excitatory but not inhibitory synaptic transmission in the rat dorsal motor nucleus of the vagus. J Neurosci 22:2998-3004.

Cajal, R. y. 1995. Histology of the nervous system of man and vertebrates. New York: Oxford University Press.

Calaresu, F.R. and Pearce, J.W. 1965. Effects on heart rate of electrical stimulation of medullary vagal structures in the cat. J Physiol 176: 241-251.

Callaway, E. M. and Katz, L. C. 1990. Emergence and refinement of clustered horizontal connections in cat striate cortex. J Neurosci 10:1134-1153.

Carey, E. M. and Foster, P. C. 1984. Phospholipid exchange activity in developing rat brain. Biochim Biophys Acta 792:48-58.

Chang, M. M., Leeman, S. E. and Niall, H. D. 1971. Amino-acid sequence of substance P. Nat New Biol 232:86-87.

Celio, M. R. 1990. Calbindin D-28k and parvalbumin in the rat nervous system.

Neuroscience 35:375-475.

Cheng, G., Zhou, X., Qu, J., Ashwell, K. W. and Paxinos, G. 2004. Central vagal sensory and motor connections: human embryonic and fetal development. Auton Neurosci 114:83-96.

Cheng, Z. and Powley, T. L. 2000. Nucleus ambiguus projections to cardiac ganglia of rat atria: an anterograde tracing study. J Comp Neurol 424:588-606.

Cheng, Z., Powley, T. L., Schwaber, J. S. and Doyle, F. J., 3rd. 1997. Vagal afferent innervation of the atria of the rat heart reconstructed with confocal microscopy. J Comp Neurol 381:1-17.

Cheng, Z., Powley, T. L., Schwaber, J. S. and Doyle, F. J., 3rd. 1999. Projections of the dorsal motor nucleus of the vagus to cardiac ganglia of rat atria: an anterograde tracing study. J Comp Neurol 410:320-341.

Cheng, Z., Zhang, H., Guo, S.Z., Wurster, R. and Gozal, D. 2004. Differential control over postaganglionic neurons in rat cardiac ganglia by NA and DmnX neurons: anatomical evidence. Am J Physiol Regul Integr Comp Physiol 286: R625-633.

Chernicky, C. L., Barnes, K. L., Ferrario, C. M. and Conomy, J. P. 1987. Projections of the

carotid sinus nerve to the medulla in the dog. Brain Res Bull 18:437-445.

Ciriello, J., Hrycyshyn, A. W. and Calaresu, F. R. 1981. Glossopharyngeal and vagal afferent projections to the brain stem of the cat: a horseradish peroxidase study. J Auton Nerv Syst 4:63-79.

Cohen, D. H., Schnall, A. M., Macdonald, R. L. and Pitts, L. H. 1970. Medullary cells of origin of vagal cardioinhibitory fibers in the pigeon. I. Anatomical studies of peripheral vagus nerve and the dorsal motor nucleus. J Comp Neurol 140:299-320.

Cohen, M. I. 1979. Neurogenesis of respiratory rhythm in the mammal. Physiol Rev 59:1105-1173.

Connors, N. A., Sullivan, J. M. and Kubb, K. S. 1983. An autoradiographic study of the distribution of fibers from the dorsal motor nucleus of the vagus to the digestive tube of the rat. Acta Anat (Basel) 115:266-271.

Contreras, R. J., Beckstead, R. M. and Norgren, R. 1982. The central projections of the trigeminal, facial, glossopharyngeal and vagus nerves: an autoradiographic study in the rat. J Auton Nerv Syst 6:303-322.

Cuello, A. C., Ribeiro-da-Silva, A., Ma, W., De Koninck, Y. and Henry, J. L. 1993.

Organization of substance P primary sensory neurons: ultrastructural and physiological correlates. Regul Pept 46:155-164.

Cunningham, E. T., Jr. and Sawchenko, P. E. 1989. A circumscribed projection from the nucleus of the solitary tract to the nucleus ambiguus in the rat: anatomical evidence for somatostatin-28-immunoreactive interneurons subserving reflex control of esophageal motility. J Neurosci 9:1668-1682.

Davies, R. O. and Kalia, M. 1981. Carotid sinus nerve projections to the brain stem in the cat. Brain Res Bull 6:531-541.

Dawes, G. S. 1974. Fetal circulation and breathing. Clin Obstet Gynaecol 1:139-149.

De Leon, M., Covenas, R., Narvaez, J. A., Aguirre, J. A. and Gonzalez-Baron, S. 1994. Distribution of calbindin D-28k-immunoreactivity in the cat brainstem. Arch Ital Biol 132:229-241.

De Leon, M., Covenas, R., Narvaez, J. A., Tramu, G., Aguirre, J. A. and Gonzalez-Baron, S. 1991. Distribution of neurotensin-like immunoreactive cell bodies and fibers in the brainstem of the adult male cat. Peptides 12:1201-1209.

De Leon, M., Covenas, R., Narvaez, J. A., Tramu, G., Aguirre, J. A. and Gonzalez-Baron, S.

1992. Distribution of cholecystokinin octapeptide in the cat brainstem: an immunocytochemical study. Arch Ital Biol 130:1-10.

de Quidt, M. E. and Emson, P. C. 1986. Distribution of neuropeptide Y-like immunoreactivity in the rat central nervous system--II. Immunohistochemical analysis. Neuroscience 18:545-618.

Del Fiacco, M., Dessi, M. L., Atzori, M. G. and Levanti, M. C. 1983. Substance P in the human brainstem. Preliminary results of its immunohistochemical localization. Brain Res 264:142-147.

Dennison, S. J., Merritt, V. E., Aprison, M. H. and Felten, D. L. 1981. Redefinition of the location of the dorsal (motor) nucleus of the vagus in the rat. Brain Res Bull 6:77-81.

Domenech-Ratto, G. 1977. Development and peripheral innervation of the palatal muscles. Acta Anat (Basel) 97:4-14.

Estes, M. L., Block, C. H. and Barnes, K. L. 1989. The canine nucleus tractus solitarii: light microscopic analysis of subnuclear divisions. Brain Res Bull 23:509-517.

Figueroa, A., Collier, S. R., Baynard, T., Giannopoulou, I., Goulopoulou, S. and Fernhall, B. 2005. Impaired vagal modulation of heart rate in individuals with Down syndrome. Clin Auton Res 15:45-50.

Filiano, J. J. and Kinney, H. C. 1992. Arcuate nucleus hypoplasia in the sudden infant death syndrome. J Neuropathol Exp Neurol 51:394-403.

Ford, T.W. and McWilliam, P.N. 1986. The effects of electrical stimulation of myelinated and non-myelinated vagal fibres on heart rate in the rabbit. J Physiol 380: 341-347.

Forutan, F., Mai, J. K., Ashwell, K. W., Lensing-Hohn, S., Nohr, D., Voss, T., Bohl, J. and Andressen, C. 2001. Organisation and maturation of the human thalamus as revealed by CD15. J Comp Neurol 437:476-495.

Fox, E. A. and Powley, T. L. 1985. Longitudinal columnar organization within the dorsal motor nucleus represents separate branches of the abdominal vagus. Brain Res 341:269-282.

Fox, E. A. and Powley, T. L. 1992. Morphology of identified preganglionic neurons in the dorsal motor nucleus of the vagus. J Comp Neurol 322:79-98.

Frost, D. O. 1984. Axonal growth and target selection during development: retinal projections to the ventrobasal complex and other "nonvisual" structures in neonatal Syrian hamsters. J Comp Neurol 230:576-592.

Fryscak, T., Zenker, W. and Kantner, D. 1984. Afferent and efferent innervation of the rat esophagus. A tracing study with horseradish peroxidase and nuclear yellow. Anat Embryol (Berl) 170:63-70.

Gai, W. P. and Blessing, W. W. 1996. Nitric oxide synthesising neurons in the central subnucleus of the nucleus tractus solitarius in humans. Neurosci Lett 204:189-192.

Gai, W. P., Messenger, J. P., Yu, Y. H., Gieroba, Z. J. and Blessing, W. W. 1995. Nitric oxide-synthesising neurons in the central subnucleus of the nucleus tractus solitarius provide a major innervation of the rostral nucleus ambiguus in the rabbit. J Comp Neurol 357:348-361.

Geis, G. S. and Wurster, R. D. 1980. Cardiac responses during stimulation of the dorsal motor nucleus and nucleus ambiguus in the cat. Circ Res 46:606-611.

Getz, B. and Sirnes, T. 1949. The localization within the dorsal motor vagal nucleus. an experimental investigation. J Comp Neurol 90:95-110.

Gibbins, I. L., Campbell, G. C., Morris, J. L., Nilsson, S. and Murphy, R. 1987. Pathway-specific connections between peptide-containing preganglionic and postganglionic neurons in the vagus nerve of the toad (Bufo marinus). J Auton Nerv Syst 20:43-55.

Gordon-Weeks, P. R. 1989. GAP-43--what does it do in the growth cone? Trends Neurosci 12:363-365.

Gray, T. S. and Magnuson, D. J. 1987. Neuropeptide neuronal efferents from the bed nucleus of the stria terminalis and central amygdaloid nucleus to the dorsal vagal complex in the rat. J Comp Neurol 262:365-374.

Gunn, C. G., Sevelius, G., Puiggari, J. and Myers, F. K. 1968. Vagal cardiomotor mechanisms in the hindbrain of the dog and cat. Am J Physiol 214:258-262.

Halasz, P. and Martin, P. 1985. Magellan: program for the quantitative analysis of histological sections. Kensington: University of New South Wales.

Hamilton, R. B. and Norgren, R. 1984. Central projections of gustatory nerves in the rat. J Comp Neurol 222:560-577.

Harding, R. and Bocking, A. D. 2001. Fetal Growth and Development. Cambridge: Cambridge University Press.

Hassiotis, M., Ashwell, K. W., Marotte, L. R., Lensing-Hohn, S. and Mai, J. K. 2002. GAP-43 Immunoreactivity in the brain of the developing and adult wallaby (Macropus

eugenii). Anat Embryol (Berl) 206:97-118.

Hayakawa, T., Takanaga, A., Tanaka, K., Maeda, S. and Seki, M. 2004. Distribution and ultrastructure of dopaminergic neurons in the dorsal motor nucleus of the vagus projecting to the stomach of the rat. Brain Res 1006:66-73.

Herbert, H., Moga, M. M. and Saper, C. B. 1990. Connections of the parabrachial nucleus with the nucleus of the solitary tract and the medullary reticular formation in the rat. J Comp Neurol 293:540-580.

Higgins, G. A. and Schwaber, J. S. 1983. Somatostatinergic projections from the central nucleus of the amygdala to the vagal nuclei. Peptides 4:657-662.

Hokfelt, T., Kellerth, J. O., Nilsson, G. and Pernow, B. 1975a. Experimental immunohistochemical studies on the localization and distribution of substance P in cat primary sensory neurons. Brain Res 100:235-252.

Hokfelt, T., Kellerth, J. O., Nilsson, G. and Pernow, B. 1975b. Substance p: localization in the central nervous system and in some primary sensory neurons. Science 190:889-890.

Hokfelt, T., Martensson, R., Bjorklund, A. and Goldstein, M. 1984. Distributional maps of tyrosine hydroxylase-immunoreactive neurons in the rat brain. In: Bjorklund, A. and

Hokfelt, T., editors. Handbook of Chemical Neuroanatomy Classical Transmitters in the CNS, Part 1. Armsterdam: Elsevier.

Honig, M. G., Hume, R. I. 1989. Dil and diO: versatile fluorescent dyes for neuronal labeling and pathway tracing [see comments]. Trends Neurosci 12: 333-335, 340-341.

Hopkins, D. A., Gootman, P. M., Gootman, N., Di Russo, S. M. and Zeballos, M. E. 1984. Brainstem cells of origin of the cervical vagus and cardiopulmonary nerves in the neonatal pig (Sus scrofa). Brain Res 306:63-72.

Hopkins, D. A. and Holstege, G. 1978. Amygdaloid projections to the mesencephalon, pons and medulla oblongata in the cat. Exp Brain Res 32:529-547.

Housley, G. D., Martin-Body, R. L., Dawson, N. J. and Sinclair, J. D. 1987. Brain stem projections of the glossopharyngeal nerve and its carotid sinus branch in the rat. Neuroscience 22:237-250.

Huang, X. F., Paxinos, G., Halasz, P., McRitchie, D. and Tork, I. 1993a. Substance P- and tyrosine hydroxylase-containing neurons in the human dorsal motor nucleus of the vagus nerve. J Comp Neurol 335:109-122.

Huang, X. F., Tork, I. and Paxinos, G. 1993b. Dorsal motor nucleus of the vagus nerve: a

cyto- and chemoarchitectonic study in the human. J Comp Neurol 330:158-182.

Humphrey, T. 1968. The development of mouth opening and related reflexes involving the oral area of human fetuses. Ala J Med Sci 5:126-157.

Hyde, T. M. and Miselis, R. R. 1992. Subnuclear organization of the human caudal nucleus of the solitary tract. Brain Res Bull 29:95-109.

Jacobson, R. D., Virag, I. and Skene, J. H. 1986. A protein associated with axon growth, GAP-43, is widely distributed and developmentally regulated in rat CNS. J Neurosci 6:1843-1855.

Jean, A. 1984. Brainstem organization of the swallowing network. Brain Behav Evol 25:109-116.

Jean, A. 1991. [The nucleus tractus solitarius: neuroanatomic, neurochemical and functional aspects]. Arch Int Physiol Biochim Biophys 99:A3-52.

Jiang, C., Fogel, R. and Zhang, X. 2003. Lateral hypothalamus modulates gut-sensitive neurons in the dorsal vagal complex. Brain Res 980:31-47.

Jones, J. F., Wang, Y. and Jordan, D. 1995. Heart rate responses to selective stimulation of cardiac vagal C fibres in anaesthetized cats, rats and rabbits. J Physiol 489 (Pt 1):203-214.

Jones, J. F., Wang, Y. and Jordan, D. 1998. Activity of C fibre cardiac vagal efferents in anaesthetized cats and rats. J Physiol 507: 869-880.

Kalia, M. 1992. Early ontogeny of the vagus nerve: an analysis of the medulla oblongata and cervical spinal cord of the postnatal rat. Neurochem Int 20:119-128.

Kalia, M., Fuxe, K., Hokfelt, T., Johansson, O., Lang, R., Ganten, D., Cuello, C. and Terenius, L. 1984. Distribution of neuropeptide immunoreactive nerve terminals within the subnuclei of the nucleus of the tractus solitarius of the rat. J Comp Neurol 222:409-444.

Kalia, M. and Mesulam, M. M. 1980a. Brain stem projections of sensory and motor components of the vagus complex in the cat: I. The cervical vagus and nodose ganglion. J Comp Neurol 193:435-465.

Kalia, M. and Mesulam, M. M. 1980b. Brain stem projections of sensory and motor components of the vagus complex in the cat: II. Laryngeal, tracheobronchial, pulmonary, cardiac, and gastrointestinal branches. J Comp Neurol 193:467-508.

Kalia, M. and Sullivan, J. M. 1982. Brainstem projections of sensory and motor components of the vagus nerve in the rat. J Comp Neurol 211:248-265.

Kapfhammer, J. P. and Schwab, M. E. 1994. Inverse patterns of myelination and GAP-43 expression in the adult CNS: neurite growth inhibitors as regulators of neuronal plasticity? J Comp Neurol 340:194-206.

Karimnamazi, H., Travers, S. P. and Travers, J. B. 2002. Oral and gastric input to the parabrachial nucleus of the rat. Brain Res 957:193-206.

Karns, L. R., Ng, S. C., Freeman, J. A. and Fishman, M. C. 1987. Cloning of complementary DNA for GAP-43, a neuronal growth-related protein. Science 236:597-600.

Katz, D. M. and Karten, H. J. 1983. Subnuclear organization of the dorsal motor nucleus of the vagus nerve in the pigeon, Columbia livia. J Comp Neurol 217:31-46.

Katz, D. M. and Karten, H. J. 1985. Topographic representation of visceral target organs within the dorsal motor nucleus of the vagus nerve of the pigeon Columba livia. J Comp Neurol 242:397-414.

Kerr, F. W. and Preshaw, R. M. 1969. Secretomotor function of the dorsal motor nucleus of the vagus. J Physiol 205:405-415.

King, C. T. and Hill, D. L. 1993. Neuroanatomical alterations in the rat nucleus of the

solitary tract following early maternal NaCl deprivation and subsequent NaCl repletion. J Comp Neurol 333:531-542.

Kinney, H. C., Filiano, J. J., White, W. F. 2001. Medullary serotonergic network deficiency in the sudden infant death syndrome: review of a 15-year study of a single dataset. J. Neuropathol Exp Neurol 60:228-247.

Kinney, H. C., Ottoson, C. K. and White, W. F. 1990. Three-dimensional distribution of 3H-naloxone binding to opiate receptors in the human fetal and infant brainstem. J Comp Neurol 291:55-78.

Kinney, H. C., Rava, L. A. and Benowitz, L. I. 1993. Anatomic distribution of the growth-associated protein GAP-43 in the developing human brainstem. J Neuropathol Exp Neurol 52:39-54.

Kitamura, S., Nagase, Y., Chen, K. and Shigenaga, Y. 1993. Nucleus ambiguus of the rabbit: cytoarchitectural subdivision and myotopical and neurotopic representations. Anat Rec 237:109-123.

Kitchell, R. L., Stromberg, M. W. and Davis, L. H. 1977. Comparative study of the dorsal motor nucleus of the vagus nerve. Am J Vet Res 38:37-49.

Koutcherov, Y., Huang, X. F., Halliday, G. M. and Paxinos, G. 2004. Organization of

human brain stem nuclei. In: Paxinos, G., editor. The Human Nervous System. 2 ed. San Diego: Elsevier Academic Press. pp 267-320.

Krowicki, Z. K. and Hornby, P. J. 1996. The inhibitory effect of substance P on gastric motor function in the nucleus raphe obscurus is mediated via nitric oxide in the dorsal vagal complex. J Auton Nerv Syst 58:177-180.

Krowicki, Z. K. and Hornby, P. J. 2000. Substance P in the dorsal motor nucleus of the vagus evokes gastric motor inhibition via neurokinin 1 receptor in rat. J Pharmacol Exp Ther 293:214-221.

Kubek, M. J., Rea, M. A., Hodes, Z. I. and Aprison, M. H. 1983. Quantitation and characterization of thyrotropin-releasing hormone in vagal nuclei and other regions of the medulla oblongata of the rat. J Neurochem 40:1307-1313.

Laughton, W. B. and Powley, T. L. 1987. Localization of efferent function in the dorsal motor nucleus of the vagus. Am J Physiol 252:R13-25.

Lawn, A. M. 1966. The localization, in the nucleus ambiguus of the rabbit, of the cells of origin of motor nerve fibers in the glossopharyngeal nerve and various branches of the vagus nerve by means of retrograde degeneration. J Comp Neurol 127:293-306.

Leslie, R., Reynolds, D. and Lawes, I. 1992. Central connections of the nuclei of the vagus nerve. In: Ritter, S.,Ritter, R. and Barnes, C., editors. Neuroanatomy and Physiology of Abdominal Vagal Afferents. Boca Raton: CRC Press. pp 81-97.

Leslie, R. A., Gwyn, D. G. and Hopkins, D. A. 1982. The ultrastructure of the subnucleus gelatinosus of the nucleus of the tractus solitarius in the cat. J Comp Neurol 206:109-118.

Lewis, M. W. and Travagli, R. A. 2001. Effects of substance P on identified neurons of the rat dorsal motor nucleus of the vagus. Am J Physiol Gastrointest Liver Physiol 281:G164-172.

Li, Y. Q., Rao, Z. R. and Shi, J. W. 1990. Substance P-like immunoreactive neurons in the nucleus tractus solitarii of the rat send their axons to the nucleus accumbens. Neurosci Lett 120:194-196.

Lindh, B., Dalsgaard, C. J., Elfvin, L. G., Hokfelt, T. and Cuello, A. C. 1983. Evidence of substance P immunoreactive neurons in dorsal root ganglia and vagal ganglia projecting to the guinea pig pylorus. Brain Res 269:365-369.

Ling, E. A., Shieh, J. Y., Wen, C. Y., Yick, T. Y. and Wong, W. C. 1987. The dorsal motor nucleus of the vagus nerve of the hamster: ultrastructure of vagal neurons and their responses to vagotomy. J Anat 152:161-172.

Liu, J. H., Yan, J., Yi, S. X., Chang, X. R., Lin, Y. P. and Hu, J. M. 2004. Effects of electroacupuncture on gastric myoelectric activity and substance P in the dorsal vagal complex of rats. Neurosci Lett 356:99-102.

Loeliger, M., Tolcos, M., Leditschke, J., Campbell, P. and Rees, S. 2000. Tracing cranial nerve pathways (glossopharyngeal, vagus, and hypoglossal) in SIDS and control infants: a DiI study. J Neuropathol Exp Neurol 59:822-829.

Loewy, A. D. 1990. Central autonomic pathways. In: Loewy, A.D. and Spyer, K.M., editors. Central Regulation of Autonomic Functions. New York: Oxford. pp 88-103.

Loewy, A. D. and Burton, H. 1978. Nuclei of the solitary tract: efferent projections to the lower brain stem and spinal cord of the cat. J Comp Neurol 181:421-449.

Loewy, A. D., McKellar, S. and Saper, C. B. 1979. Direct projections from the A5 catecholamine cell group to the intermediolateral cell column. Brain Res 174:309-314.

Loewy, A. D. and Spyer, K. M. 1990. Vagal preganglionic neurons. In: Loewy, A.D. and Spyer, K.M., editors. Central Regulation of Autonomic Functions. New York: Oxford. pp 68-87.

Lorke, D. E., Kwong, W. H., Chan, W. Y. and Yew, D. T. 2003. Development of

catecholaminergic neurons in the human medulla oblongata. Life Sci 73:1315-1331.

Lundy, R. and Norgren, R. 2004. Gustatory system. In: Paxinos, G., editor. The Rat Nervous System. 3 ed. San Diego: Academic Press. pp 891-921.

Lynn, R. B., Hyde, T. M., Cooperman, R. R. and Miselis, R. R. 1996. Distribution of bombesin-like immunoreactivity in the nucleus of the solitary tract and dorsal motor nucleus of the rat and human: colocalization with tyrosine hydroxylase. J Comp Neurol 369:552-570.

Ma, W. L., Zhang, W. B., Feng, G. and Cai, Y. L. 2005. Calbindin D28k-containing neurons in the paratrigeminal nucleus receive convergent nociceptive information and project to nucleus of the solitary tract in rat. Brain Res 1038:132-140.

Macchi, V., Snenghi, R., De Caro, R. and Parenti, A. 2002. Monolateral hypoplasia of the motor vagal nuclei in a case of sudden infant death syndrome. J Anat 200:195-198.

Mai, J. K., Stephens, P. H., Hopf, A. and Cuello, A. C. 1986. Substance P in the human brain. Neuroscience 17:709-739.

McLean, J. H. and Hopkins, D. A. 1985. Ultrastructure of the dorsal motor nucleus of the vagus nerve in monkey with a comparison of synaptology in monkey and cat. J Comp

Neurol 231:162-174.

McRitchie, D. A. and Tork, I. 1993. The internal organization of the human solitary nucleus. Brain Res Bull 31:171-193.

McRitchie, D. A. and Tork, I. 1994. Distribution of substance P-like immunoreactive neurons and terminals throughout the nucleus of the solitary tract in the human brainstem. J Comp Neurol 343:83-101.

Meiri, K. F., Pfenninger, K. H. and Willard, M. B. 1986. Growth-associated protein, GAP-43, a polypeptide that is induced when neurons extend axons, is a component of growth cones and corresponds to pp46, a major polypeptide of a subcellular fraction enriched in growth cones. Proc Natl Acad Sci U S A 83:3537-3541.

Menetrey, D. and Basbaum, A. I. 1987. Spinal and trigeminal projections to the nucleus of the solitary tract: a possible substrate for somatovisceral and viscerovisceral reflex activation. J Comp Neurol 255:439-450.

Menetrey, D., De Pommery, J., Baimbridge, K. G. and Thomasset, M. 1992. Calbindin-D28K (CaBP28k)-like Immunoreactivity in Ascending Projections. Eur J Neurosci 4:61-69.

Mitchell, G. A. and Warwick, R. 1955. The dorsal vagal nucleus. Acta Anat (Basel) 25:371-395.

Moore, K. L. 1977. The Developing Human. Clinically Orientated Embryology. Philadelphia: W. B. Saunders.

Muller, F. and O'Rahilly, R. 1985. The first appearance of the neural tube and optic primordium in the human embryo at stage 10. Anat Embryol (Berl) 172:157-169.

Muller, F. and O'Rahilly, R. 1990. The human brain at stages 18-20, including the choroid plexuses and the amygdaloid and septal nuclei. Anat Embryol (Berl) 182:285-306.

Muller, F. and O'Rahilly, R. 2004. Embryonic development of the central nervous system. In: Paxinos, G., editor. The Human Nervous System. 2 ed. San Diego: Elsevier Academic Press. pp 22-48.

Muller, F., O'Rahilly, R. and Tucker, J. A. 1981. The human larynx at the end of the embryonic period proper. I. The laryngeal and infrahyoid muscles and their innervation. Acta Otolaryngol 91:323-336.

Nageotte, J. 1906. The par intermedia or nervus intermedius of Wrisberg, and the bulbopontine gustatory nucleus ion man. Rev Neurol Psychiatr 4:472-488.

Nara, T., Goto, N. and Hamano, S. 1991. Development of the human dorsal nucleus of vagus nerve: a morphometric study. J Auton Nerv Syst 33:267-275.

Neve, R. L., Finch, E. A., Bird, E. D. and Benowitz, L. I. 1988. Growth-associated protein GAP-43 is expressed selectively in associative regions of the adult human brain. Proc Natl Acad Sci U S A 85:3638-3642.

Nomura, H., Shiosaka, S., Inagaki, S., Ishimoto, I., Senba, E., Sakanaka, M., Takatsuki, K., Matsuzaki, T., Kubota, Y., Saito, H., Takase, S., Kogure, K. and Tohyama, M. 1982. Distribution of substance P-like immunoreactivity in the lower brainstem of the human fetus: an immunohistochemical study. Brain Res 252:315-325.

Norgren, R. 1978. Projections from the nucleus of the solitary tract in the rat. Neuroscience 3:207-218.

O'Kusky, J. R. and Norman, M. G. 1992. Sudden infant death syndrome: postnatal changes in the numerical density and total number of neurons in the hypoglossal nucleus. J Neuropathol Exp Neurol 51:577-584.

Olszewski, J. and Baxter, D. 1954. Cytoarchitecture of the human brain stem. N.Y.: Lippincott.

Olszewski, J. and Baxter, D. 1982. Cytoarchitecture of the human brain stem. Basel: S. Karger.

Pagani, F. D., Norman, W. P., Kasbekar, D. K. and Gillis, R. A. 1985. Localization of sites within dorsal motor nucleus of vagus that affect gastric motility. Am J Physiol 249:G73-84.

Paxinos, G. and Huang, X. 1995. Atlas of the Human Brainstem. San Diego: Academic Press.

Pego-Reigosa, R., Covenas, R., Tramu, G. and Pesini, P. 2000. Distribution of met-enkephalin immunoreactivity in the diencephalon and the brainstem of the dog. J Chem Neuroanat 19:243-258.

Pendleton, R. G., Rasheed, A., Roychowdhury, R. and Hillman, R. 1998. A new role for catecholamines: ontogenesis. Trends Pharmacol Sci 19:248-251.

Pereyra, P. M., Zhang, W., Schmidt, M. and Becker, L. E. 1992. Development of myelinated and unmyelinated fibers of human vagus nerve during the first year of life. J Neurol Sci 110:107-113.

Price, J. L. and Amaral, D. G. 1981. An autoradiographic study of the projections of the central nucleus of the monkey amygdala. J Neurosci 1:1242-1259.

Pritchard, T. and Norgren, R. 2004. Gustatory system. In: Paxinos, G., editor. The Human Nervous System. 2 ed. San Diego: Academic Press. pp 1171-1197.

Puelles, L. and Verney, C. 1998. Early neuromeric distribution of tyrosine-hydroxylase-immunoreactive neurons in human embryos. J Comp Neurol 394:283-308.

Qi, B. Q., Merei, J., Farmer, P., Hasthorpe, S., Myers, N. A., Beasley, S. W. and Hutson, J. M. 1997. The vagus and recurrent laryngeal nerves in the rodent experimental model of esophageal atresia. J Pediatr Surg 32:1580-1586.

Ricardo, J. A. and Koh, E. T. 1978. Anatomical evidence of direct projections from the nucleus of the solitary tract to the hypothalamus, amygdala, and other forebrain structures in the rat. Brain Res 153:1-26.

Rikard-Bell, G. C., Tork, I., Sullivan, C. and Scheibner, T. 1990. Distribution of substance P-like immunoreactive fibres and terminals in the medulla oblongata of the human infant. Neuroscience 34:133-148.

Rinaman, L. 2003. Postnatal development of hypothalamic inputs to the dorsal vagal complex in rats. Physiol Behav 79:65-70.

Rinaman, L. and Levitt, P. 1993. Establishment of vagal sensorimotor circuits during fetal development in rats. J Neurobiol 24:641-659.

Rinaman, L. and Miselis, R. R. 1987. The organization of vagal innervation of rat pancreas using cholera toxin-horseradish peroxidase conjugate. J Auton Nerv Syst 21:109-125.

Ritter, S., Ritter, R. C. and Barnes, C. D. 1992. Neuroanatomy and physiology of abdominal vagal afferents. Boca Raton: CRC Press.

Rogers, R. C. and Hermann, G. E. 1985. Dorsal medullary oxytocin, vasopressin, oxytocin antagonist, and TRH effects on gastric acid secretion and heart rate. Peptides 6:1143-1148.

Rogers, R. C., Kita, H., Butcher, L. L. and Novin, D. 1980. Afferent projections to the dorsal motor nucleus of the vagus. Brain Res Bull 5:365-373.

Rogers, R. C., McTigue, D. M. and Hermann, G. E. 1995. Vagovagal reflex control of digestion: afferent modulation by neural and "endoneurocrine" factors. Am J Physiol

268:G1-10.

Rogers, R. C., Travagli, R. A. and Hermann, G. E. 2003. Noradrenergic neurons in the rat solitary nucleus participate in the esophageal-gastric relaxation reflex. Am J Physiol Regul Integr Comp Physiol 285:R479-489.

Ross, C. A., Ruggiero, D. A. and Reis, D. J. 1985. Projections from the nucleus tractus solitarii to the rostral ventrolateral medulla. J Comp Neurol 242:511-534.

Ruggiero, D. A., Mtui, E. P., Otake, K. and Anwar, M. 1996. Central and primary visceral afferents to nucleus tractus solitarii may generate nitric oxide as a membrane-permeant neuronal messenger. J Comp Neurol 364:51-67.

Sachis, P. N., Armstrong, D. L., Becker, L. E. and Bryan, A. C. 1982. Myelination of the human vagus nerve from 24 weeks postconceptional age to adolescence. J Neuropathol Exp Neurol 41:466-472.

Saito, R., Takano, Y. and Kamiya, H. O. 2003. Roles of substance P and NK(1) receptor in the brainstem in the development of emesis. J Pharmacol Sci 91:87-94.

Saper, C. B. 1995. Central Autonomic System. In: Paxinos, G., editor. The Rat Nervous System. San Diego, CA: Academic Press. pp 107-135.

Sase, M., Miwa, I., Sumie, M., Nakata, M., Sugino, N. and Ross, M. G. 2005. Ontogeny of gastric emptying patterns in the human fetus. J Matern Fetal Neonatal Med 17:213-217.

Sase, M., Tamura, H., Ueda, K. and Kato, H. 1999. Sonographic evaluation of antepartum development of fetal gastric motility. Ultrasound Obstet Gynecol 13:323-326.

Sato, K., Momose-Sato, Y., Hirota, A., Sakai, T. and Kamino, K. 1998. Optical mapping of neural responses in the embryonic rat brainstem with reference to the early functional organization of vagal nuclei. J Neurosci 18:1345-1362.

Satoda, T., Takahashi, O., Uchida, T. and Mizuno, N. 1995. An anterograde-retrograde labeling study of the carotid sinus nerve of the Japanese monkey (Macaca fuscata). Neurosci Res 22:381-387.

Sawaguchi, T., Ozawa, Y., Patricia, F., Kadhim, H., Groswasser, J., Sottiaux, M., Takashima, S., Nishida, H. and Kahn, A. 2003. Catecholaminergic neurons in the brain-stem and sleep apnea in SIDS victims. Early Hum Dev 75 Suppl:S41-50.

Sawchenko, P. E. and Swanson, L. W. 1982. Immunohistochemical identification of neurons in the paraventricular nucleus of the hypothalamus that project to the medulla or to the spinal cord in the rat. J Comp Neurol 205:260-272.

Saxon, D. W. and Hopkins, D. A. 1998. Efferent and collateral organization of paratrigeminal nucleus projections: an anterograde and retrograde fluorescent tracer study in the rat. J Comp Neurol 402:93-110.

Schoenen, J. and Faull, R. L. M. 2004. Spinal cord: cyto- and chemoarchitecture. In: Paxinos, G., editor. The Human Nervous System. 2 ed. San Diego: Elsevier Academic Press. pp 190-232.

Schwaber, J. S., Kapp, B. S. and Higgins, G. 1980. The origin and extent of direct amygdala projections to the region of the dorsal motor nucleus of the vagus and the nucleus of the solitary tract. Neurosci Lett 20:15-20.

Schwaller, B., Buchwald, P., Blumcke, I., Celio, M. R. and Hunziker, W. 1993. Characterization of a polyclonal antiserum against the purified human recombinant calcium binding protein calretinin. Cell Calcium 14:639-648.

Schwaller, B., Meyer, M. and Schiffmann, S. 2002. 'New' functions for 'old' proteins: the role of the calcium-binding proteins calbindin D-28k, calretinin and parvalbumin, in cerebellar physiology. Studies with knockout mice. Cerebellum 1:241-258.

Schwarzacher, S. W. 2002. Cajal's prophetic functional considerations on respiratory reflexes: new questions about old answers. Prog Brain Res 136:435-442.

Shapiro, R. E. and Miselis, R. R. 1985. The central organization of the vagus nerve innervating the stomach of the rat. J Comp Neurol 238:473-488.

Smolen, A. J. and Truex, R. C. 1977. The dorsal motor nucleus of the vagus nerve of the cat: localization of preganglionic neurons by quantitative histological methods. Anat Rec 189:555-565.

Song, A., Ashwell, K. W. and Tracey, D. J. 2000. Development of the rat phrenic nucleus and its connections with brainstem respiratory nuclei. Anat Embryol (Berl) 202:159-177.

Spencer, S. E. and Talman, W. T. 1986. Modulation of gastric and arterial pressure by nucleus tractus solitarius in rat. Am J Physiol 250:R996-1002.

Stuesse, S. L., Cruce, W. L. and Powell, K. S. 1984. Organization within the cranial IX-X complex in ranid frogs: a horseradish peroxidase transport study. J Comp Neurol 222:358-365.

Sugimoto, T., Fujiyoshi, Y., He, Y. F., Xiao, C. and Ichikawa, H. 1997. Trigeminal primary projection to the rat brain stem sensory trigeminal nuclear complex and surrounding structures revealed by anterograde transport of cholera toxin B subunit-conjugated and Bandeiraea simplicifolia isolectin B4-conjugated horseradish peroxidase. Neurosci Res

28:361-371.

Swanson, L. W., Sawchenko, P. E., Rivier, J. and Vale, W. W. 1983. Organization of ovine corticotropin-releasing factor immunoreactive cells and fibers in the rat brain: an immunohistochemical study. Neuroendocrinology 36:165-186.

Taber, E. 1961. The cytoarchitecture of the brain stem of the cat. I. Brain stem nuclei of cat. J Comp Neurol 116:27-69.

Talman, W. T. and Reis, D. J. 1981. Baroreflex actions of substance P microinjected into the nucleus tractus solitarii in rat: a consequence of local distortion. Brain Res 220:402-407.

Ter Horst, G. J., de Boer, P., Luiten, P. G. and van Willigen, J. D. 1989. Ascending projections from the solitary tract nucleus to the hypothalamus. A Phaseolus vulgaris lectin tracing study in the rat. Neuroscience 31:785-797.

Todo, K. 1977. Vagal preganglionic innervation of the cat heart--an attempt to identify the medullary "heart area" by the retrograde axoplasmic transport of horseradish peroxidase. Jpn Circ J 41:1341-1352.

Tolcos, M., McGregor, H., Walker, D. and Rees, S. 2000. Chronic prenatal exposure to

carbon monoxide results in a reduction in tyrosine hydroxylase-immunoreactivity and an increase in choline acetyltransferase-immunoreactivity in the fetal medulla: implications for Sudden Infant Death Syndrome. J Neuropathol Exp Neurol 59:218-228.

Tork, I., McRitchie, D., Rikard-Bell, G. C. and Paxinos, G. 1990. Autonomic regulatory centers in the medulla oblongata. In: Paxinos, G., editor. Human Nervous System. San Diego, CA: Academic Press. pp 221-259.

Torrealba, F. and Claps, A. 1988. The carotid sinus connections: a WGA-HRP study in the cat. Brain Res 455:134-143.

Torvik, A. 1956. Afferent connections to the sensory trigeminal nuclei, the nucleus of the solitary tract and adjacent structures: an experimental study in the rat. J Comp Neurol 106:51.

Travers, J. B. and Norgren, R. 1983. Afferent projections to the oral motor nuclei in the rat. J Comp Neurol 220:280-298.

van der Kooy, D. 1984. Area postrema: site where cholecystokinin acts to decrease food intake. Brain Res 295:345-347.

Verney, C., Zecevic, N. and Ezan, P. 2001. Expression of calbindin D28K in the

dopaminergic mesotelencephalic system in embryonic and fetal human brain. J Comp Neurol 429:45-58.

Waite, P. M., Ho, S. and Henderson, T. A. 1995. A novel preparation for investigating trigeminal connections in fetal rat. Soc Neurosci Abstr 21:1531.

Wang, J., Chen, Y., Li, K., Sun, F. 2005. GABAergic neurons innervating the preganglionic cardiac vagal neurons in the dorsal motor nucleus receive tonic glutamatergic control. Acta Physiologica Sinica 57: 761-765.

Wang, L. G., Rao, Z. R., Li, H. M. and Li, J. S. 1993. Prenatal ontogeny of substance P-like immunoreactivity in the nucleus tractus solitarii and dorsal motor nucleus of the vagus nerve of the human fetus: an immunocytochemical study. Brain Res 605:9-17.

Wang, Z. J., Rao, Z. R. and Shi, J. W. 1992. Tyrosine hydroxylase-, neurotensin-, or cholecystokinin-containing neurons in the nucleus tractus solitarii send projection fibers to the nucleus accumbens in the rat. Brain Res 578:347-350.

Whitehead, M. C. 1986. Anatomy of the gustatory system in the hamster: synaptology of facial afferent terminals in the solitary nucleus. J Comp Neurol 244:72-85.

Whitehead, M. C. 1988. Neuronal architecture of the nucleus of the solitary tract in the

hamster. J Comp Neurol 276:547-572.

Whitehead, M. C. 1990. Subdivisions and neuron types of the nucleus of the solitary tract that project to the parabrachial nucleus in the hamster. J Comp Neurol 301:554-574.

Windle, W. F. and Fitzgerald, J. E. 1937. Development of the spinal reflex mechanism in human embryos. J Comp Neurol 67:493-509.

WMA. 1964. WORLD MEDICAL ASSOCIATION DECLARATION OF HELSINKI: Ethical Principles for Medical Research Involving Human Subjects.

Woolley, D.C., McWilliam, P.N., Ford, T.W. and Clarke, R.W. 1987. The effect of selective electrical stimulation of non-myelinated vagal fibres on heart rate in the rabbit. J Auton Nerv Syst 21: 215-221.

Wozniak, W. and O'Rahilly, R. 1981. Fine structure and myelination of the developing human vagus nerve. Acta Anat (Basel) 109:218-230.

Xiong, Y., Okada, J., Tomizawa, S., Takayama, K. and Miura, M. 1998. Difference in topology, and numbers of barosensitive catecholaminergic and cholinergic neurons in the medulla between SHR and WKY rats. J Auton Nerv Syst 70: 200-208.

Yamazoe, M., Shiosaka, S., Shibasaki, T., Ling, N., Tateishi, K., Hashimura, E., Hamaoka, T., Kimmel, J. R., Matsuo, H. and Tohyama, M. 1984. Distribution of six neuropeptides in the nucleus tractus solitarii of the rat: an immunohistochemical analysis. Neuroscience 13:1243-1266.

Yao, G. L., Kiyama, H. and Tohyama, M. 1993. Distribution of GAP-43 (B50/F1) mRNA in the adult rat brain by in situ hybridization using an alkaline phosphatase labeled probe. Brain Res Mol Brain Res 18:1-16.

Yew, D. T., Luo, C. B., Zheng, D. R., Guan, Y. L., Lin, Y. Q. and Chen, W. Z. 1990. Development and localization of enkephalin and substance P in the nucleus of tractus solitarius in the medulla oblongata of human fetuses. Neuroscience 34:491-498.

Zhang, L. L. and Ashwell, K. W. 2001a. The development of cranial nerve and visceral afferents to the nucleus of the solitary tract in the rat. Anat Embryol (Berl) 204:135-151.

Zhang, L. L. and Ashwell, K. W. 2001b. Development of the cyto- and chemoarchitectural organization of the rat nucleus of the solitary tract. Anat Embryol (Berl) 203:265-282.

Zec, N., Filiano, J.J., Kinney, H.C. 1997. Anatomic relationships of the arcuate nucleus of the medulla: A DiI-labeling study. J Neuropatholo Exp Neurol 56: 509-522.

Zec, N. and Kinney, H.C. 2001. Anatomic relationships of the human nucleus paragigantocellularis lateralis. A DiI labeling study. Auto Neurosci 89: 110-124.

Zec, N. and Kinney, H.C. 2003. Anatomic relationships of the human nucleus of the solitary tract: A DiI labeling study. Auto Neurosci 105: 131-144.

Zou, X. C. and Martin, G. F. 1995. The distribution of GAP-43 immunoreactivity in the central nervous system of adult opossums (Didelphis virginiana) with notes on their development. Brain Behav Evol 45:63-83.

Abbreviations

4V	fourth ventricle
5n	trigeminal nerve
7n	facial nerve
9n	glossopharyngeal nerve
10Ca	dorsal motor nucleus of vagus, caudal
10CaI	dorsal motor nucleus of vagus, caudointermediate
10CeI	dorsal motor nucleus of vagus, centrointermediate
10DI	dorsal motor nucleus of vagus, dorsointermediate
10DR	dorsal motor nucleus of vagus, dorsorostral
10Gn	inferior ganglion of vagus nerve
10n	vagus nerve
10N	dorsal motor nucleus of vagus
10RI	dorsal motor nucleus of vagus, rostrointermediate
10Tr	vagal trigone
10VI	dorsal motor nucleus of vagus, ventrointermediate
10VR	dorsal motor nucleus of vagus, ventrorostral
12n	hypoglossal nerve
12N	hypoglossal nucleus
A2	A2 noradrenaline cells
A2/C2	A2/C2 noradrenaline and/or adrenaline cells
Amb	ambiguus nucleus
AP	area Postrema
Cb	calbindin
CC	central canal
CDPMn	caudal dorsal paramedian nucleus
CeC	central cervical nucleus
chp	choroids plexus
Cr	calretinin
Cu	cuneate nucleus
DiI	1,1'-dioctadecyl-3,3,3',3' tetramethylindocarbocyanine percholorate
DPGi	dorsal paragigantocellular nucleus
DrF	dorsal motor nucleus of vagus, dorsal fringe
E	ependyma and subependymal layers
ECu	external cuneate nucleus
EF	epifascicular nucleus
GAP-43	growth associated protein 43
Gr	gracile nucleus
ia	internal arcuate fibers
In	intercalated nucleus of the medulla
IPo	interpositus nucleus
IRt	intermediate reticular zone
LMP	last menstrual period
MA	marginal zone of myelencephalon
MeF	dorsal motor nucleus of vagus, medial fringe
MPCu	medial pericuneate nucleus
MVePC	medial veistibular nucleus, parvicellular part
MVeMC	medial veistibular nucleus, magnocelluar part
MZ	mantle zone of myelencephalon
PCRt	parvicellular reticular nucleus
PCuMx	pericuneate matrix
Pr	prepositus nucleus
PSol	parasolitary nucleus
sl	sulcus limitans
sol	solitary tract
Sol	solitary nucleus
SolC	solitary nucleus, commissural
SolD	solitary nucleus, dorsal
SolDL	solitary nucleus, dorsolateral
SolG	solitary nucleus, gelatinosus
SolI	solitary nucleus, interstitial
SolIM	solitary nucleus, intermediate
SolM	solitary nucleus, medial
SolPa	solitary nucleus, paracommissural
SolV	solitary nucleus, ventral
SolVL	solitary nucleus, ventrolateral
SP	substance P
sp5	spinal trigeminal tract
Sp5I	spinal trigeminal nucleus, interpolaris part
SpVe	spinal vestibular nucleus
TH	tyrosine hydroxylase
Z	nucleus Z